Carbon cycle changes during the end-Marjuman (Cambrian) extinction in the Southern Appalachians

Angela M. Gerhardt

Thesis submitted to the faculty of the Virginia Polytechnic Institute and State University in partial fulfillment of the requirements for the degree of

Master of Science
In
Geosciences

Benjamin C. Gill, Committee Chair
Shuhai Xiao
Brian W. Romans

May 28, 2014
Blacksburg, VA

Keywords: Steptoean Positive Carbon Isotope Excursion, ocean anoxia, stable isotope geochemistry, Nolichucky Formation, Appalachian geology, end-Marjuman extinction

Carbon cycle changes during the end-Marjuman (Cambrian) extinction in the Southern Appalachians

Angela M. Gerhardt

ABSTRACT

The late Cambrian-early Ordovician transition contains several trilobite extinctions. The first of these extinctions (the end-Marjuman) is thought to coincide with the Steptoean Positive Carbon Isotope Excursion or SPICE, a large and rapid excursion in the marine carbon isotope record. This excursion, which is expressed in sedimentary successions globally, is thought to represent a large perturbation to the carbon cycle during this time. Additionally, a limited amount of carbon isotope data from the Deadwood Formation in the Black Hills of South Dakota suggests the possibility of a small negative $\delta^{13}C$ excursion near the extinction and preceding the SPICE. Previous high-resolution biostratigraphy has identified an expanded record of extinction event within the Nolichucky Formation of the Southern Appalachians making it an excellent candidate for the study of the precise relationship between the extinction and changes in the carbon cycle. This investigation confirms the onset of the SPICE occurs at the extinction boundary however no negative $\delta^{13}C$ excursion occurs at the extinction boundary. Further there is no systematic relationship between local facies changes and $\delta^{13}C$ or the extinction interval across the basin, which suggests that global environmental changes were responsible for both the $\delta^{13}C$ record and the extinction event.

DEDICATION

I dedicate my thesis to my parents
Matthew A. Gerhardt & Annette F. Gerhardt
Who have always encouraged my curiosity and support my every decision
And
To my niece and nephew
Annalyse M.J. Cortez and Benjamin A. Cortez
Who inspire me to lead by example

ACKNOWLEDGEMENTS

All of my efforts would be lost if it wasn't for the guidance of my Advisor Benjamin Gill. I'd like to thank Ben for maintaining a lighthearted work environment while still challenging my intellect. It has been a pleasure to be your first Master student. I would like to thank the members of my committee Brian Romans and Shuhai Xiao for continued insight and direction.

The foundation of my success thus far is attributed to the education I received at Virginia Tech and the University of California, Riverside. It has been an honor to be a part of the geoscience department at both universities. I'd like to thank Jeremy Owens and Harmony Colella for their mentorship; they both strongly influence my decision to attend graduate school.

To Matthew Petroff and Alexandra Menza, thank you for assisting me in sample processing. It takes a steady hand and patience to drill all of those samples and your time is appreciated.

Of course the experience of graduate school is truly amplified by the genuine friendships gained. With that, I'd like to thank Kristen McCall, Lyndsey Funkhouser, and Hannah King for being my support system even through the most stressful times. Just as important, I'd like to thank my office mates Theodore Them, Neal Auchter, Cody Mason, Patrick Boyle, and Ty Buller for being a continuous source of entertainment and knowledge.

Finally, I would like to thank my family members Matthew Gerhardt, Annette Gerhardt, Arianne Cortez, Johnny Cortez, and Jessica Gerhardt for being supportive, hilarious and patient. You all are my motivation.

Table of contents

List of Figures

List of Tables

1. Introduction

Mass extinctions represent critical events in the history of life on Earth and important boundaries within the geological timescale. The Phanerozoic is marked by both major and minor mass extinctions that are manifested in the paleontological record and were likely caused by several environmental and biological factors that can be deciphered from geochemical records (e.g. Hönisch et al., 2012). In particular, the later Cambrian was characterized by three extinction events that affected mainly shallow marine shelf communities of trilobites and brachiopods (Palmer, 1979; Saltzman et al., 1998; Perfetta, 1999). The first of these extinctions occurred at the Marjumiid-Pterocephaliid biomere boundary (here referred to as the end-Marjuman extinction) which coincides with the initiation of a globally recognized perturbation to the carbon isotope record referred to as the Steptoean Positive Carbon Isotope Excursion, or SPICE (Brasier, 1993; Saltzman et al., 1998). The coincidence of the SPICE and the end-Marjuman extinction has led to several hypotheses regarding the relationship between and the cause of these two events. For example, an increase in organic matter burial under widespread deep marine euxinic conditions has been proposed to both explain the SPICE and end-Marjuman extinction (Gill et al., 2011). Additionally, carbon isotope records from the Deadwood Formation (Fm.) in the Black Hills of South Dakota show a small (1‰) negative $\delta^{13}C$ excursion occurred at the extinction boundary, preceding the initiation of the SPICE (Perfetta et al., 1999). Perfetta et al. (1999) suggested that the negative shift in $\delta^{13}C$ is linked to cold, deep, nutrient-rich ^{12}C-enriched marine waters that invaded the warm, shallow water environments. However, this negative excursion has yet to be identified in stratigraphic successions elsewhere and thus, could be the result of changes in the chemistry confined to that location.

The majority of previous studies concerning the SPICE have focused on epicontinental stratigraphic successions from western Laurentia and Gondwana (Figure 1), but few studies have focused on the passive margin of Laurentia (eastern North America) in great detail. The Cambrian-Ordovician passive margin succession of Laurentia makes up the Great American Carbonate Bank and which extends to portions

of the Southern Appalachians, the location of this study. This region represents an excellent location to study the relationship between changes in the carbon cycle based on the expanded nature of the extinction interval in the Southern Appalachians (Rasetti, 1965; Palmer, 1979). In northeastern Tennessee and southwestern Virginia the extinction interval is contained within the lithological units of the Nolichucky Formation. The units that comprise the Nolichucky Formation are interpreted as an intrashelf basin consisting of peritidal and subtidal carbonate and shale facies (Markello and Read, 1981; Hasson and Hasse, 1988; Weber, 1988). This formation has been the subject of several biostratigraphic studies that have identified the end-Marjuman extinction in this unit (Derby, 1965; Rasetti, 1965; Cuggy, 1996). This study is the first high-resolution geochemical analysis of the Nolichucky Formation and investigates the relationship between changes in the biosphere, sea level, and the carbon cycle during this interval of the late Cambrian.

1.1 End-Marjuman extinction

The most abundant fossils in the late Cambrian and early Ordovician strata are trilobites, brachiopods, and conodonts (Palmer, 1965a; Miller, 1988; Taylor, 2012). Early biostratigraphic studies of the late Cambrian by Palmer (1965a) and Longacre (1970) recognized that this interval was punctuated by three trilobite extinction events followed by diversification events. The first of these extinctions occurred at the boundary between the Guzhangian and Furongian International Stages of the Cambrian (Figure 2). In western North America this extinction is identified as the boundary between regional Marjuman and Steptoean Stages and is thus referred to in this thesis as the end-Marjuman extinction.

The ecological patterns of the extinction interval suggest the abrupt extinction of a diverse assemblage of shallow marine trilobite faunas (those faunas inhabiting the shelf) that were replaced by a low diversity assemblage of olenimorph trilobite fauna (normally found in more distal deep-water facies). In general, the morphology of olenid fauna

suggests that they were well-adapted to low oxygen environments (Fortey, 1985), as they are normally found in the deep, off-platform environment(s) (Stitt, 1971; Palmer, 1984; Westrop and Ludvigsen, 1987; Taylor, 2006). In detail, the extinctions appear to have occurred in two phases: the first was an extinction of the majority of the shallow-water trilobite assemblage (*Crepicephalus* Zone fauna), but with the survival of a few of the trilobites from this assemblage (*Coosella perplexa* Subzone fauna). The second phase involved the extinction of the remaining shallow-water trilobites and their replacement by the olenimorph fauna (*Aphelaspis* zone fauna). The *Coosella perplexa* subzone, located between these two extinctions, has been termed the "critical interval" by some authors (Stitt, 1971; Palmer, 1979; Taylor, 2006).

Following the extinction, the diversity of the shallow-water trilobite assemblage gradually increased, only again to be affected by another mass extinction exhibiting the same ecological patterns as the previous (Stitt, 1971; Palmer, 1984). This stratigraphic pattern of extinction and diversification in the late Cambrian trilobite communities has been referred to as a "biomere", which is a biostratigraphic unit whose boundaries are defined by the extinction events (Palmer, 1984). For a more thorough review of the stages, zonations, and the history of the biomere concept, refer to Taylor et al. (2012). In addition to its recognition on Laurentia, this extinction interval has subsequently been shown to be of global significance with the identification of correlative extinctions in other sedimentary basins from other distinct paleocontinents (Figures 1, 2) (Opik, 1963; Peng et al., 2004a).

The mechanism for the extinction of shelf communities at the Marjuman-Steptoean boundary is still the subject of ongoing debate. The mechanisms that were originally proposed were based solely on the paleontological and sedimentological data. These include drastic temperature changes (Opik, 1966; Lochman-Balk, 1970), a combination of climatic cooling and a rise in the thermocline, which acted to cool the shelf areas (Stitt 1975; Taylor 1977), and/or an ocean transgression which led to a lateral shift in facies and overrode inner shelf facies (Ludvigsen, 1982; Palmer, 1984; Westrop

and Ludvigsen, 1987). However, there appears to be no coherent continent-wide pattern of sedimentary changes associated with the biomere boundary (Palmer, 1984).

Geochemical studies have also been utilized to infer the cause of the extinction. Orth et al. (1984) searched for an iridium anomaly at the boundary for evidence of an impact (similar to that used by Alvarez et al. (1980) to demonstrate an extraterrestrial impact was associated with the K-Pg boundary), but they did not find one. More recent geochemical studies led to the recognition of the SPICE and made a case for widespread anoxia (Saltzman et al., 1998) and euxinia (Gill et al., 2011), however the timing and driver for these environmental changes are still not clear. Additionally, data from Perfetta et al (1999) support a rise in the thermocline and they suggested that the short-lived -1‰ shift in $\delta^{13}C$ across the extinction horizon was attributed to ^{12}C-enriched cold, deep waters invading the shelf, driven by changes in ocean circulation.

However, the majority of these studies examined sections where the extinction interval is relatively condensed. Investigating the details of the carbon isotope record in the southern Appalachians, where there is an expanded section of critical zone (*Coosella perplexa* Subzone), will help assess the timing of environmental drivers that potentially caused the extinction.

1.2 Carbon isotopes as a paleoproxy

Stratigraphic changes in the carbon isotope composition ($\delta^{13}C$ defined in methods section) of marine carbonates can be used to track the carbon isotope composition of the ocean water in which they precipitated (Scholle and Arthur, 1980; Saltzman et al., 1998; Ripperdan, 2001). Carbon isotope fractionations (changes in the ratio of the stable isotopes caused by slight differences in masses and therefore energies) between its two stable isotopes, ^{12}C and ^{13}C, occur during a wide range of environmental processes such as evaporation, condensation, photosynthesis, organic metabolisms, and mineral precipitation (Marshall, 1992). However, the carbon isotope fractionation

between dissolved inorganic carbon (DIC) and carbonate minerals is relatively small and not significantly sensitive to changes in temperature, leaving the $\delta^{13}C$ of ancient marine carbonates a robust proxy to reconstruct the isotope composition of DIC in ancient ocean waters (Scholle and Arthur, 1980). Additionally, early, low temperature diagenesis appears to average the isotopic composition of carbonate sediments that were originally heterogeneous (Brazier et al., 1993).

Previous studies suggested that over the last 3.5 billion years the $\delta^{13}C$ value of ancient oceans has remained within ±3‰ from the Pee Dee Belemnite standard (PDB) (Veizer and Hoefs, 1976; Schidlowski et al., 1983; Ripperdan, 2001). Large deviations from the PDB (now replaced by Vienna Pee Dee Belemnite or VPDB) standard represent perturbations to the carbon cycle (residence time of carbon in the ocean is ~100 kiloyears (kyrs)) that left the ocean reservoir enriched in ^{12}C or ^{13}C (Ripperdan, 2001). Several of these perturbations have been correlated with major events in the geologic record, in particular mass extinctions (Ripperdan, 2001). Positive carbon isotope excursions reflect a relative enrichment of the ocean reservoir in ^{13}C (or depletion of ^{12}C) and can be interpreted as the result of one or a combination of the following factors: (1) an increase in organic productivity, and/or an associated increase in the fraction of carbon buried as organic matter; (2) increased sedimentation rates within oceans with associated increases in burial rate of organic matter; and (3) enhanced preservation of organic material caused by an expanded oxygen-minimum zone or marine anoxia (Brasier et al. 1994; Glumac and Walker, 1998; Kump and Arthur 1999; among others). Negative carbon isotope excursions represent a relative enrichment in ^{12}C in the ocean reservoir and are normally interpreted as the result of one or a combination of the following factors: (1) a decrease in bioproductivity; (2) increased oxidation of organic carbon (3) an associated increase in the percent of organic-rich rocks exposed to weathering; and/or (4) an increase in volcanic activity (Kump 1991; Ripperdan, 2001). Considering that a variety of factors can be involved in perturbing the carbon cycle, only so much can be inferred solely from carbon isotope records throughout the geologic record. Therefore, it is best to couple $\delta^{13}C$ data with other data. Of particular utility is the complementary analysis of redox-sensitive elements/isotopes.

2. The Nolichucky Formation

In the study area the extinction interval is contained with the lithostratigraphic unit of the Nolichucky Fm., which is part of the Conasauga Group. The Nolichucky Fm. (sometimes referred to as the Nolichucky Shale or Conasauga Shale) consists of a 0-300 meter thick succession of peritidal and subtidal carbonates and shales (Markello and Read, 1981). It is exposed in multiple strike belts within the fold and thrust belt of the Valley and Ridge Province of the Appalachian Mountains in eastern North America (Palmer 1971; Markello and Read 1981; Markello and Read, 1982; Hasson and Haase, 1988; Read and Repetski, 2012). This study examines five outcrops in the region of northeastern Tennessee to southwestern Virginia (Figure 3a).

2.1 Basin development

Deposition on the passive margin of Laurentia initiated post-Neoproterozoic rifting (Srinivasan and Walker, 1993; Read and Eriksson, 2012), which resulted in a number of salients and recesses (Aleinikoff et al., 1995; Thomas 2006, Read and Eriksson, 2012). This resulted in two large depocenters separated by the Virginia promontory: the Conasauga (centered in Tennessee) and the Pennsylvania (centered in northern Virginia to south-central Pennsylvania) (Colton, 1970; Thomas 1977; Read 1989a, b; Read and Eriksson, 2012). A phase of renewed rifting during the Middle Cambrian led to the development of the Rome Trough and coincident subsidence that formed the southern Appalachian Conasauga intrashelf basin (Hasson and Hasse, 1988).

Isopach maps suggest this intrashelf basin was elliptical in shape (Hasson and Hasse, 1988) and this would become the depocenter for the Nolichucky Fm. (Figure 3b). Read and Repetski (2012) reported that inferred subsidence rates were 7cm/k.y. (higher if compaction is considered), typical of a passive margin. The Conasauga intrashelf basin was bounded to the west by the Laurentian craton and by a rimmed carbonate platform

(Elbrook Formation) to the south and east (Figure 3b, c) (Markello and Read, 1981; Hasson and Hasse, 1988). The Rome Trough, located in what is now eastern central Kentucky, formed the northern boundary (Weber 1988). Siliciclastic input to the basin sourced from the exposed craton via a large delta system to the northwest of the basin (now in the subsurface of present day Ohio) that is represented by the Kerbel Fm. (Janssens, 1973). Carbonate sedimentation was restricted to the carbonate platform margin, which prograded from the east into the basin. The Conasauga sequence is characterized by three distinct phases of deposition during the middle and late Cambrian (Rodgers, 1953): a succession of carbonate lithologies to the east and southeast, a western and northwestern succession dominated by shale, and a central succession of interbedded carbonate and shale formations (Srinivasan and Walker, 1993). Therefore, the Nolichucky Fm. represents a mixed siliciclastic-carbonate ramp system.

2.2 Sequences within the Nolichucky Fm.

The Conasauga Group was deposited during the middle to early late Cambrian, an interval of relatively warm climate (Read and Repetski, 2012). The development of the Nolichucky Fm. lies within the second-order Sauk II (or C-3 in Read and Repetski, 2012; Eriksson and Read, 2013) depositional supersequence (5-30 m.y.) (Figure 3). Five third-order sequences (0.5-5 m.y.) are recognized within the Nolichucky Fm., where platform carbonates represented by the Maryville Limestone, Bradley Creek Members and Maynardville Limestone interfinger with the basinal shale facies represented by Lower and Upper Shale Members (Markello and Read, 1982; Hasson and Haase, 1988; Read and Repetski, 2012). This interfingering was limited to the slope margins of the intrashelf basin. Finally, small-scale shallowing-upward cycles (parasequences) attributed to higher frequency (10-100 k.y.) sea level fluctuations are observed on 1-10 meter scale. The stratigraphic distribution of interbedded shale and flat-pebble conglomerate beds shows weak cyclicity, but may be better attributed to storm-dominated shoreface deposits (Markello and Read, 1982; Myrow et al., 2004).

2.3 Biostratigraphy of the Nolichucky Fm.

The biostratigraphy of the Nolichucky Fm. is unique, as its upper shale member represents an expanded section of the end-Marjuman extinction. The Bradley Creek Member and Upper Shale contain the two trilobite zones and one subzone of interest for this study: in stratigraphic order, the *Crepicephalus* Zone, *Coosella perplexa* subzone, and the *Aphelaspis* Zone. Unfortunately, as Rasetti (1965) pointed out, fossiliferous horizons within the Nolichucky occur irregularly, which can make it difficult to correlate from section to section. Nonetheless, the presence of the critical interval (trilobite Subzone *Coosella perplexa* defined in the section above) allows for a higher resolution investigation of facies changes and carbon cycle changes across the extinction horizon (Derby, 1965; Rasetti, 1965; Cuggy, 1996).

3. Methods

3.1 Field work

Field locations were initially chosen using available biostratigraphic records that had identified the extinction interval (Derby, 1965; Rasetti, 1965; Cuggy, 1996). Ultimately, five outcrop locations ranging from southwestern Virginia and northern Tennessee (Figure 3a) were studied based on the quality and accessibility of each exposure. Fieldwork was carried out in autumn of 2012 and 2013 and the spring of 2013 and 2014. Two of these locations are in northeastern Tennessee and three are in southwestern Virginia. Each section was measured and logged using the following protocol: (1) lithofacies descriptions were performed at the decimeter scale, (2) facies representing depositional trends and unique features (sedimentary structures, grain types, ichnofossils, fossil, etc.) were also noted, (3) a modified Dunham classification scheme (Folk, 1959; Dunham, 1962) was employed to describe carbonate samples, and (4) carbonates were collected at one meter intervals, unless the quality of the outcrop or type

of lithology was not suitable for geochemical analysis. The lack of biostratigraphic control at the Lebanon section resulted in incomplete sampling; there is no geochemical data for the first 26 meters.

3.2 Sample preparation

A rock saw with a diamond tipped blade was used to remove weathered surfaces, as a fresh surface is required for proper geochemical analysis. A handheld Dremel tool was used to produce a powder while targeting carbonate mud lithologies (Kaufman et al., 1991) for $\delta^{13}C$ and elemental analysis (Marshall, 1992). In cases where mud lithologies were not present, fine-grained lithologies proved to be sufficient. Diagenetic assessment took place after the initial $\delta^{13}C$ analysis.

3.3 Petrographic analysis

Twenty-seven samples of representative of five lithologies (mudstone, trilobite packstone/grainstone, thrombolite, oolite, and flat pebble conglomerate) were selected for petrographic thin section. The thin sections were examined for petrographic characterization and diagenetic fabrics. Diagenetic alteration can be physically expressed by recrystallization/cementation (calcite spar or microspar), micritization (the transformation of carbonate grains into fine-grained calcite generally removing all internal structure), and/or the presence of dolomite. Alizarin red staining was used to verify the distribution of calcite versus dolomite within samples. Dolomite, calcite veins, stylolites, and glauconite-rich areas were generally avoided when sampling for $\delta^{13}C$ and elemental composition of the carbonate minerals.

3.4 Geochemical analyses

3.4a Carbonate carbon and oxygen isotope analysis

Roughly 0.350 milligrams of carbonate powder from each sample was reacted with 100% ortho-phosphoric acid at 70°C for 4-8 hours. Carbon and oxygen isotope data were obtained by measuring the CO_2 gas evolved upon acidification of the sample. Samples were measured on an Isoprime 100 isotope-ratio mass spectrometer (IRMS) coupled with a peripheral MultiFlow-Geo headspace sampler in the Stable Isotope Facility in the Department of Geosciences at Virginia Polytechnic Institute and State University. Carbon and oxygen isotope compositions are reported in standard delta notation as per mil (‰) deviations from Vienna Pee Dee Belemnite (VPDB):

$$\delta^{13}C = \left[\frac{\left(\frac{^{13}C}{^{12}C}_{sample} - \frac{^{13}C}{^{12}C}_{Standard} \right)}{\frac{^{13}C}{^{12}C}_{Standard}} \right] \times 1000$$

Eighty percent of samples were replicated at least once and were equal to or better than 0.1‰ for $\delta^{13}C$ ±0.1‰ (1σ), and ±0.3‰ for $\delta^{18}O$ ±0.2‰ (1σ). Repeated measurements of the IAEA-CO-1, CO-9 and NBS-18 standards were ±0.04‰ for $\delta^{13}C$, and ±0.18‰ for $\delta^{18}O$ ±0.2‰ (1σ).

3.4b Elemental analysis

Elemental analysis of calcium (Ca), magnesium (Mg), manganese (Mn), iron (Fe), strontium (Sr), and aluminum (Al) in the carbonate portion of the sample were carried out on an inductively coupled plasma atomic emission spectrometer (ICP-AES) housed in the Crop & Soil Environmental Sciences Department at Virginia Polytechnic Institute and State University. For this procedure, 100 - 300 milligrams of powder was dissolved in trace metal grade acetic acid (a weak acid was used to target the carbonate fraction of the sample to avoid the breakdown of pyrite or secondary lithologies). The samples were

then centrifuged, decanted, and finally diluted to a 4% acetic acid dilution before analysis. ICP-AES detection limits for Al, Fe, Mn, Sr, Mg, and Ca are 0.006 ppm, 0.003 ppm, 0.0003 ppm, 0.0002 ppm, 0.028 ppm, and 0.016 ppm respectively. The reproducibility of the data set is 7% or better.

4. Results

4.1 Lithofacies descriptions

The five stratigraphic sections measured are characterized by seven lithofacies in the context mixed siliciclastic-carbonate ramp expressed in Table 1. Refer to the diagram in Figure 4 to illustrate the environmental interpretations from Table 1.

Table 1. Lithofacies Descriptions		
Facies	**Description**	**Environmental interpretation**
Grey shale	Predominantly deeply weathered fissile shale. Grey in color. Occurrences of trace fossils (horizontal burrows) often observed in float.	Distal intrashelf basin – below storm wave base
Green shale	Predominantly shale weathered into mud chips. Green in color.	Distal intrashelf basin – below storm wave base
Interbedded shale/limestone	Dominated by calcareous grey shale with occurrences of thin (2-5cm) discontinuous beds of peloidal carbonate mudstone. Less common are beds of trilobite wackestone, intraclast/trilobite packstone, and trilobite grainstone.	Carbonate ramp margin
Limestone: a general facies for carbonate lithologies	Carbonate mudstone Trilobite wackestone, packstone, grainstone	Subtidal carbonate ramp – little to no tidal influence.
Flat pebble conglomerate	Intraclast (flat pebble conglomerate) packstone.	Storm deposits
Ribbon Rock	An interbedded carbonate mudstone and shale unit that is predominately 5-10cm thick beds of carbonate mud, broken up by thin (2-5 cm) grey shale beds.	Deep carbonate ramp
Dolostone	A limestone facies that has been predominantly dolomitized (replaced with dolomite). It is often recognized as single (<1m thick) beds, except at the top of the Washburn Section where it is more prevalent.	Post-depositional alteration of original lithologies
Thrombolite	Clotted microbial textures	Microbial mound/ patch reefs on the carbonate ramp
Oolite	Well-sorted ooid grainstone often associated with thrombolitic, and less common stromatolitic textures. Ooids are generally 2 mm in diameter and many appear to be dolomitized.	Shallow subtidal carbonate-ramp

Symbols (Figure 6a) are added to the stratigraphic columns to indicate clast composition (flat-pebble conglomerates, trilobite fragments, etc.), the presence of accessory minerals (e.g. glauconite), and the presence of larger scale sedimentary features/structures (sedimentary dikes, thrombolitic textures/mounds, etc.). Flat pebble conglomerate occasionally cap small-scale shale to mudstone potentially representing shoaling cycles. Each cycle begins with 0-1 meter of shale to interbedded shale/limestone facies, followed by 0.2 to 2 meter carbonate mudstone and/or interbedded limestone/shale facies. The Three Springs and Dickensonville sections preserve these shale-mudstone-conglomerate cycles best. For detailed stratigraphic columns, sample locations and descriptions refer to Appendices A and B.

4.2 Petrographic assessment of diagenesis

Of the twenty-seven samples that were analyzed, eight are displayed in Figure 5 since they represent the most common fabrics. Three samples W-24, T-11, and D-10 illustrate ideal lithologies for $\delta^{13}C$ sampling: carbonate muds with low porosity, which inhibited post-depositional fluid flow. Generally, pure mudstones and/or flat pebble mud clasts show coherent trends in and reproducibility of $\delta^{13}C$ values. Samples W-44, T-25, T-40, Du-27, and D-36 illustrate lithologies that are more likely to display altered primary $\delta^{13}C$ signals (Figure 5). Carbonate mud can be prone to dissolution and reprecipitation as microspar (a common diagenetic fabric usually 4-30 micrometers in diameter) through a process called sparitization. Samples with extensive sparitization or unavoidable calcite veins often had $\delta^{13}C$ values negatively skewed from the rest of the population of the data. The majority of the samples with larger clasts (packstones and grainstones) also showed signs of sparitization and the addition of diagenetic cements.

4.3 Geochemical patterns

Carbon isotope values are presented in Figure 6 with corresponding lithologic sections. Isotope values of both carbon and oxygen are displayed in Appendix B with corresponding trace metal concentrations. Contact with meteoric waters can alter the primary isotopic and elemental chemistry of rocks (Lohmann, 1988). Geochemical trends such as, the meteoric calcite line (Lohmann, 1988) and trace metal concentrations are useful tools in assessing the extent of diagenetic alteration a rock has undergone. It is common that $\delta^{18}O$ values become more negative with alteration of meteoric waters (Brand and Veizer, 1981; Lohmann, 1988). Additionally, depletions in Sr concentrations and/or the enrichment of Fe, Mn, and Mg are common elemental changes equilibrated with increasing diagenetic alteration (Brand and Veizer, 1980; Lohmann, 1988). Samples with $\delta^{13}C$ values in each section were omitted if their $\delta^{18}O$ versus $\delta^{13}C$ plotted outside of the main population and showed elemental diagenetic trends (e.g. Sr/Ca ratios much lower than the mean value of the main sample population in its corresponding section)(Figure 7). Samples with high Fe, and Mg values were also considered to be compromised.

4.3a Washburn section

Within the basal 14 meters of section, which contains *Crepicephalus* and *Coosella perplexa* biozones, $\delta^{13}C$ values remain tightly grouped between -0.5‰ and +1‰ (Figure 5b). $\delta^{13}C$ values steadily increase to roughly +4‰ in the overlying 30 meters of section directly after the extinction boundary at the base of the *Aphelaspis* Zone (Figure 6b). $\delta^{18}O$ values in this section range from -6.7‰ to -8.3‰, with one outlier W-1 having a value of -9.4‰ (Figure 7a).

4.3b Three Springs section

The $\delta^{13}C$ values remain tightly grouped within -0.5‰ and +1‰ within the lowermost 23 meters of this section, which contain the pre-extinction *Crepicephalus* and *Coosella perplexa* biozones (Figure 6c). $\delta^{13}C$ values are variable but overall show an increase to roughly +3‰ over the 19 meters of section above the extinction boundary at

the base of the *Aphelaspis* Zone. Generally, these rocks were highly weathered and petrographic analysis confirms extensive sparitization of rocks with lower than expected $\delta^{13}C$ values. The $\delta^{18}O$ values in this section range -7.6‰ to -11.11‰, which constitutes the low range of the five sections (Figure 7b).

4.3c Duffield section

The basal 8 meters of this section contains the *Coosella perplexa* biozone (Figure 6d). The *Crepicephalus* biozone is not present in this section (Derby, 1965; Cuggy, 1996). $\delta^{13}C$ values remain tightly grouped between -0.1‰ and +1.1‰ in the *Coosella perplexa* Subzone, but steadily begin to rise from +1‰ to +3.5‰ over the overlying 26 meters of section at the *Aphelaspis* Zone. $\delta^{18}O$ values in this section vary between -6.6‰ to -10.8‰ (Figure 6c).

4.3d Dickensonville section

The *Crepicephalus* Zone lies within the 22 meters of section before transitioning into the *Coosella perplexa* Subzone. Roughly 4 meters of biostratigraphic data is missing between the *Coosella perplexa* Subzone and *Aphelaspis* Zone, which could potentially drop the end-Marjuman extinction boundary to the 41-meter mark, instead of its current position at the 45-meter mark. $\delta^{13}C$ values remain tightly grouped within -0.5‰ and +1.1‰ within the 47 meters of section (Figure 6e). The 12 meters of section lack carbon isotope data due to a covered interval as well as a heavily-weathered shale interval. There is a sudden shift in $\delta^{13}C$ values to +2.5‰ at the 60-meter mark and steadily increases to +3.8‰ in the last 9 meters of section. This section has the highest resolution pre-extinction history due to this outcrop's exquisite quality. $\delta^{18}O$ values range from -6.4‰ to -9.7‰, with sample D-48 having outlier value of -12.5‰ (Figure 7d).

4.3e Lebanon section

Carbon isotope data are limited to the upper 22 meters of this section because; there is no biostratigraphic control (Figure 6f). $\delta^{13}C$ values begin at 1‰ and gradually

shift to 2‰ beneath a covered interval. Values above the covered interval are tightly grouped within 3‰ and 4‰. $\delta^{18}O$ -5.8‰ to -8.6‰ (Figure 7e).

5. Discussion

The spread of strongly negative $\delta^{18}O$ values suggests post-depositional alteration of the oxygen isotope composition of carbonates during burial, which is typical of ancient carbonates. The negative oxygen isotope values at the Three Springs section suggest that the most significant alteration occurred at this outcrop (Figure 7). In any case, it broadly appears that the $\delta^{13}C_{carbonate}$ values maintained their original isotopic signature. Trace metal analysis and petrographic analysis of samples that displayed anomalous values — negative carbon isotope values which deviated from main population data trends — suggest that these samples had undergone significant diagenetic overprinting and therefore are not likely representative of the primary, local seawater chemistry. However, sparitization or micritization, which is observed in many of the samples, do not appear to have altered the $\delta^{13}C$ values. Original $\delta^{13}C$ values are commonly buffered during carbonate diagenesis when the chemistry of the later fluid is dominated by the original carbonate chemistry of rock (i.e. the same inorganic carbon is liberated from the rock during the dissolution of the carbonate minerals and then is precipitated as new carbonate minerals during diagenesis) (Brand and Veizer, 1981; Lohman, 1988). This appears to be the case with most of the samples from Nolichucky Formation.

The $\delta^{13}C$ values that have no obvious signs of significant diagenetic alteration, as assessed with petrological or geochemical data ($\delta^{18}O$ and trace metals), are considered to represent the ancient seawater chemistry in which the carbonates precipitated. In each section, $\delta^{13}C$ data show no significant changes in the negative or positive direction throughout the *Crepicephalus* Zone (Figure 6, 8). Additionally, the *Coosella perplexa* Subzone is also characterized by little variation in $\delta^{13}C$ values in each stratigraphic section. It is only at the base of the *Aphelaspis* Zone that $\delta^{13}C$ values begin to gradually shift in the

positive direction in each section. Generally, the $\delta^{13}C$ values gradually reach +3 to +4‰ over a few 10s of meters: this positive shift represents the rising limb and the peak of the Steptoean Positive Carbon Isotope Excursion (SPICE). The *Aphelaspis* Zone is characterized by the invasion of the interpreted low-oxygen tolerant Olenimorph trilobites onto the shelf areas. Therefore, this data set confirms that the initiation of the SPICE was in fact concurrent with the invasion of the Olenimorph fauna and potentially both these event were driven by the same mechanism (e.g. the spread of dysoxia/anoxia), similar to that observed from previous studies (e.g. Wignall and Twitchett, 1996). A caveat to this relationship is that the end-Marjuman extinction occurred in two phases, the first of which is not concurrent with a carbon isotope excursion. The absence of a perturbation in $\delta^{13}C$ values during the first extinction in shallow water fauna at the *Crepicephalus* and *Coosella perplexa* transition is an intriguing scenario.

It is possible that a perturbation to the carbon cycle at the first extinction occurs at timescales less than the residence time of carbon (~100 kyrs in the modern oceanic setting), which would result in a delayed $\delta^{13}C$ signal. Thus, an estimate of the minimum and maximum time recorded in the *Coosella perplexa* subzone is useful to test this hypothesis. The Washburn section and Dickensonville section serve as the minimum (5 meters) and maximum (24 meters) end members of the *Coosella perplexa* Subzone, respectively. It appears that the *Coosella perplexa* Subzone represents anywhere from 83 ky and 166 ky at the Washburn section and 400 kyrs to 800 kyrs at the Dickensonville section. Time estimations are based on ~6 cm/kyrs depositional rate derived from the Gradstein et al. (2012) timescale (compaction not considered) and ~3 cm/kyrs depositional rates reported from sedimentary successions in the southern Appalachians (Osleger and Read, 1993). The time estimates in Washburn fit the model for a delayed response, but the time recorded at Dickensonville would suggest a perturbation would be recorded. Although not definitive, it is within the realm of possibility that there is a delay in the carbon isotope record relative to the actual perturbation.

The Nolichucky Fm. shows no evidence for a short-lived negative 1‰ shift prior to the onset of the SPICE, as observed in the dataset from the Deadwood Fm. in South

Dakota (Perfetta et al., 1999). The Three Springs section (Figure 5c) does have a single data point that would represent a -1‰ $\delta^{13}C$ shift directly after the end-Marjuman extinction. However, petrographic analysis of that sample (T-25) has revealed that it has undergone pervasive sparitization (Figure 5f). Given this information, the fact the shift is constrained by a single data point and that none of the other sections display a similar trend, this sample has likely been altered and its $\delta^{13}C$ value is most likely not primary.

The lack of a coherent negative $\delta^{13}C$ trend in the Nolichucky data suggests that the negative carbon isotope excursion observed in the Black Hills was not a global trend. One potential explanation for the Black Hills data involves the fact that the negative carbon isotope values occur directly below an unconformity. This suggests that meteoric fluids may have altered the original carbonate chemistry during erosion and exposure of the section. Alternatively, if the negative $\delta^{13}C$ shift truly records a primary signal, it would represent a localized event given the lack of evidence for it in the Nolichucky Fm. and other sedimentary basins.

The two-phase nature of the end-Marjuman extinction is often thought to have been associated with sea level change (Ludvigsen, 1982; Palmer, 1984; Westrop and Ludvigsen, 1987). However, there is no uniform pattern of sedimentary changes associated with the end-Marjuman extinction on a continent-wide scale (Palmer, 1984). It is observed that the base of the *Coosella perplexa* Subzone coincides with a change from shallow-water carbonate facies to deeper water shale/carbonate facies, but this observation is limited to only the Dickensonville section. The *Aphelaspis* Zone also displays a similar shallow- to deep-water facies pattern, but this can only be correlated across the Washburn and Three Springs sections. Furthermore, the presence of microbial mounds — thought to be indicative of shallow-water settings (Myrow et al., 2004) — both below and soon after the extinction horizon, suggests that there is no clear relationship between the extinction horizon and sea level locally in the Conasauga Basin. Therefore, it would be premature to draw further conclusions about the association between the extinction and local sea level in this study.

Carbon isotopes alone are not sufficient to pinpoint the driver of the end-Marjuman extinction. However, Gill et al. (2011) used geochemical data from several sedimentary basins worldwide to investigate the global redox conditions during the SPICE interval. Those data suggested that widespread euxinic conditions spread at the initiation of the SPICE (Gill et al., 2011). This scenario is consistent with the carbon isotope and paleontological patterns observed in the Conasauga Basin: the SPICE initiates at the final extinction and the invasion of the olenimorph fauna. The application of sulfur isotope data and additional redox-sensitive paleoproxies (e.g. iodine and manganese concentrations) to the Nolichucky Fm. sections would further help to delineate the relationship between changes in redox state of the ocean and the end-Marjuman extinction.

6. Conclusion

This study is the first high-resolution study of the stratigraphic relationship between the end-Marjuman extinction, sea level and carbon cycle changes. This study confirms that the onset of the SPICE coincided with the end-Marjuman extinction boundary within the Conasauga Basin of the Southern Appalachians. It also reveals that there is no negative shift in $\delta^{13}C$ values at the onset of the SPICE, as seen in the Black Hills stratigraphic section. This suggests that the $\delta^{13}C$ shifts in the Black Hills are either the product of diagenesis or an environmental signal local to the Black Hills. The end-Marjuman extinction is independent of major facies shift in the Conasauga Basin, throwing into doubt the purported relationship between sea level rise and the extinction event. Although, a larger basin wide analysis that includes proximal and distal regions of the basin is required to truly test the role that sea level may have played. This study does not shed new light on the driving mechanism for the extinction; however, it provides higher resolution insights into the sequence of events. Based on relationships between the SPICE and geochemical patterns observed elsewhere, anoxia and/or euxinia are likely candidates as the extinction driver. The application of redox-sensitive proxies to

the sections from the Conasauga Basin will ultimately test the relationship between changes in redox state of the ocean and the end-Marjuman extinction.

References

Aleinikoff, J. N., Zartman, R. E., Walter, M., Rankin, D. W., Lyttle, P. T., and Burton, W. C., 1995. U-Pb ages of metarhyolites of the Catoctin and Mount Rogers formations, central and southern Appalachians: evidence for two pulses of Iapetan rifting: American Journal of Science 295, 428-454.

Alvarez, L.W., Alvarez, W., Asaro, F., Michel, H.V., 1980. Extraterrestrial Cause for the Cretaceous-Tertiary Extinction. Science, New Series 208 (4448), 1095-1108.

Brand, U., Veizer, J., 1980. Chemical Diagenesis of Multicomponent Cabonate System-1: Trace Elements. Sedimentary Petrology 50(4), 1219-1236.

Brand, U., Veizer, J., 1981. Chemical Diagenesis of Multicomponent Cabonate System-2: Stable Isotopes. Sedimentary Petrology 51(3), 987-997.

Brasier, M.D., 1993. Towards a carbon isotope stratigraphy of the Cambrian system: Potential of the Great Basin succession, *in* Hailwood, E.A., and Kidd, R.B., eds., High resolution stratigraphy: The Geological Society of London Special Publication 70, 341–350.

Colton, G. W., 1970. The Appalachian Basin – Its depositional sequences and their geologic relationships, in Fisher, G. W., Pettijohn, F .J., and Reed, J. C., Jr., eds., Studies of Appalachian Geology: Central and Southern: New York, Interscience Publishers, 5-47.

Cuggy, M. B., 1996. Patterns of Faunal Change at an Upper Cambrian trilobite extinction event, Nolichucky Formation Tennessee and Virginia. Masters Thesis, Brock University.

Derby, J. R., 1965, Paleontology and stratigraphy of the Nolichucky Formation in southwest Virginia and northeast Tennessee: PhD thesis, Virginia Polytechnic Institute, and State University.

Elrick, M. B., Rieboldt, S., Saltzman, M. R., & Mckay, R. M., 2011. Oxygen-isotope trends and seawater temperature changes across the Late Cambrian Steptoean positive carbon-isotope excursion (SPICE event). Geology 39(10), 987–990. doi:10.1130/G32109.1

Foreman, J.L., Walker, K.R., Weber, L.J., and Dreier, R.B., 1991, Slope and basinal carbonate deposition in the Nolichucky Shale (upper Cambrian), east Tennessee: Effect of carbonate suppression by siliciclastic deposition on basin-margin morphology, in Lomando, A.J., and Harris, P.M., eds., Mixed Carbonate–Siliciclastic Sequences: SEPM Core Workshop No. 15, SEPM (Society for Sedimentary Geology), 511–539.

Fortey, R.A., 1985. Pelagic trilobites as an example of deducing the life habits of extinct arthropods. Earth Sciences 76 (2-3), 219-230.

Gill, B. C., Lyons, T. W., Young, S. A., Kump, L. R., Knoll, A. H., & Saltzman, M. R., 2011. Geochemical evidence for widespread euxinia in the Later Cambrian ocean. Nature 469(7328), 80–83. doi:10.1038/nature09700

Glumac, B., 2011. High-resolution stratigraphy and correlation of Cambrian strata using carbon isotopes: an example from the southern Appalachians, USA. Carbonates and Evaporites 26(3), 287–297. doi:10.1007/s13146-011-0065-2

Glumac, B., & Walker, K., 1998. A Late Cambrian positive carbon-isotope excursion in the Southern Appalachians; relation to biostratigraphy, sequence stratigraphy, environments of deposition, and diagenesis. Journal of Sedimentary Research 68(6), 1212–1222.

Glumac, B., Walker, K. R., 2000. Carbonate deposition and sequence stratigraphy of the terminal Cambrian Grand Cycle the southern Appalachians, U.S.A. Journal of Sedimentary Research 70(4), 952–963.

Hasson, K. O., Haase, C. S., 1988. Lithofacies and paleogeography of the Conasauga Group, (Middle and Late Cambrian) in the Valley and Ridge province of east Tennessee. Geological Society of America Bulletin 100, 234–246.

Helton, W.L., 1967. Lithostratigraphy of Conasauga Group Between Rogersville and Kingsport, Tennessee PhD diss., University of Tennessee.

Honisch, B., Ridgewell, A., Schmidt, D.N., Thomas, E., Gibbs, S.J, Sluijs, A., Zeebe, R., Kump, L., et al., 2012. The Geologic Record of Ocean Acidification. Science 2 335(6072), 1058-1063.

Janssens, A., 1973. Stratigraphy of Cambrian and Lower Ordovician rocks in Ohio: Ohio Division of Geological Survey Bulletin 64, 197

Kaufman, A. J., Hayes, J. M., Knoll, A. H., Germs, G. J. B., 1991. Isotopic compositions of carbonates and organic carbon from upper Proterozoic successions in Namibia: stratigraphic variation and the effects of diagenesis and metamorphism. Precambrian Research 49, 301–327.

Kump, L. R., 1991. Interpreting carbon-isotope excursions; Strangelove oceans. Geology 19, 299–302.

Kump, L.R., Arthur, M.A., 1999. Interpreting carbon-isotope excursions: carbonates and organic matter. Chemical Geology 161 (1-3), 181-198.

Lohman, K.C., 1988. Geochemical Patterns of Meteroric Diagenetic Systems and Their Application to Studies of Paleokarst. Springer New York, 58-80.

Lochman-Balk, C., 1970. Upper Cambrian Faunal Patterns on the Craton. Geological Society of America Bulletin 81 (11), 3197-3224

Lochman-Balk, C., Wilson, J. L., 1958. Cambrian biostratigraphy in North America: Journal of Paleontology 32, 312–350.

Longacre, S. A., 1970. Trilobites of the Upper Cambrian Ptychaspid biomere, Wilberns Formation, central Texas: Paleontological Society Memoir 4, Journal of Paleontology 44 supp., 70.

Ludvigsen, R., 1982. Upper Cambrian and Lower Ordovician trilobite biostratigraphy of the Rabbitkettle Formation, western District of Mackenzie: Royal Ontario Museum Life Sciences Contributions 134, 187.

Markello, J. R., 1979. Carbonate ramp to deeper shale-shelf transi- tions of an Upper Cambrian (Dresbachian) shelf embayment, Nolichucky Formation, southwest Virginia: Master's thesis, Virginia Polytech. Inst, and State University, 162.

Markello, J. R., Read, J. F., 1981. Carbonate ramp-to-deeper shale shelf transitions of an Upper Cambrian intrashelf basin, Nolichucky Formation, Southwest Virginia Appalachians. Sedimentology 28, 573–597.

Markello, J. R., Read, J. F., 1982. Upper Cambrian Intrashelf Basin, Nolichucky Formation, Southwest Virginia Appalachians. AAPG Bulletin 66(7), 860–878.

Marshall, J.D., 1992. Climatic and oceanographic isotopic signals from the carbonate rock record and their preservation. Geological Magazine 129, 143-160.

Miller, J.F., 1988. Conodonts as biostratigraphic tools for redefinition and correlation of the Cambrian-Ordovician Boundary. Geological Magazine 125, 349-362.

Myrow P.M., Tice, P., Archuleta, B., Clark, B., Taylor, J.F., Ripperdan, R.L., 2004. Flat-pebble conglomerate: its multiple origins and relationship to metre-scale depositional cycles. Sedimentology 51, 973-996.

Osleger, D., Read, J.F., 1993. Comparative analysis of methods used to define eustatic variation in outcrop: Late Cambrian interbasinal sequence development. American Journal of Sceince 293, 157-216.

Opik, A.A., 1963. Early Upper Cambrian fossils from Queensland. Bureau of Mineral Resources of Australia Bulletin 64, 1-133.

Opik,A.A., 1966. The early Upper Cambrian crisis and its correlation. Royal Society of New South Wales Journal and Proceedings 100, 9–14.

Orth, C., Knight, J., Quintana, L., Gilmore, J., & Palmer, A. R., 1984. A search for iridium abundance anomalies at two late Cambrian biomere boundaries in Western Utah. Science, 163–165.

Palmer, A. R., 1965a. Trilobites of the Late Cambrian Pterocephaliid biomere in the Great Basin, United States: U.S. Geological Survey Professional Paper 493, 105.

Palmer, A. R., 1979. Biomere boundaries re-examined. Alcheringa: an Australasian J. of Palaeontology 3(1), 33–41. doi:10.1080/03115517908565438

Palmer, A. R., 1984. The Biomere Problem: Evolution of an Idea. Journal of Paleontology 58(3), 599–611.

Peng, S.C., Babcock, L.E., Robison, R.A., Lin, H.L., Ress, M.N., Saltzman, M.R., 2004a. Global Standard Stratotype-section and Point (GSSP) of the Furongian Series and Paibian Stage (Cambrian). Lethaia 37, 365-379.

Perfetta, P. J., Shelton, K. L., & Stitt, J., 1999. Carbon isotope evidence for deep-water invasion at the Marjumiid-Pterocephaliid biomere boundary, Black Hills, USA: A common origin for biotic crises on Late Cambrian shelves. Geology 27(5), 403–406.

Rasetti, F., 1965. Upper Cambrian trilobite faunas of northeastern Tennessee. Smithsonian Miscellaneous Collections 148, 127.

Read, J.F., Eriksson, K.A., 2012. Chapter 3: Paleozoic Sedimentary Successions of the Virginia Valley and Ridge and Plateau. In prep.

Read, J.F., Repetski, J.E., 2012. Cambrian – lower Middle Ordovician passive carbonate margin, southern Appalachians, in J. R. Derby, R. D. Fritz, S. A. Longacre, W. A. Morgan, and C. A. Sternbach, eds., The great American carbonate bank: The geology and economic resources of the Cambrian – Ordovician Sauk megasequence of Laurentia: AAPG Memoir 98, 357 – 382.

Ripperdan, R.L., 2001. Stratigraphic Variation in Marine Carbonate Carbon Isotope Ratios. Stable Isotope Geochemistry; Reviews in Mineralogy & Geochemistry 43, 637-659.

Rodgers, J., 1953. Geologic map of East Tennessee with explanatory text: Tennessee Dept. Consev., Div. Geology Bulletin 58(2), 168.
Saltzman, M. R., Runnegar, B., & Lohmann, K. C., 1998. Carbon isotope stratigraphy of Upper Cambrian (Steptoean Stage) sequences of the eastern Great Basin: Record of a global oceanographic event. Geological Society of America Bulletin 110, 285–297.

Saltzman, M. R., Ripperdan, R. L., Brasier, M. D., Lohmann, K. C., Reichart, R. A., Chang, W. T., Shanchi, P., Erga;iev, E.K., Runnegar, B., 2000. A global carbon isotope excursion (SPICE) during the Late Cambrian: relation to trilobite extinctions, organic-matter burial and sea level. Palaeogeography, Palaeoclimatology, Palaeoecology 162, 211–223.

Saltzman, M. R., Cowan, C. A., Runkel, A. C., Runnegar, B., Stewart, M., & Palmer, A. R., 2004. The Late Cambrian Spice ($\delta^{13}C$) Event and the Sauk II-SAUK III Regression: New Evidence from Laurentian Basins in Utah, Iowa and Newfoundland. Journal of Sedimentary Research 74(3), 366–377.

Saltzman, M. R., Young, S. A., Kump, L. R., Gill, B. C., Lyons, T. W., & Runnegar, B., 2011. Pulse of atmospheric oxygen during the late Cambrian. Proceedings of the National Academy of Sciences 108(10), 3876–3881.

Schidlowski M., Hayes J.M., Kaplan I.R., 1983. Isotopic inferences of ancient biochemistries: carbon sulfur, hydrogen, and nitrogen. *In* Schopf JW (ed) Earth's Earliest Biosphere: Its Origin and Evolution. Princeton University Press, Princeton, NJ, 149-186.

Scholle, P. A., and Arthur, M. A., 1980. Carbon isotope fluctuations in Cretaceous pelagic limestones: Potential stratigraphic and petroleum exploration tool: American Association of Petroleum Geologists Bulletin 64, 67–87.

Srinivasan, K., Walker, K.R., 1993. Sequence stratigraphy of an intrashelf basin carbonate ramp to rimmed platform transition: Maryville Limestone (Middle Cambrian), southern Appalachains. Geological Society of American Bulletin 105, 883-896.

Stitt, J. H., 1971. Repeating evolutionary pattern in Late Cambrian trilobite biomeres: Journal of Paleontology 45, 178–181.

Stitt, J. H., 1975. Adaptive radiation, trilobite paleoecology, and extinction, Ptychaspid biomere, Late Cambrian of Oklahoma: Fossils and Strata 4, 381–390.

Taylor, J. F., 2006. History and status of the biomere concept. Memoirs of the Association of Australasian Palaeontologists 32, 247–265.

Taylor, J.F., Repetski, J.E., Loch, J.D., Leslie, S.A., 2012. Biostratigraphy and Chronostratigraphy of the Cambrian-Ordovician Great American Carbonate Bank. in J. R. Derby, R. D. Fritz, S. A. Longacre, W. A. Morgan, and C. A. Sternbach, eds., The great American carbonate bank: The geology and economic resources of the Cambrian – Ordovician Sauk megasequence of Laurentia: AAPG Memoir 98, 15 – 35.

Thomas, W. A., 1977. Evolution of Appalachian-Ouachita salients and recesses from reentrants and promontories in the continental margin: American Journal of Science 277, 1233-1278.

Thomas, W. A., 2006. Tectonic inheritance at a continental margin: GSA Today 16, 4-11.

Veizer J., Hoefs J., 1976. The nature of 18O/16O and 13C/12C secular trends in sedimentary carbonate rocks. Geochim Cosmochim Acta 40, 1387-1395.

Weber, L. J.Jr., 1988. Paleoenvironmental Analysis and Test of Stratigraphic Cyclicity in the Nolichucky Shale and Maynardville Limestone (Upper Cambrian) in Central East Tennessee. PhD diss., University of Tennessee.

Westrop, S.R., Ludvigsen, R., 1987. Biogerographic Control of Trilobite Mass Extinction at an Upper Cambrain "Biomere" Boundary. Paleobiology 13, 84-99

Wignall, P.R., Twitchett, R.J., 1996. Oceanic anoxia and the end Permian mass extinction. Science 272 (5265), 1155-1158. Doi: 10.1126/science.272.5265.1155

Figure 1

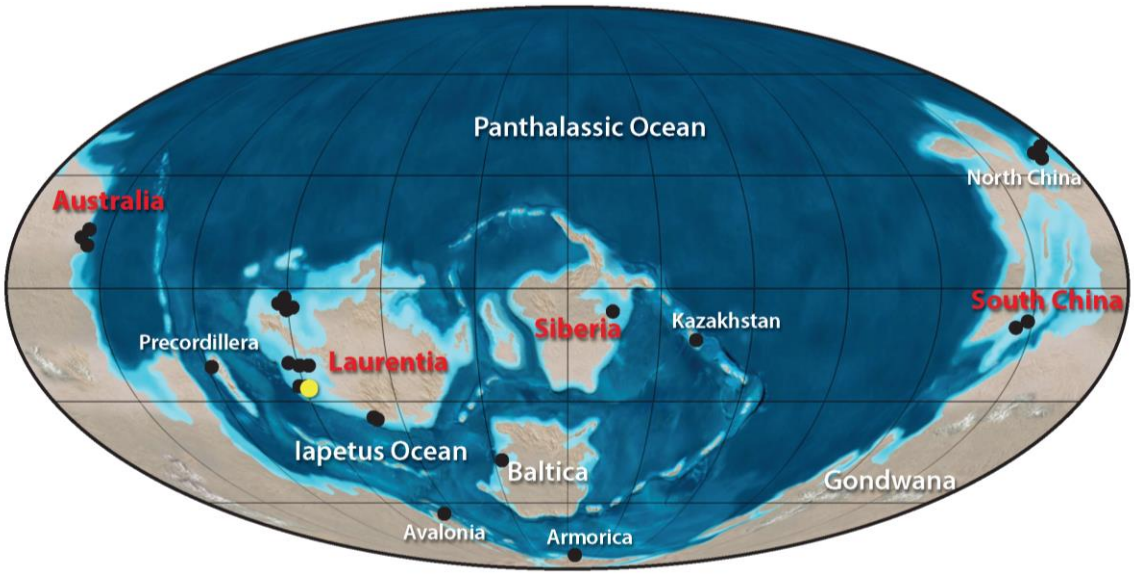

Figure 1. Late Cambrian Earth. A paleo-reconstruction of Earth ~500 mya modified from Blakey. Black circles indicate locations where the SPICE is observed in the modern. Paleocontinents in red letering indicate locations where the end-Marjuman extinction has been observed in the modern. The yellow circle indicates the approximate location of the study area.

Figure 2

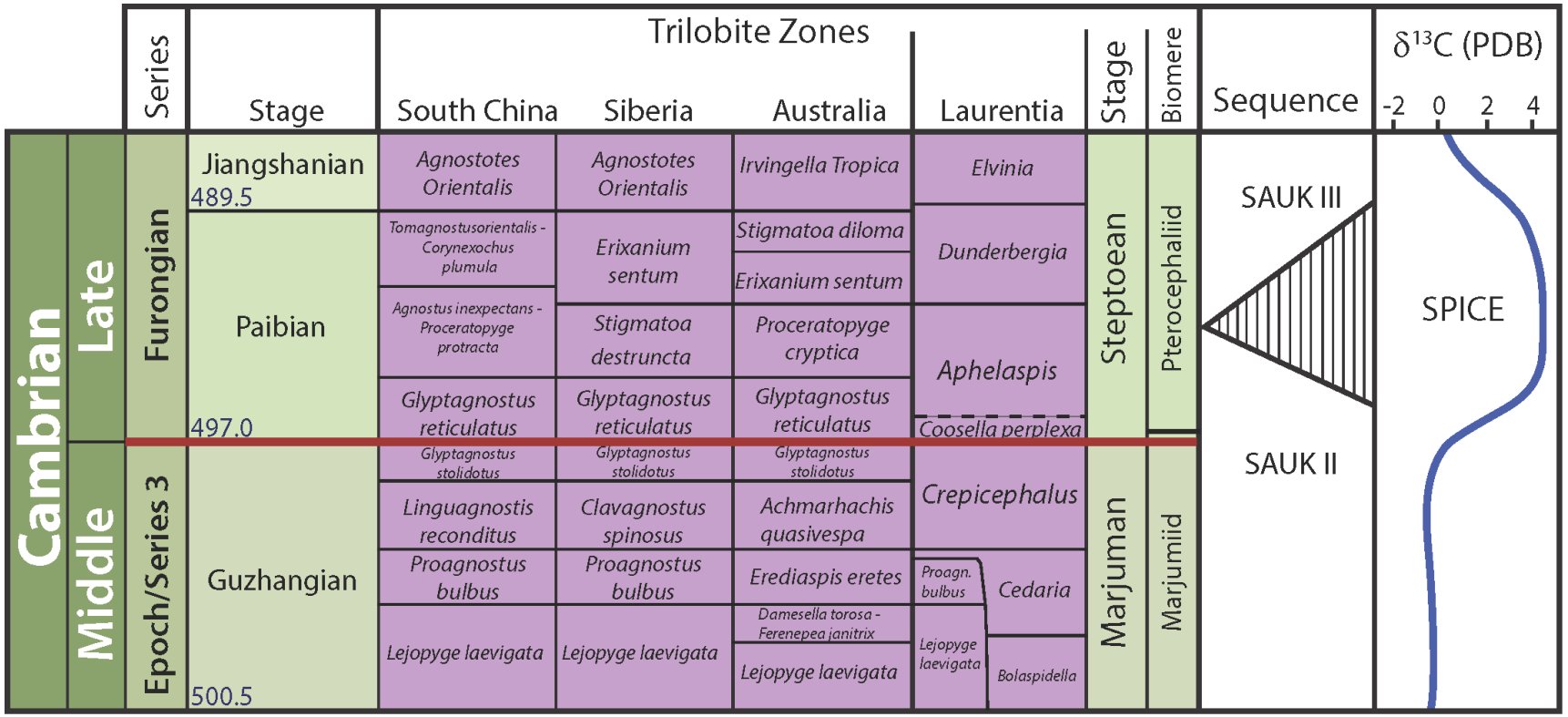

Figure 2. Upper Cambrian chronostratigraphic and biostratigraphic subdivisions. Chart is focused on the end-Marjuman extinction (red line). Shown are regional biostratigraphic zonal scheme correlated with Laurentian stages, and biomeres. Also shown is the SPICE and the sequences of the SAUK megasequence. Figure modified from Peng et al., 2012, Taylor et al., 2012, and Saltzman et al., 2004.

Figure 3

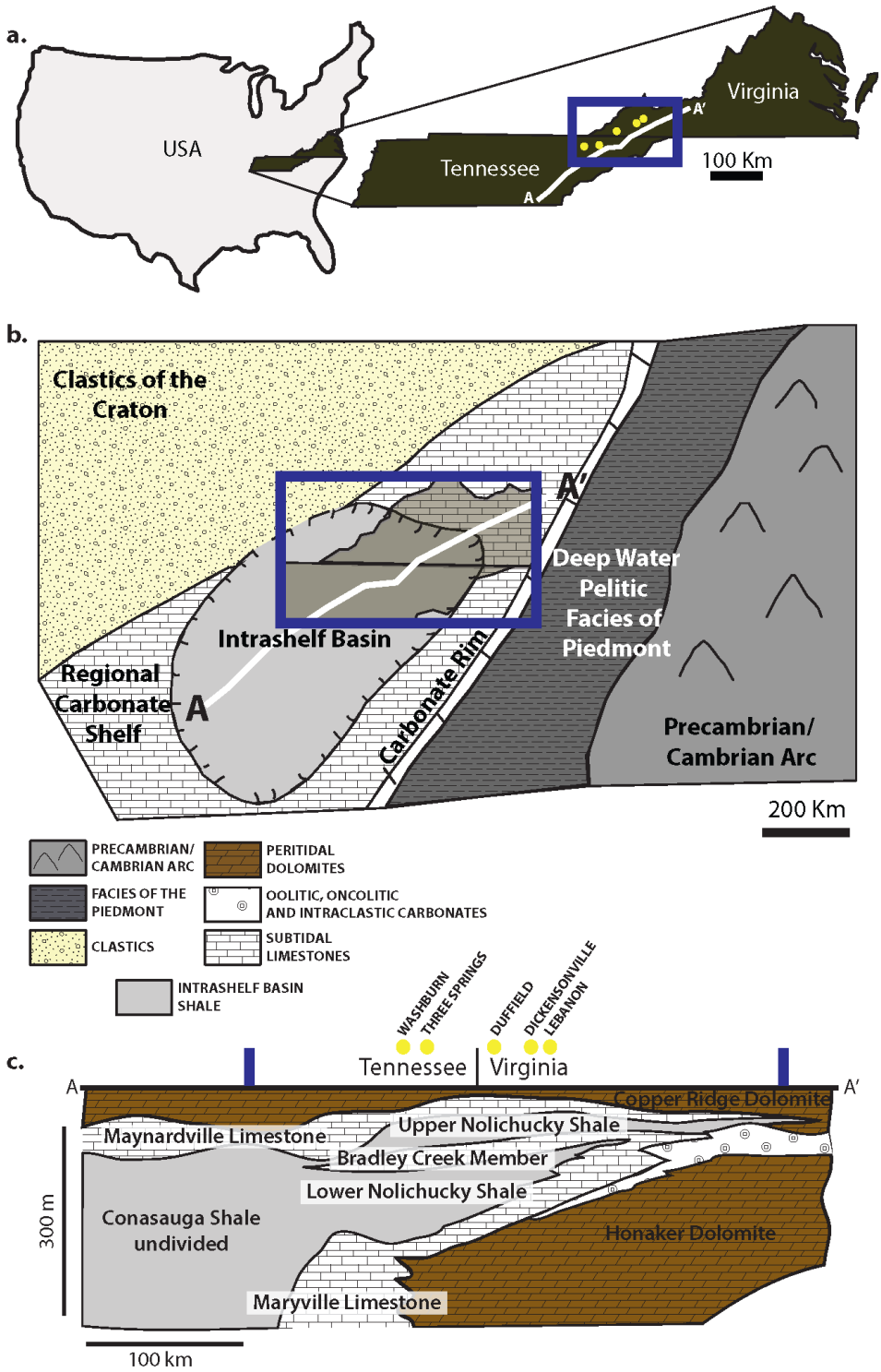
a.
USA
Tennessee
Virginia
A
A'
100 Km
b.
Clastics of the Craton
Intrashelf Basin
Regional Carbonate Shelf
Carbonate Rim
Deep Water Pelitic Facies of Piedmont
Precambrian/ Cambrian Arc
200 Km
PRECAMBRIAN/ CAMBRIAN ARC
FACIES OF THE PIEDMONT
CLASTICS
INTRASHELF BASIN SHALE
PERITIDAL DOLOMITES
OOLITIC, ONCOLITIC AND INTRACLASTIC CARBONATES
SUBTIDAL LIMESTONES
WASHBURN
THREE SPRINGS
DUFFIELD
DICKENSONVILLE
LEBANON
c.
Tennessee
Virginia
Copper Ridge Dolomite
Upper Nolichucky Shale
Maynardville Limestone
Bradley Creek Member
Lower Nolichucky Shale
Conasauga Shale undivided
Honaker Dolomite
Maryville Limestone
300 m
100 km

Figure 3. Regional setting of the Nolichucky Fm. a. Locality image of United States, Virginia and Tennessee. Expanded image of Virginia and Tennessee outlines the study area in a blue box with approximate outcrop locations as yellow circles. The white A-A' refers to the cross section in Figure 3.c. (Modified from Markello and Read, 1982). **b.** is a palinspastic regional map of the Nolichucky intrashelf basin (Modified from Markello and Read, 1982). **c.** a regional cross section focused on the Nolichucky Fm.

Figure 4

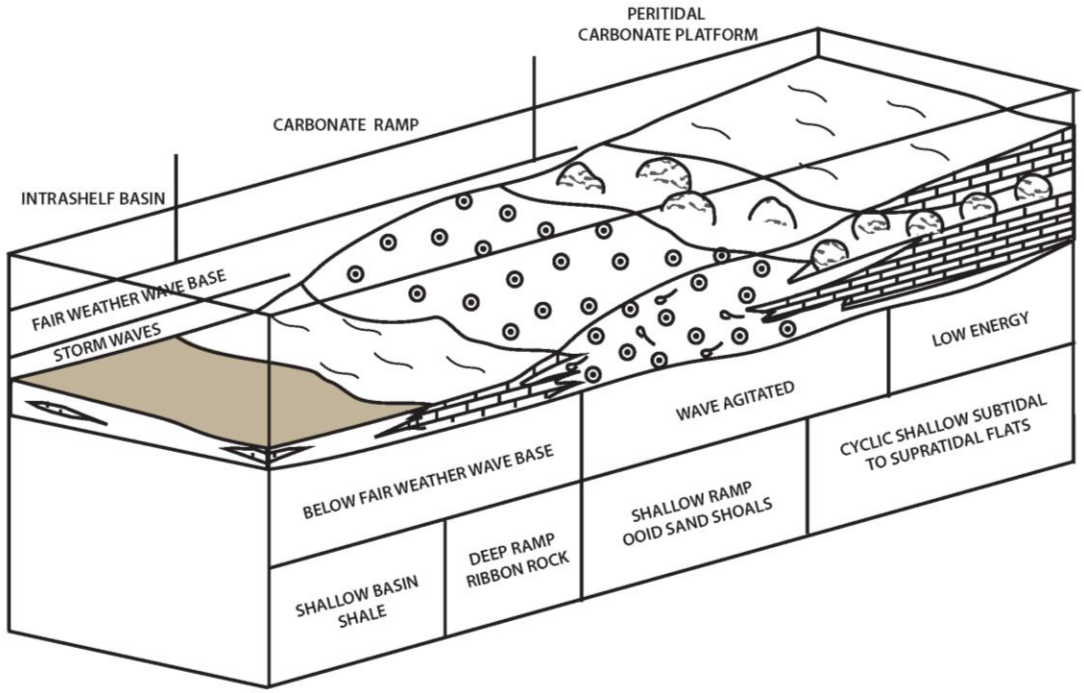

Figure 4. Depositional environment. A schematic of the carbonate platform to intrashelf basin modified from Markello and Read (1981) to accompany Table 1.

Figure 5

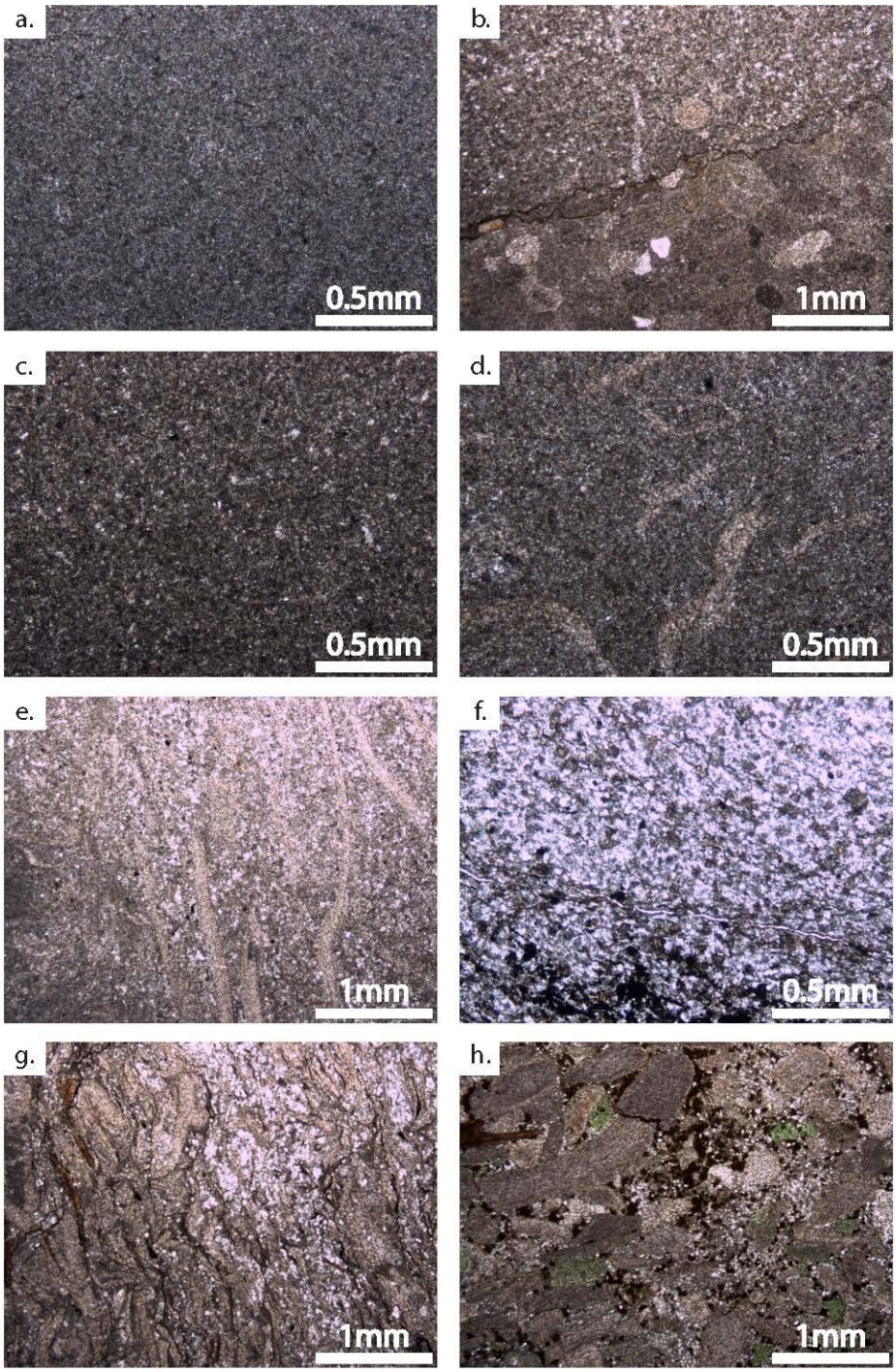

Figure 5. Photomicrographs for diagenetic assessment. a. Sample W-24 of the Washburn Section is a pure peloidal mudstone with little to no sparitization. **b.** Sample T-11 of the Three Springs Section is a flat pebble clast (top) accentuated by a stylolite in carbonate mud matrix (bottom). It appears that both the matrix and intraclast contain microspar, though the spar is much smaller the in the intraclast. **c.** Sample D-10 of the Dickensonville Section is a pure peloidal mudstone with microspar throughout. **d.** Sample W-44 of the Washburn Section is a trilobite packstone/grainstone where the trilobite skeletal fragments have been micritized. e. Sample T-40 is a peloidal mudstone to micritized trilobite wackestone with abundant in microspar. **f.** Sample T-25 of the Three Springs Section is a mudstone that has undergone extensively sparitization. **g.** Sample Du-27 of the Duffield Section is a trilobite wackestone that grades into a mudstone abundant in microspar and opaque minerals (shown). **h.** Sample D-36 of the Dickensonville Section is a trilobite packstone abundant in calcite spar and glauconite filled pores.

Figure 6a

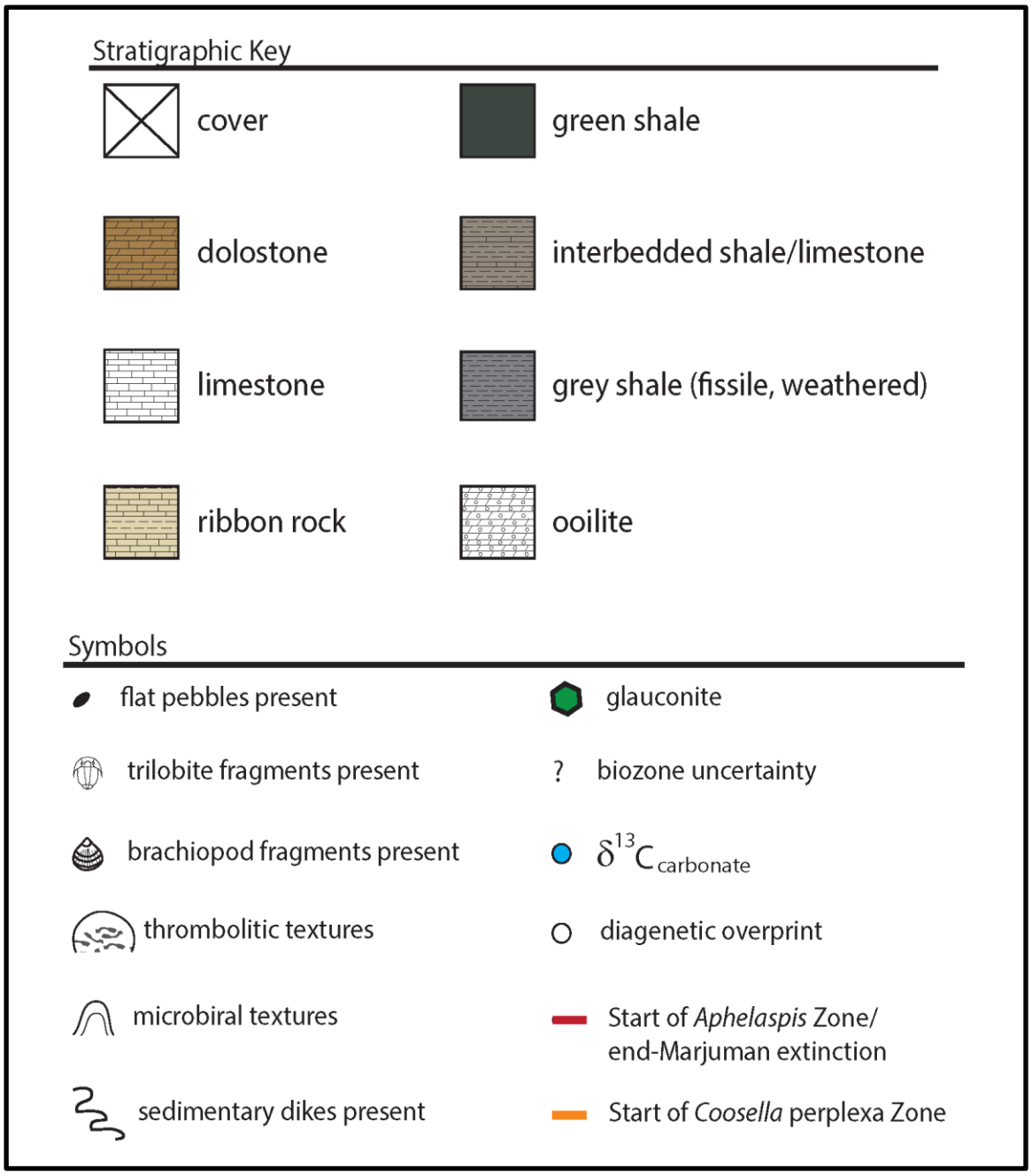
Stratigraphic Key
cover
green shale
dolostone
interbedded shale/limestone
limestone
grey shale (fissile, weathered)
ribbon rock
ooilite
Symbols
flat pebbles present
glauconite
trilobite fragments present
? biozone uncertainty
brachiopod fragments present
$\delta^{13}C_{carbonate}$
thrombolitic textures
diagenetic overprint
microbiral textures
Start of *Aphelaspis* Zone/ end-Marjuman extinction
sedimentary dikes present
Start of *Coosella* perplexa Zone

Figure 6b

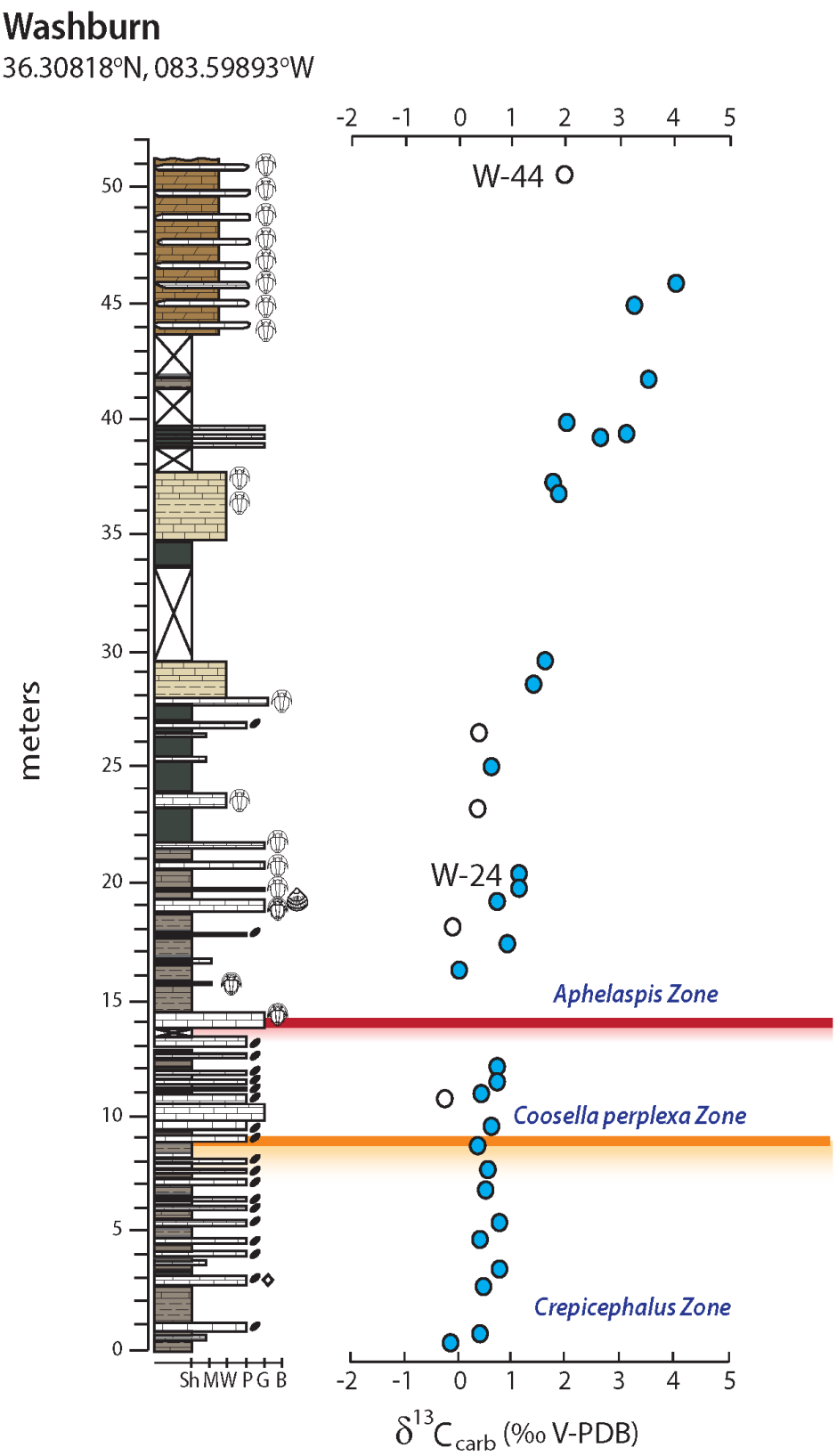
Washburn
36.30818°N, 083.59893°W
-2 -1 0 1 2 3 4 5
W-44
W-24
meters
50
45
40
35
30
25
20
15
10
5
0
Sh MW P G B
Aphelaspis Zone
Coosella perplexa Zone
Crepicephalus Zone
δ13Ccarb (‰ V-PDB)

Figure 6c

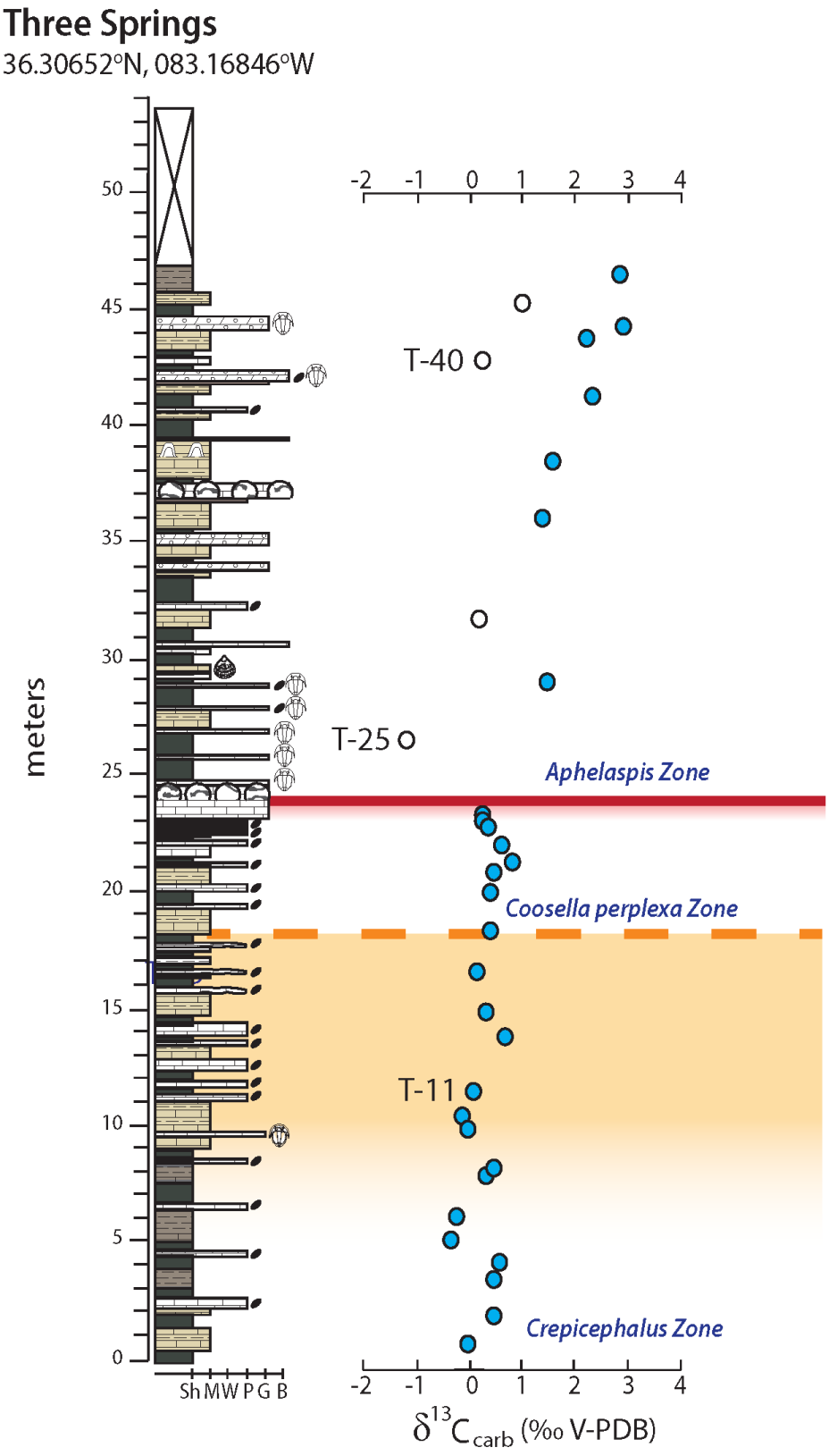
Three Springs
36.30652°N, 083.16846°W
meters
50
45
40
35
30
25
20
15
10
5
0
Sh MW P G B
-2 -1 0 1 2 3 4
T-40
T-25
T-11
Aphelaspis Zone
Coosella perplexa Zone
Crepicephalus Zone
-2 -1 0 1 2 3 4
δ13Ccarb (‰ V-PDB)

Figure 6d

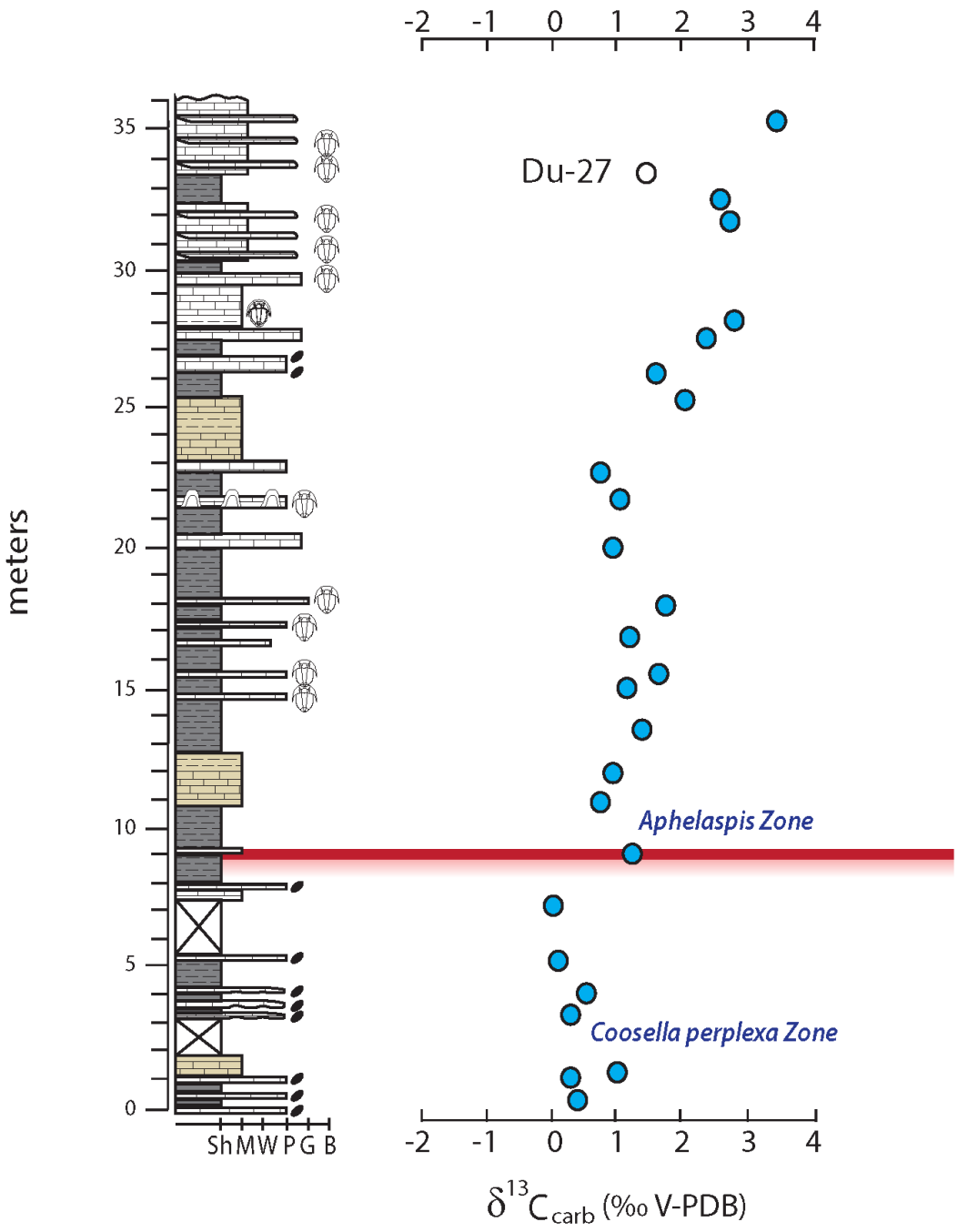
Duffield
36.70140°N, 082.77380°W
meters
35
30
25
20
15
10
5
0
Sh M W P G B
-2 -1 0 1 2 3 4
Du-27
Aphelaspis Zone
Coosella perplexa Zone
-2 -1 0 1 2 3 4
δ13Ccarb (‰ V-PDB)

Figure 6e

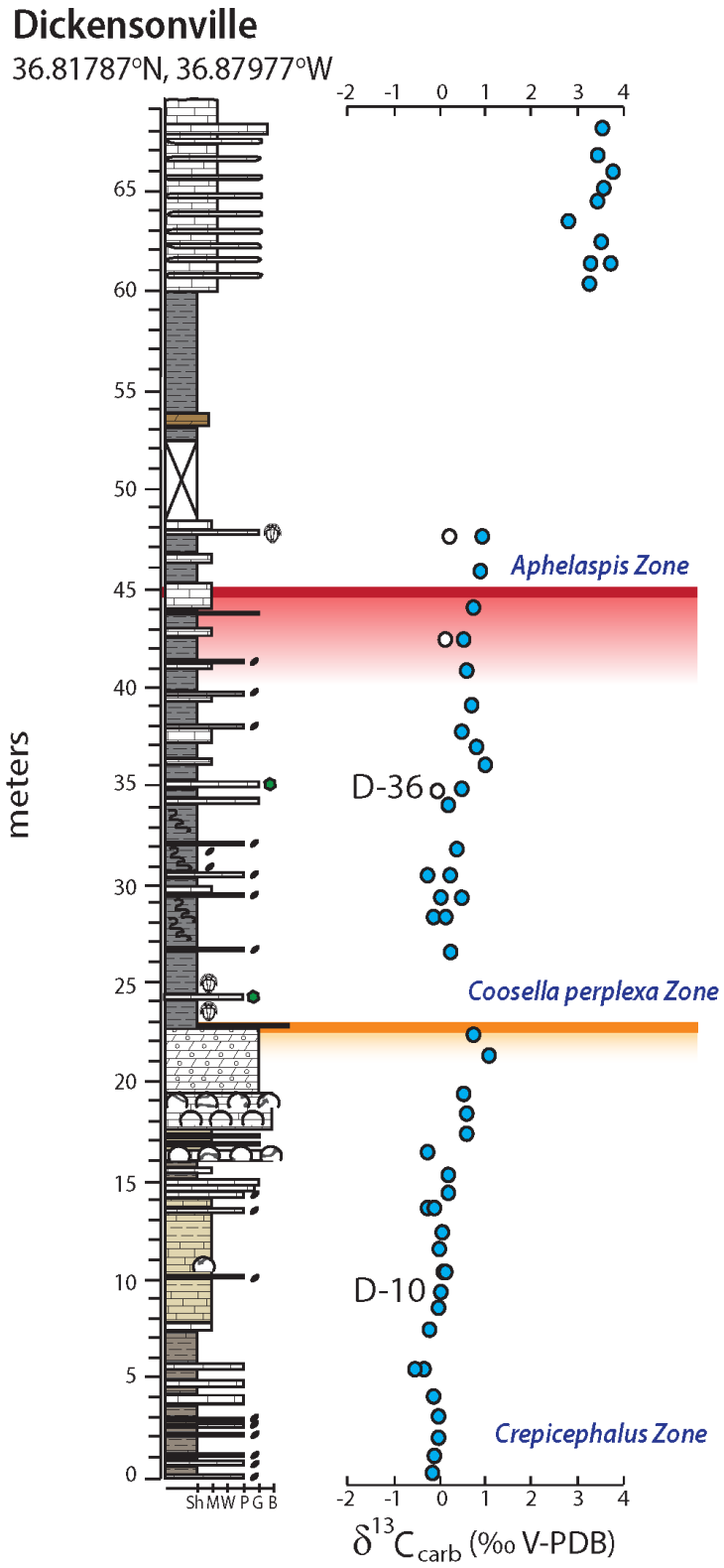
Dickensonville
36.81787°N, 36.87977°W
meters
0
5
10
15
20
25
30
35
40
45
50
55
60
65
Sh MW P G B
-2 -1 0 1 2 3 4
Aphelaspis Zone
Coosella perplexa Zone
Crepicephalus Zone
D-36
D-10
δ13Ccarb (‰ V-PDB)

Figure 6f

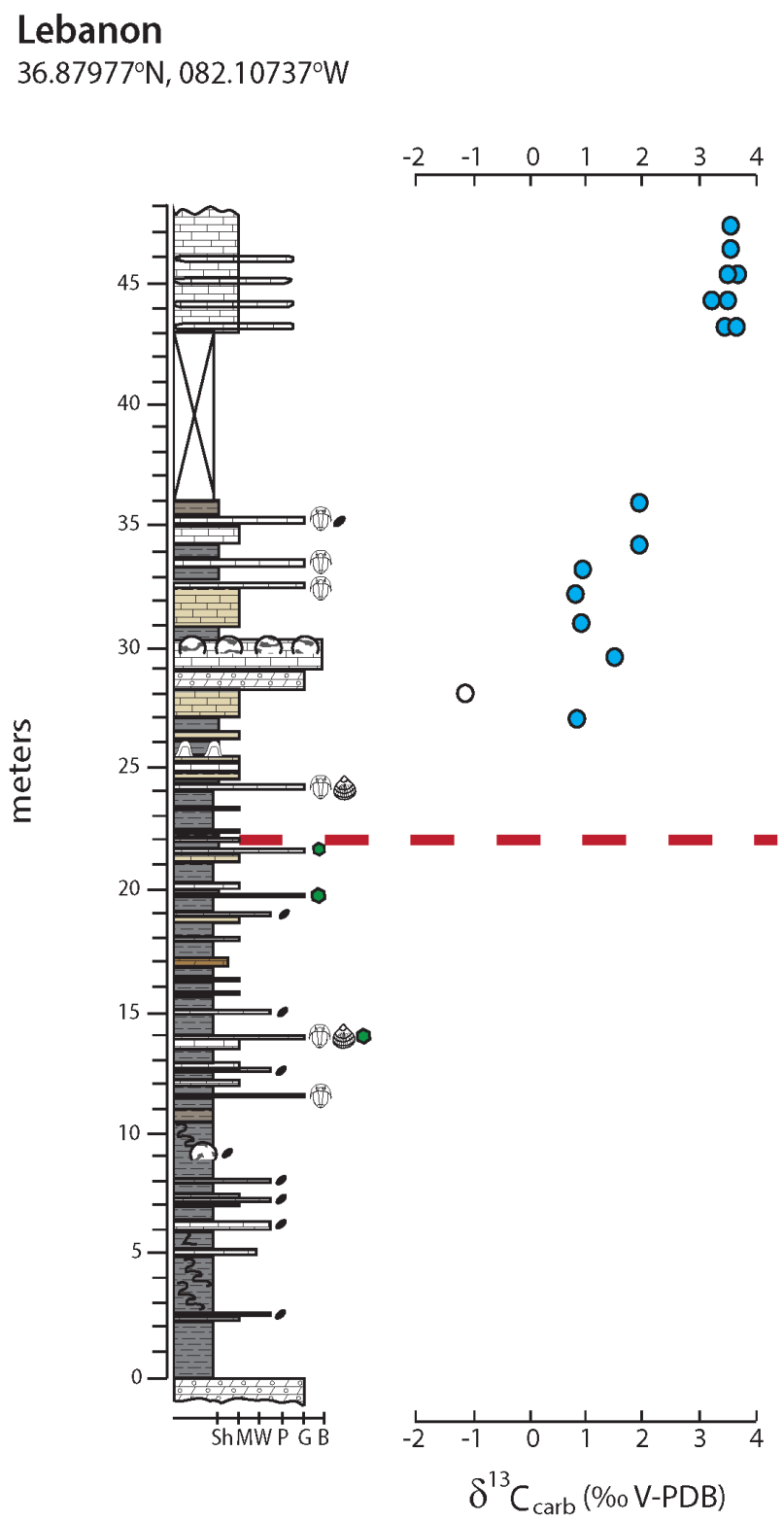
Lebanon
36.87977°N, 082.10737°W
meters
0
5
10
15
20
25
30
35
40
45
Sh MW P G B
-2 -1 0 1 2 3 4
-2 -1 0 1 2 3 4
δ13Ccarb (‰ V-PDB)

Figure 6. Measured stratigraphic sections and correlating carbon isotope values. **a.** Stratigraphy and symbol key to accompany Figure b. c. d. e. f. **b.** Washburn section. **c.** Three Springs section. **d.** Duffield section. **e.** Dickensonville section. **f.** Lebanon section. Orange and red shading indicates the range of biozone uncertainty within sections with biostratigraphic control.

Figure 7

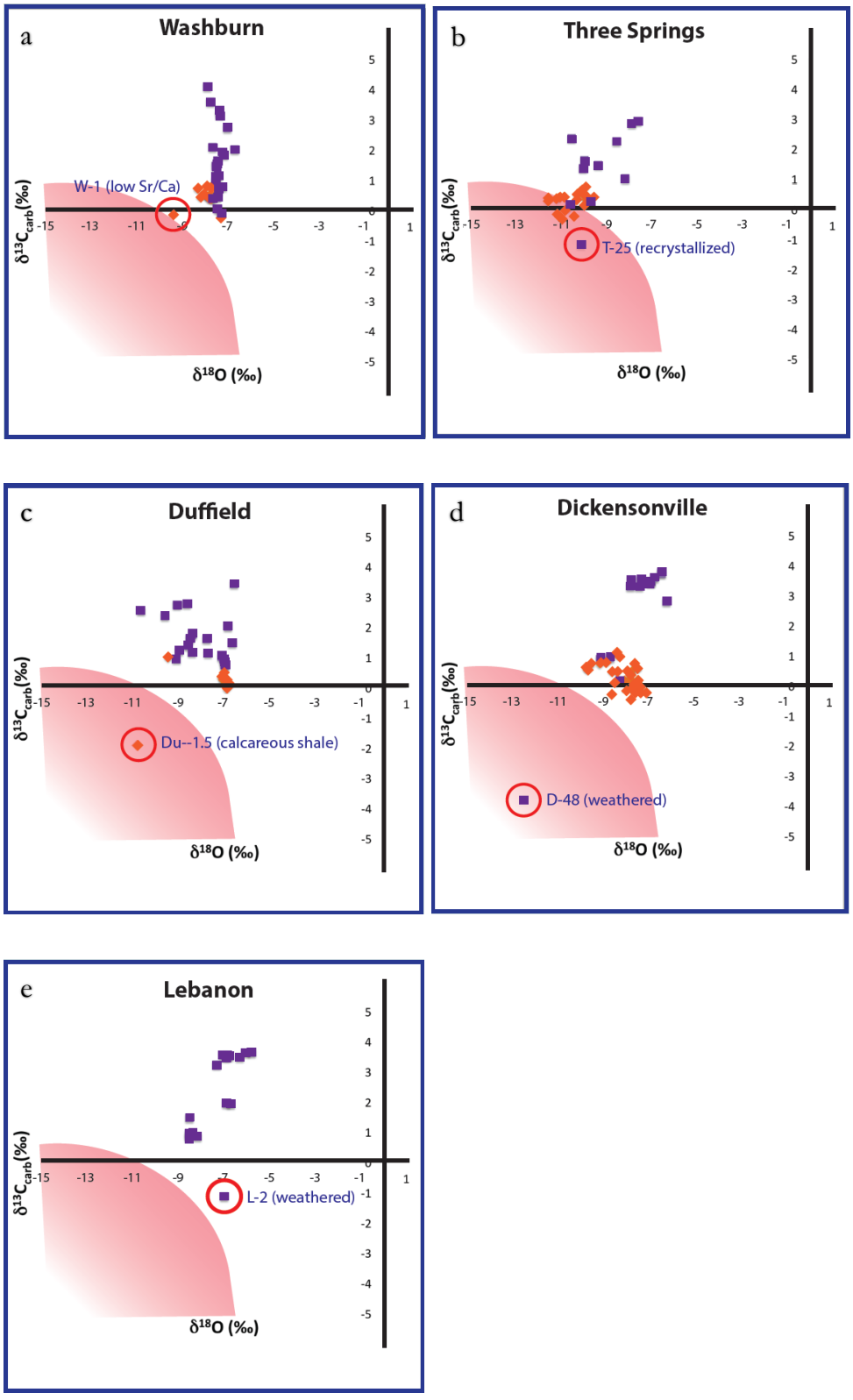
a
Washburn
W-1 (low Sr/Ca)
δ13Ccarb (‰)
δ18O (‰)
b
Three Springs
T-25 (recrystallized)
δ13Ccarb (‰)
δ18O (‰)
c
Duffield
Du--1.5 (calcareous shale)
δ13Ccarb (‰)
δ18O (‰)
d
Dickensonville
D-48 (weathered)
δ13Ccarb (‰)
δ18O (‰)
e
Lebanon
L-2 (weathered)
δ13Ccarb (‰)
δ18O (‰)

Figure 7. Plot of $\delta^{18}O$ versus $\delta^{13}C$ for each section. Data categorized into pre-SPICE (orange) and SPICE (purple) trends. Open red circles highlight outliers with additional elemental or petrographic diagenetic support. Shaded area is the range of potentially altered data. **a.** Washburn Section. **b.** Three Springs section. **c.** Duffield section. **d.** Dickensonville section. **e.** Lebanon section

Figure 8

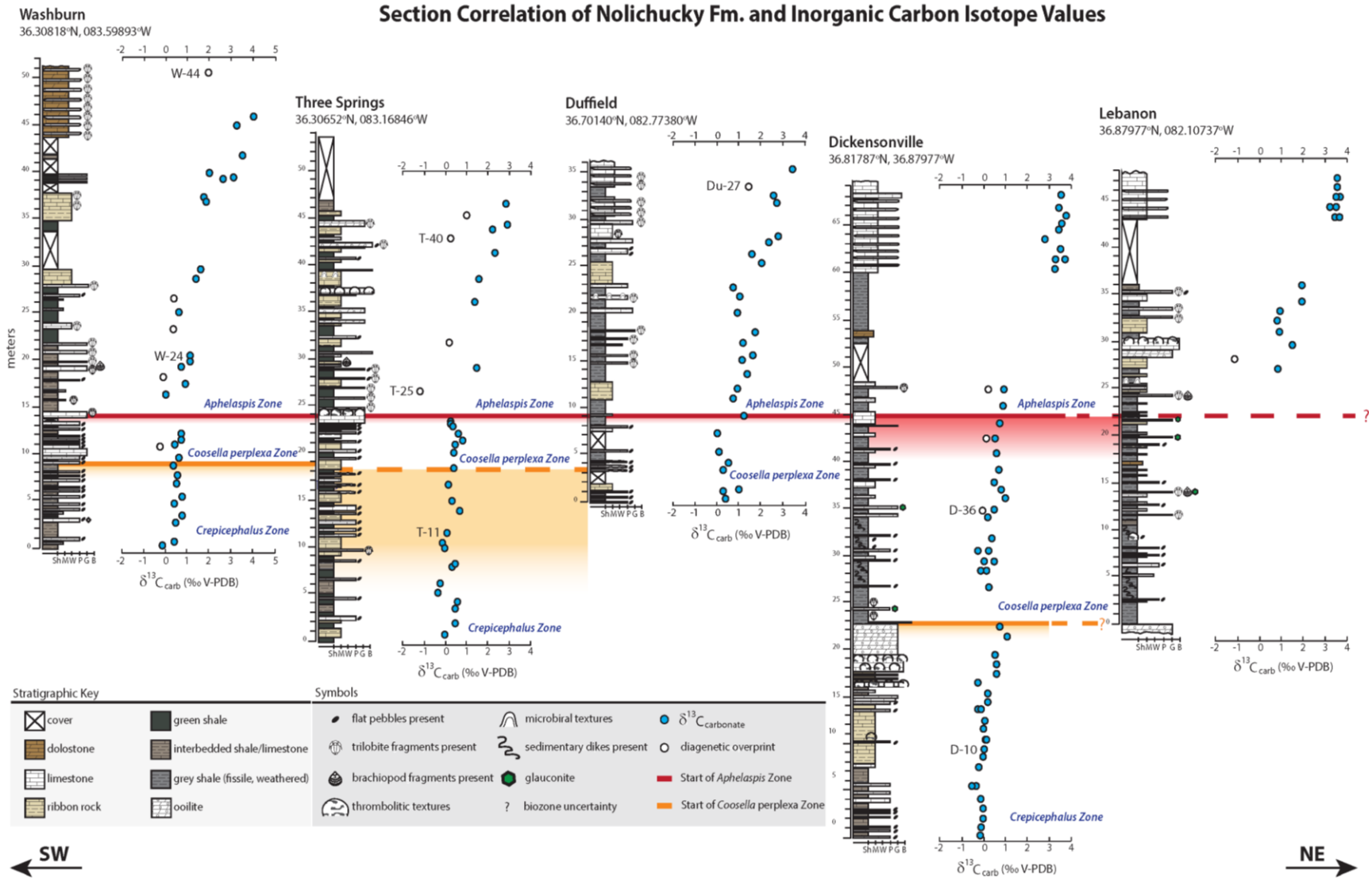
Section Correlation of Nolichucky Fm. and Inorganic Carbon Isotope Values
Washburn
36.30818°N, 083.59893°W
Three Springs
36.30652°N, 083.16846°W
Duffield
36.70140°N, 082.77380°W
Dickensonville
36.81787°N, 36.87977°W
Lebanon
36.87977°N, 082.10737°W
W-44
W-24
T-40
T-25
T-11
Du-27
D-36
D-10
Aphelaspis Zone
Coosella perplexa Zone
Crepicephalus Zone
meters
δ13Ccarb (‰ V-PDB)
Sh M W P G B
Stratigraphic Key
cover
dolostone
limestone
ribbon rock
green shale
interbedded shale/limestone
grey shale (fissile, weathered)
ooilite
Symbols
flat pebbles present
trilobite fragments present
brachiopod fragments present
thrombolitic textures
microbiral textures
sedimentary dikes present
glauconite
biozone uncertainty
δ13Ccarbonate
diagenetic overprint
Start of Aphelaspis Zone
Start of Coosella perplexa Zone
SW
NE

Figure 8. Section correlation of the Nolichucky Fm. and inorganic carbon isotope values. A summary figure of data collected in this study. Outcrop sections correlated from southwest to northeast along the end-Marjuman extinction horizon (red line). Also shown are the carbon isotope values (blue circles). Samples names (W-44, W-24, T-40, T-25, T-11, Du-27, D-36, D-10) correspond with petrographic images in Figure 4.

Appendix A. Field measurments and observations

A detailed summary to include the latitude and longitude of each outcrop location, along with corresponding elevation and bed attitude. Sample names and specific locations are to the left of each columnar section and field descriptions are to the right. Each sections field description will be in reference to the first facies described in the Dickensonville section (indicated by roman numerals) as it was the first section to be measured. Additional notes and/or differences in those facies first described are added to the roman numeral.

Dickensonville Section

36.81787°N, 36.87977°W
Elevation: 703m, Attitude: 79°, 24°S

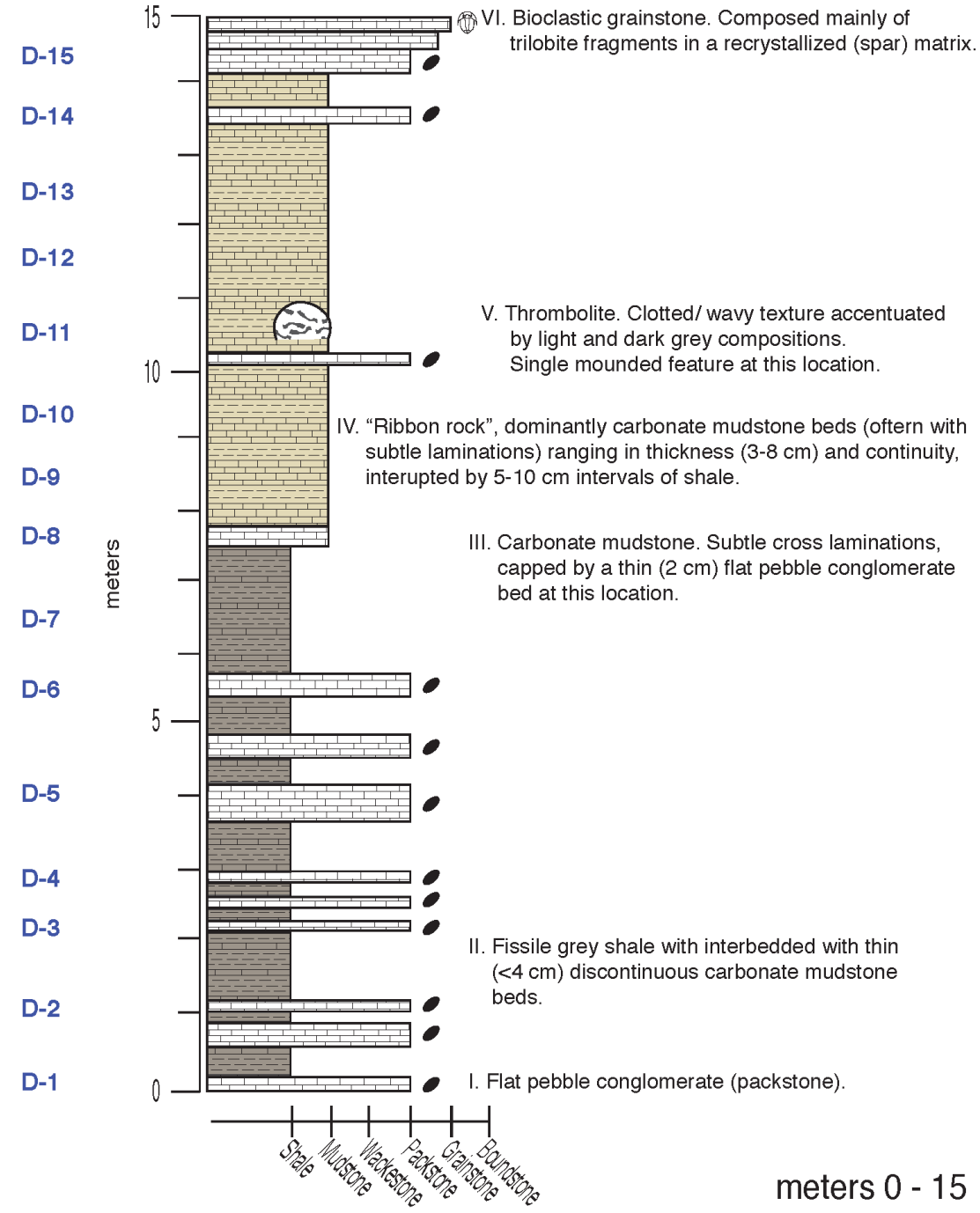

Dickensonville Section

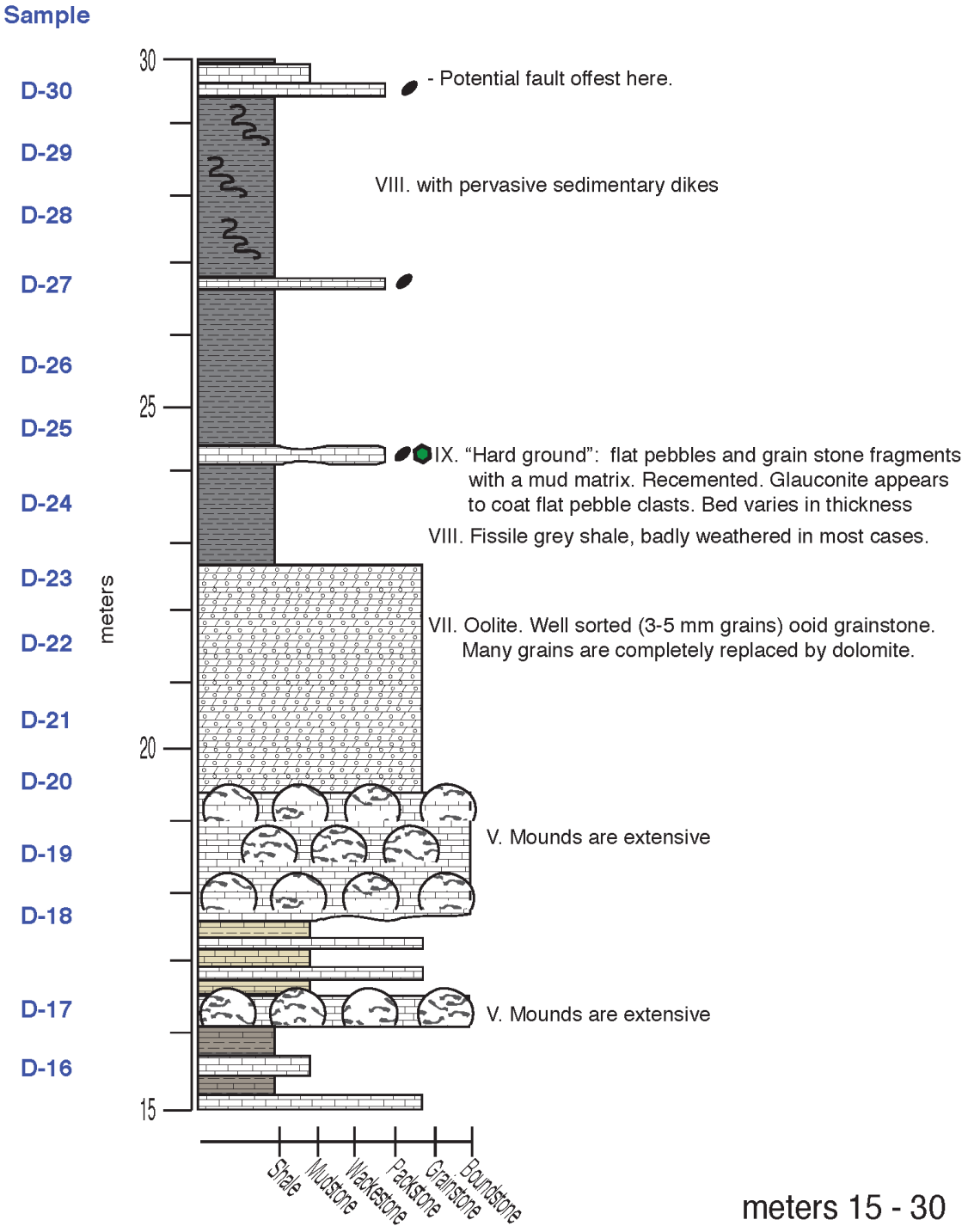

Dickensonville Section

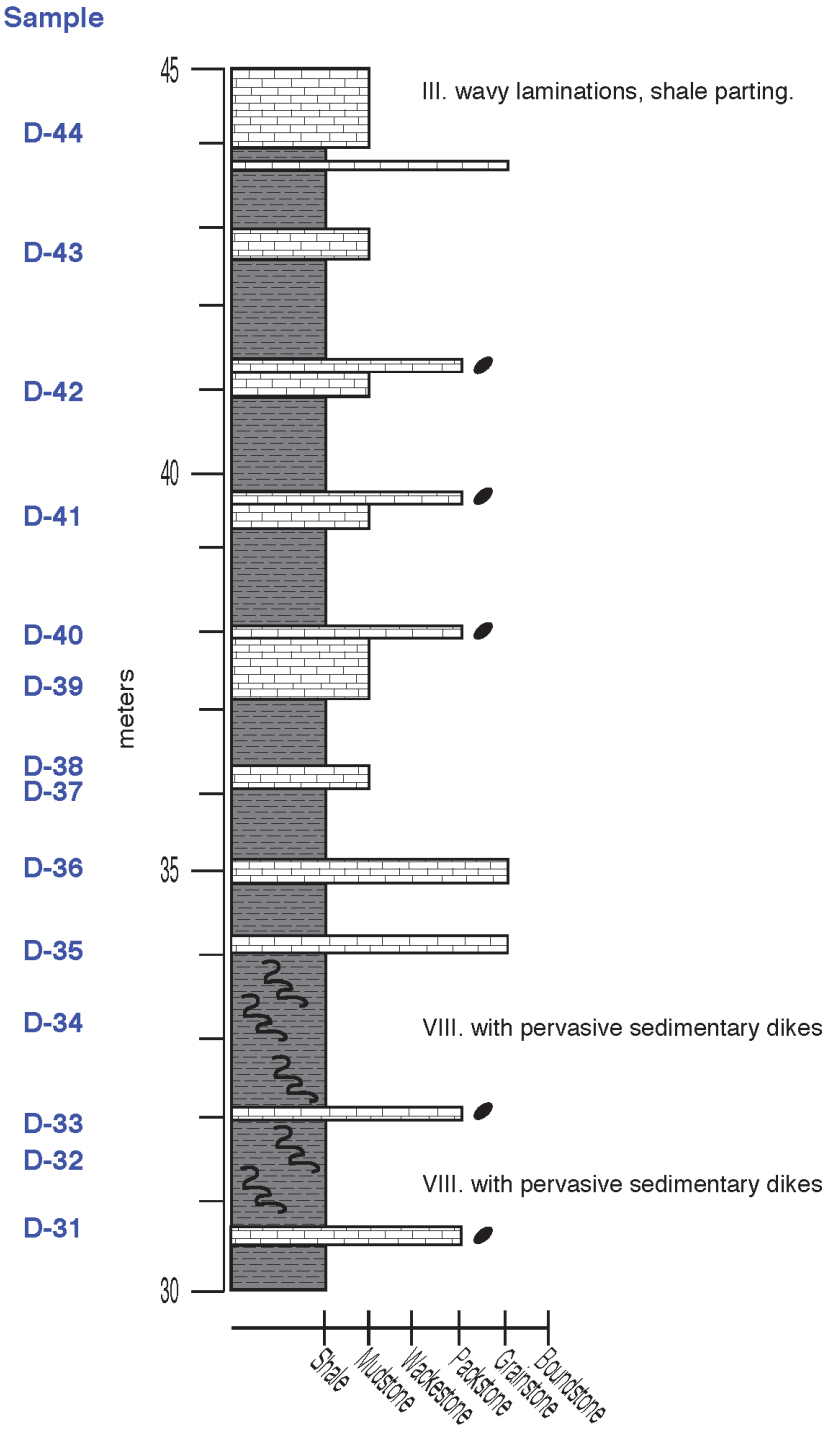

meters 30 - 45

Dickensonville Section

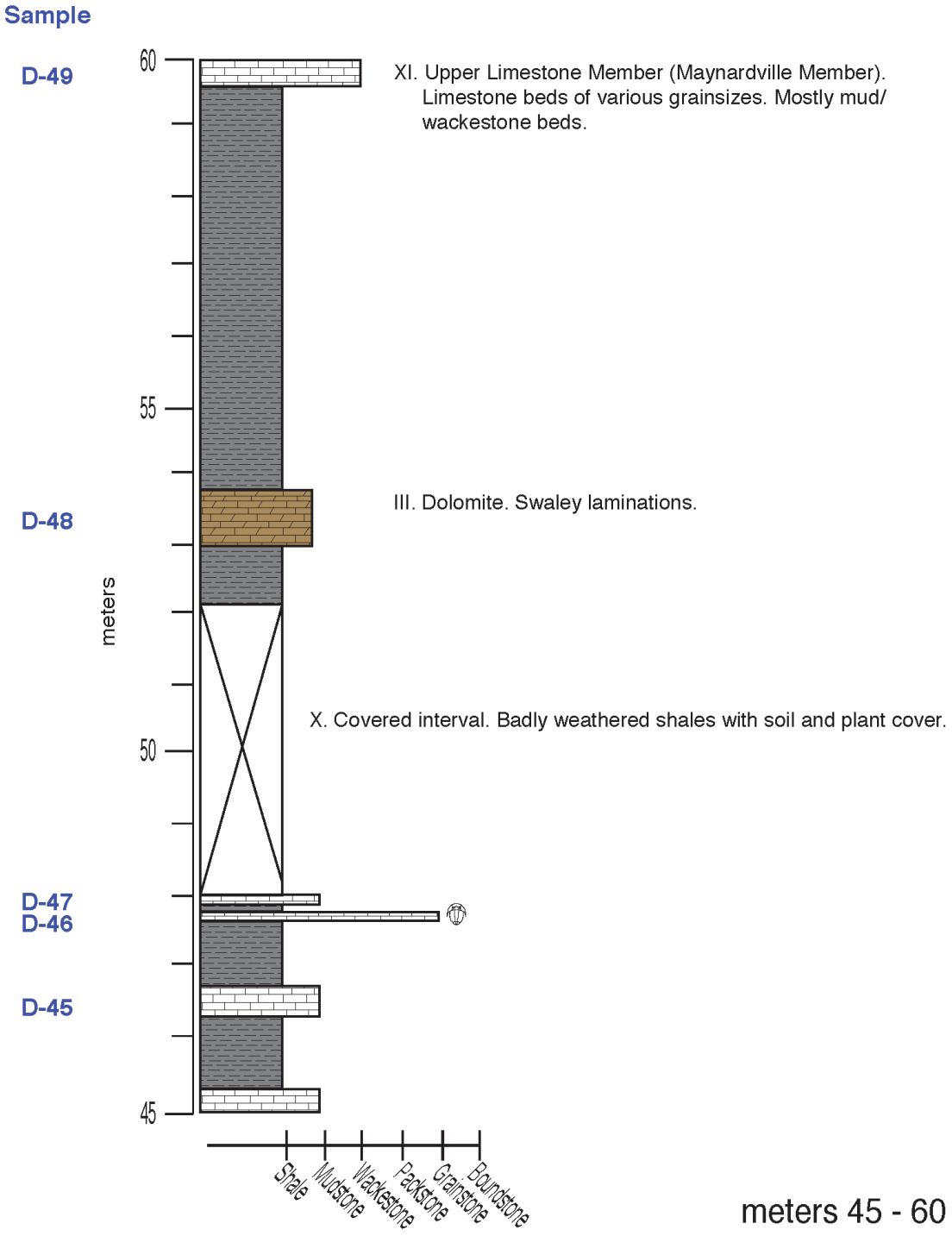

Dickensonville Section

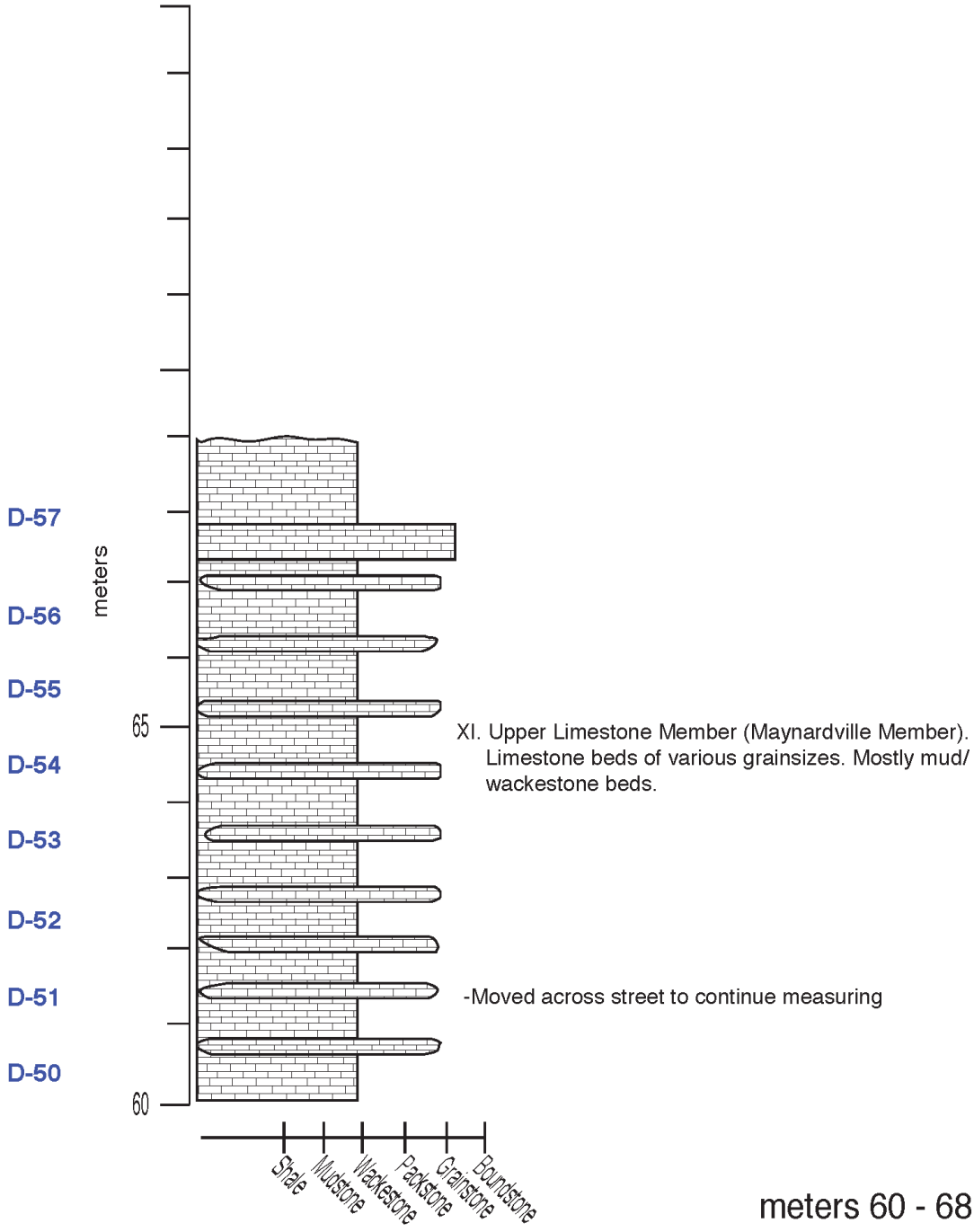

Washburn Section

36.30818°N, 083.59893°W
Elevation: 413m, Attitude: 89°,45°S

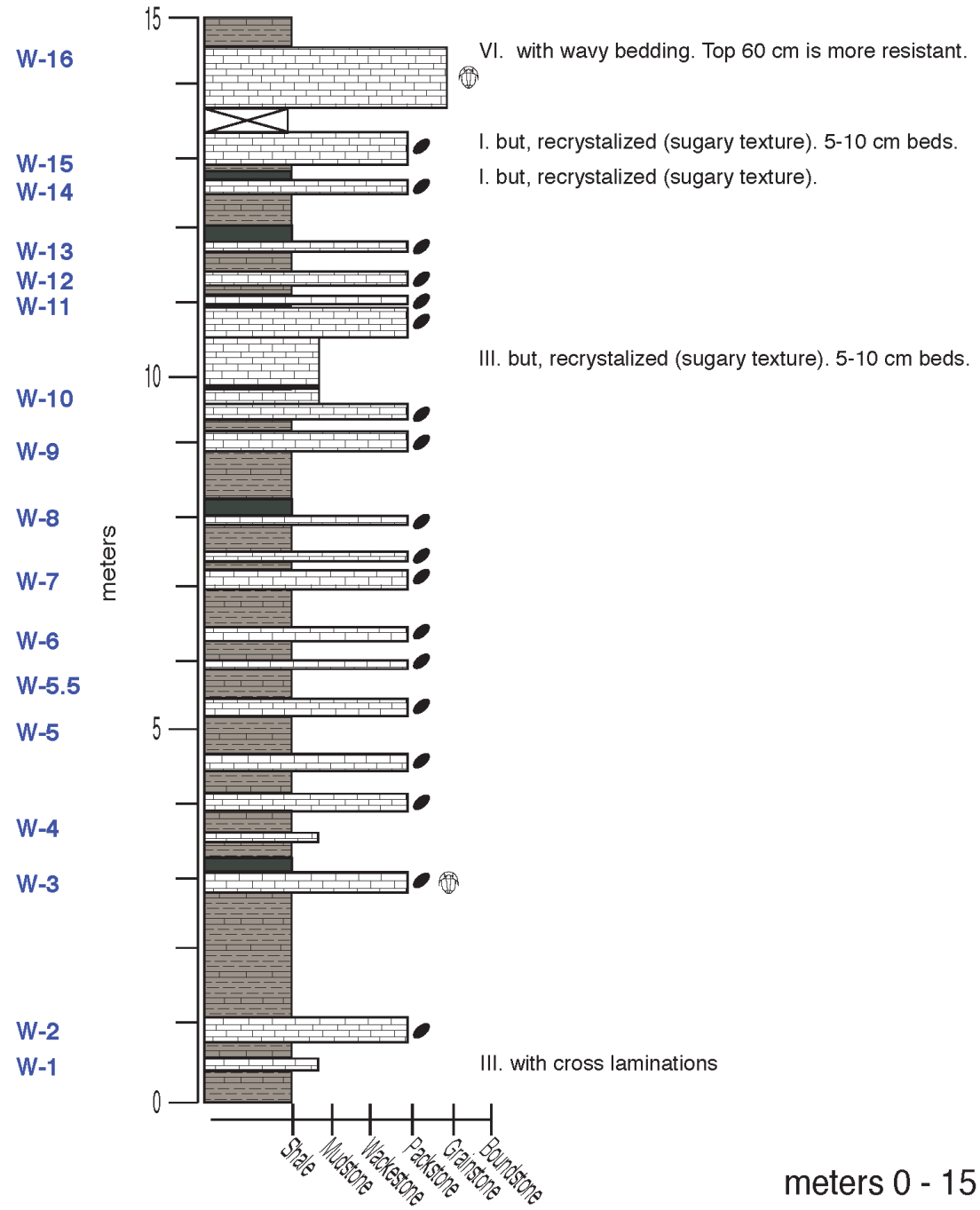

Washburn Section

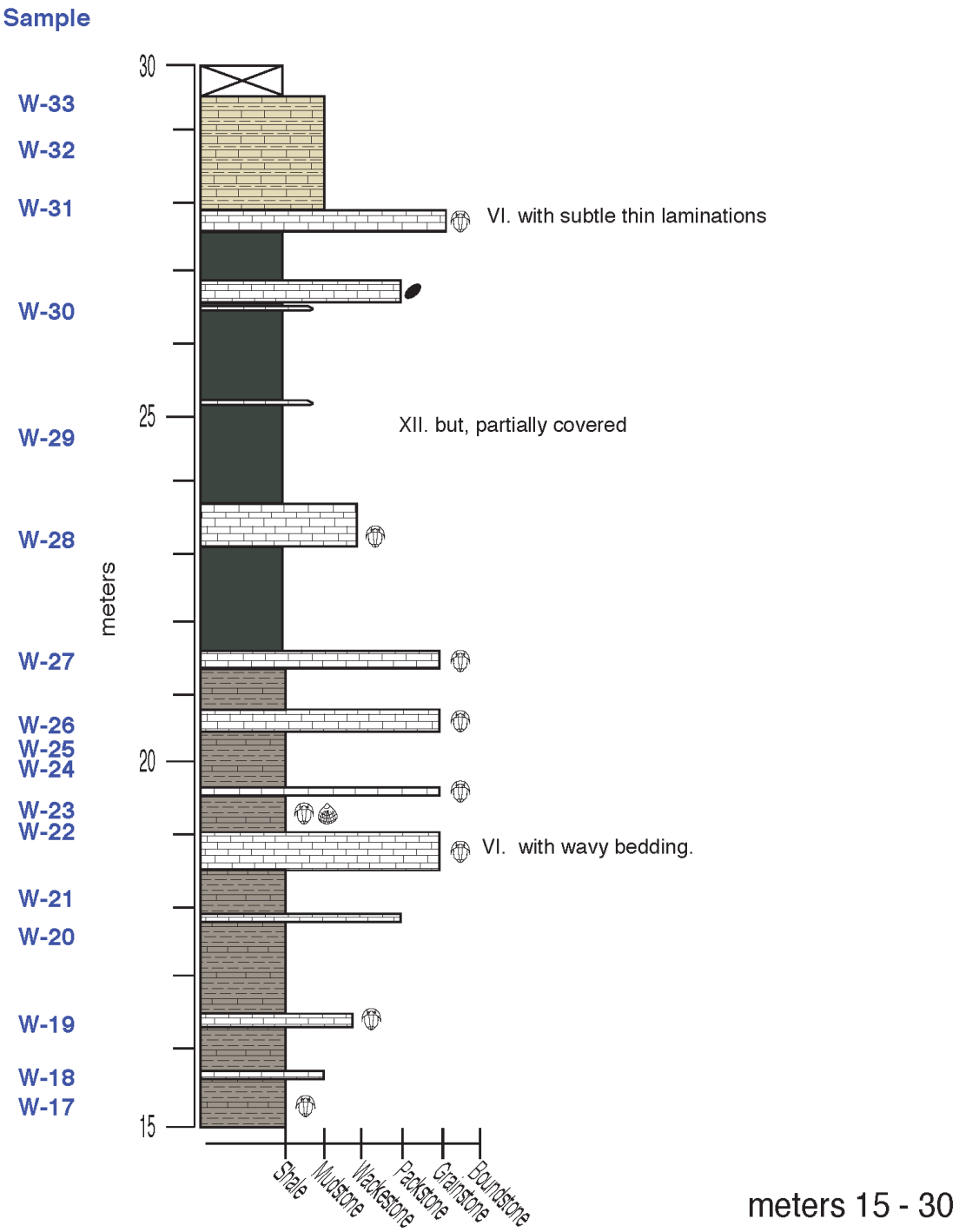

Washburn Section

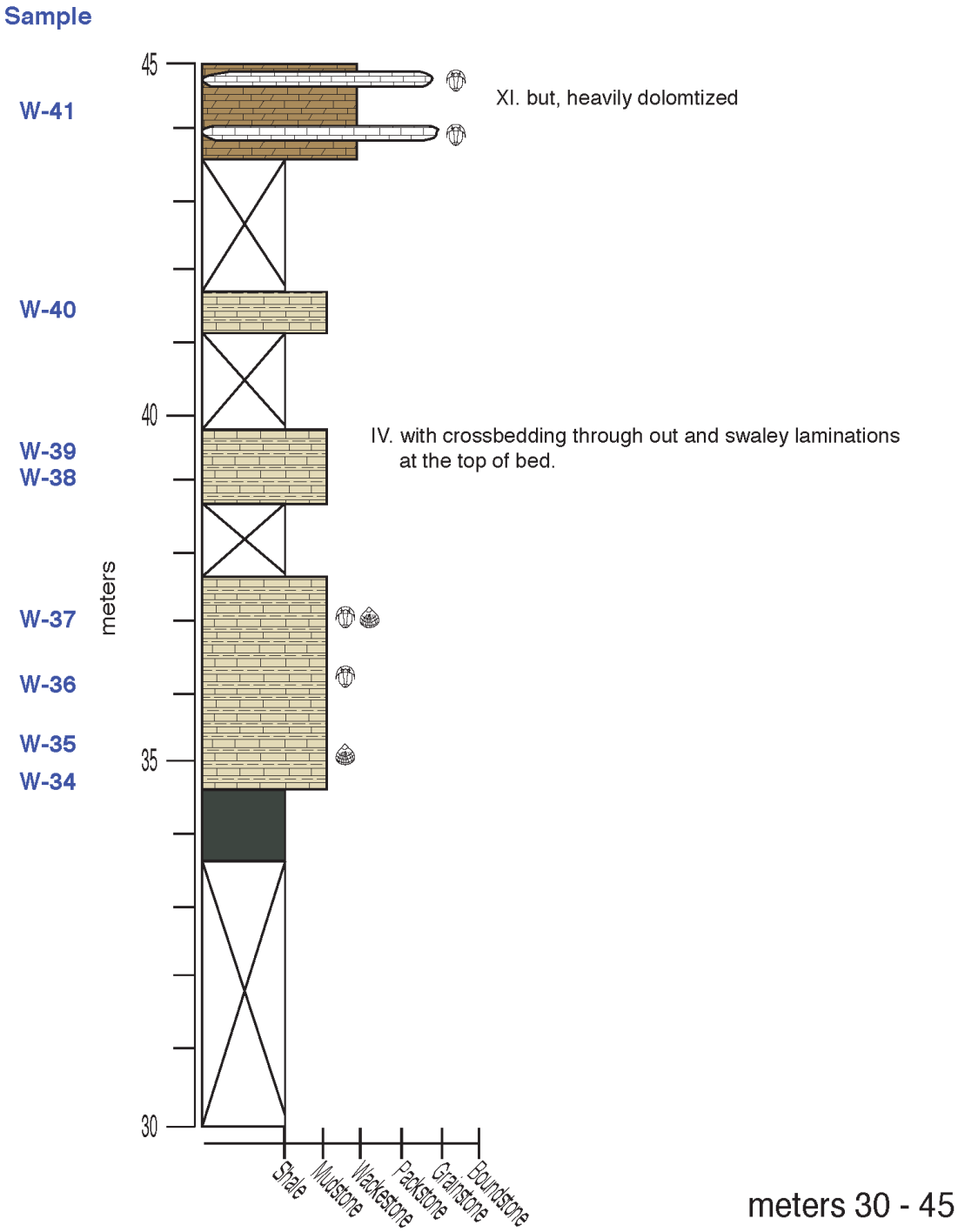

Washburn Section

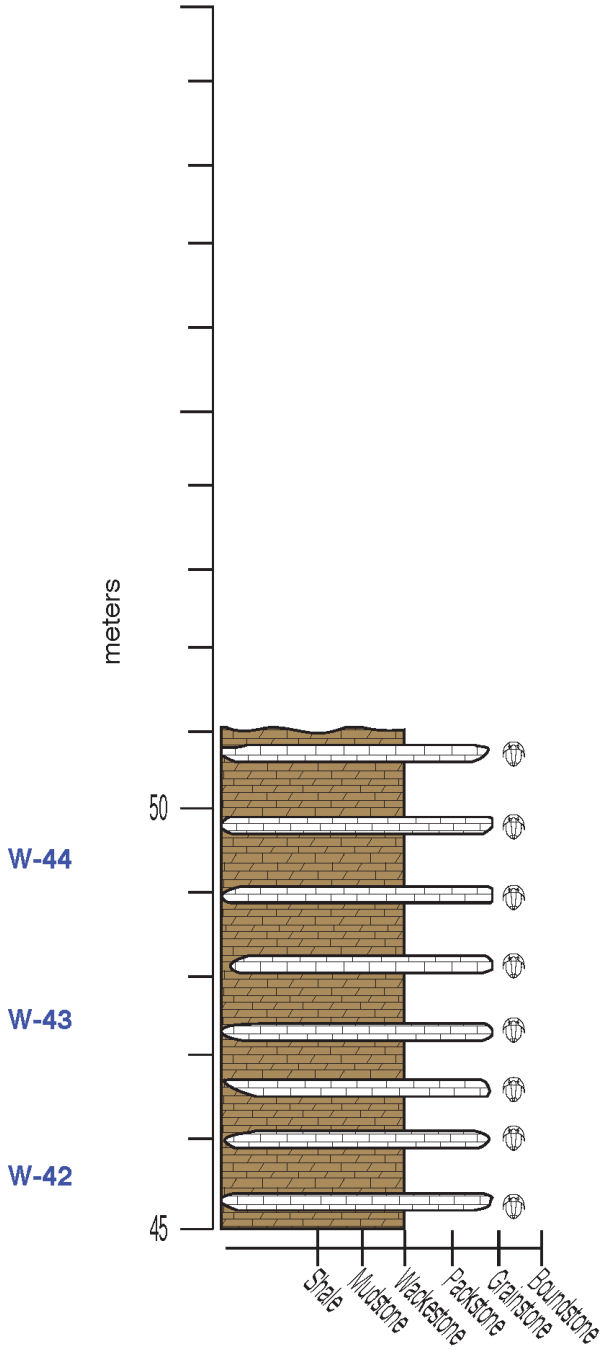

XI. but, heavily dolomtized

meters 45 - 50

Three Springs Section

36.30652°N, 083.16846°W
Elevation: 375m, Attitude: 40°,26°S

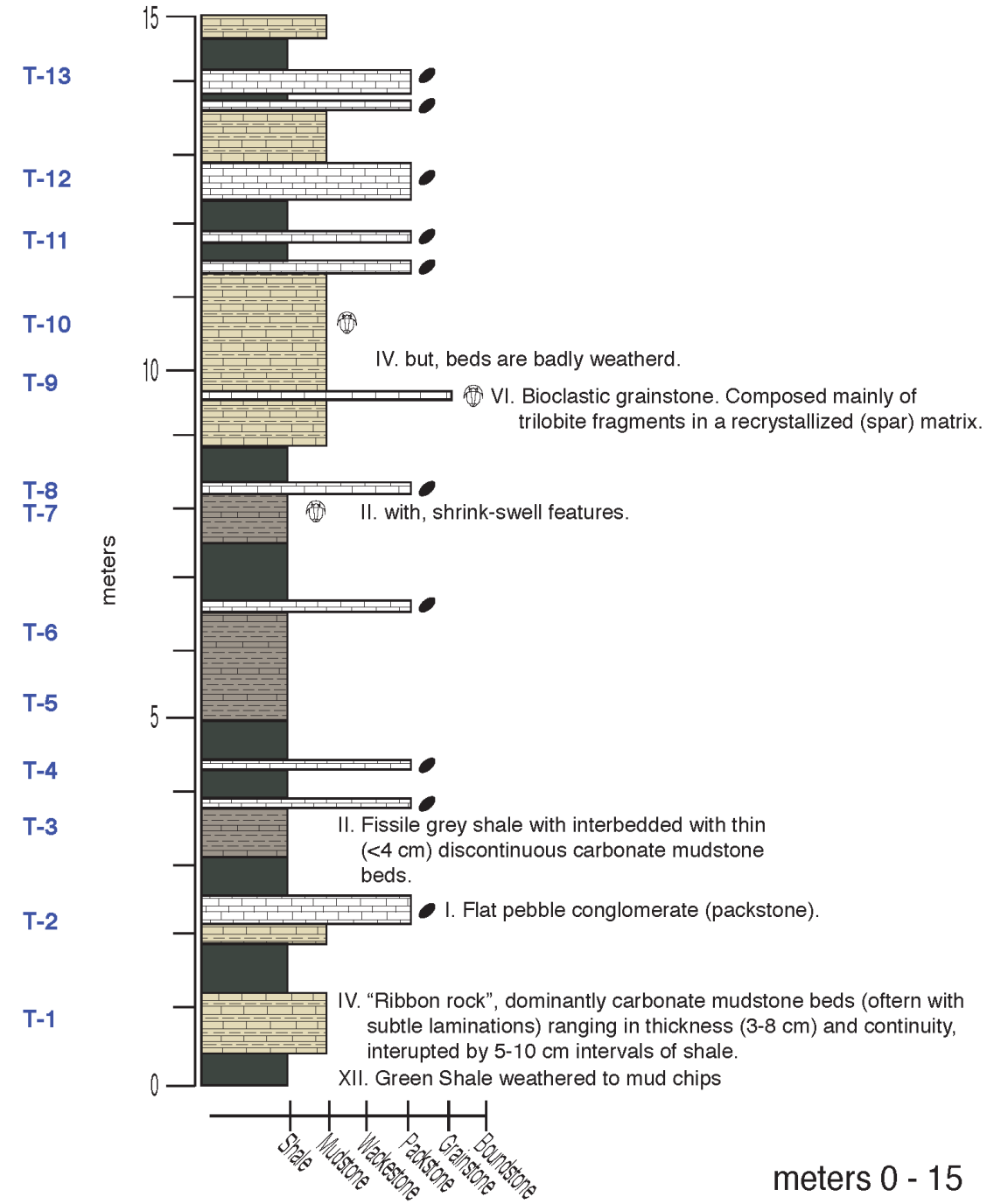

Three Springs Section

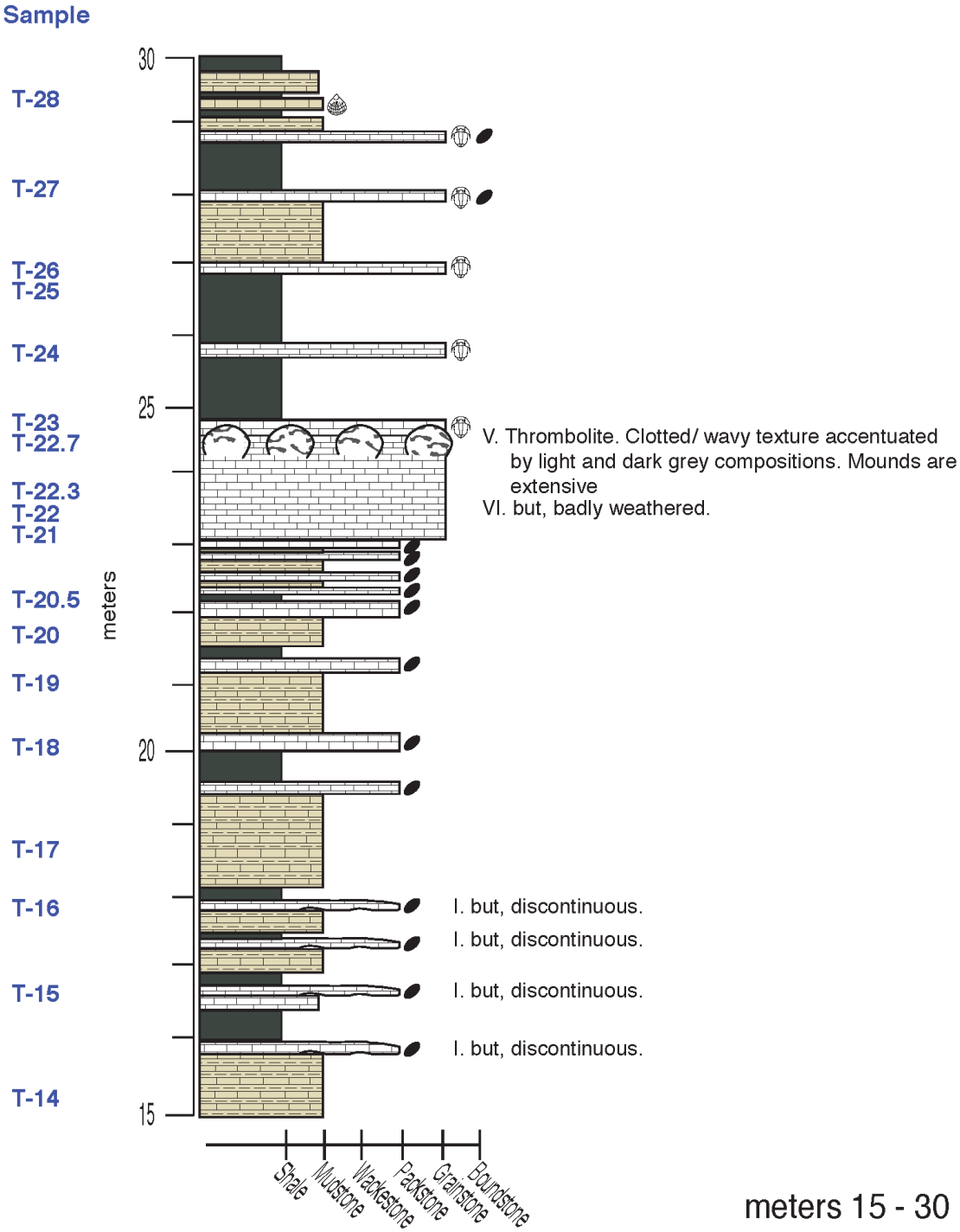

meters 15 - 30

Three Springs Section

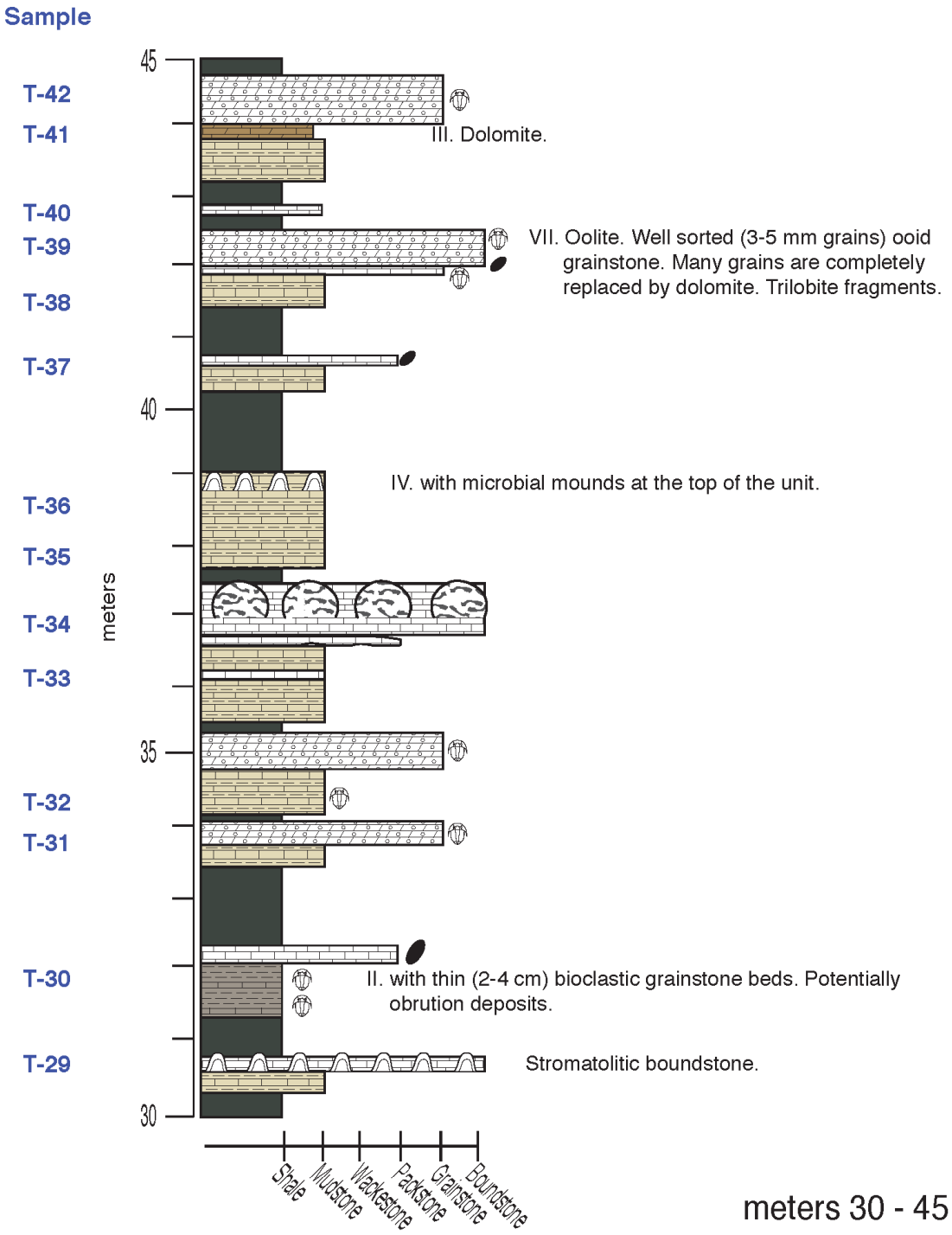

Three Springs Section

Sample

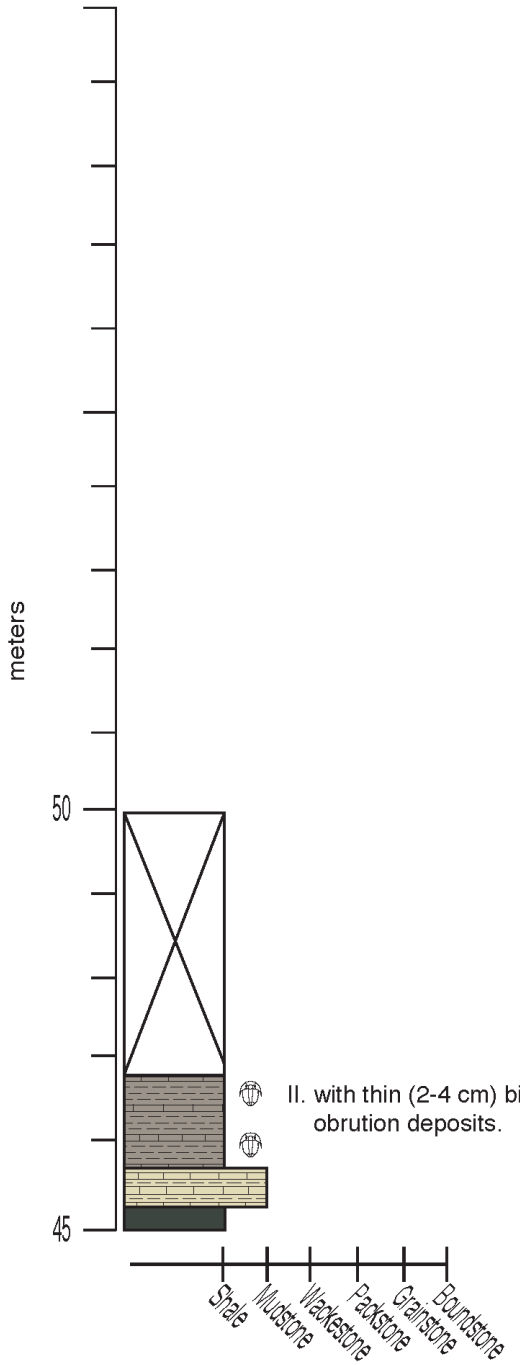

T-44

II. with thin (2-4 cm) bioclastic grainstone beds. Potentially obrution deposits.

T-43

meters 45 - 50

Duffield Section

36.70140°N, 082.77380°W
Elevation: 501m, Attitude: 34°, 24°S

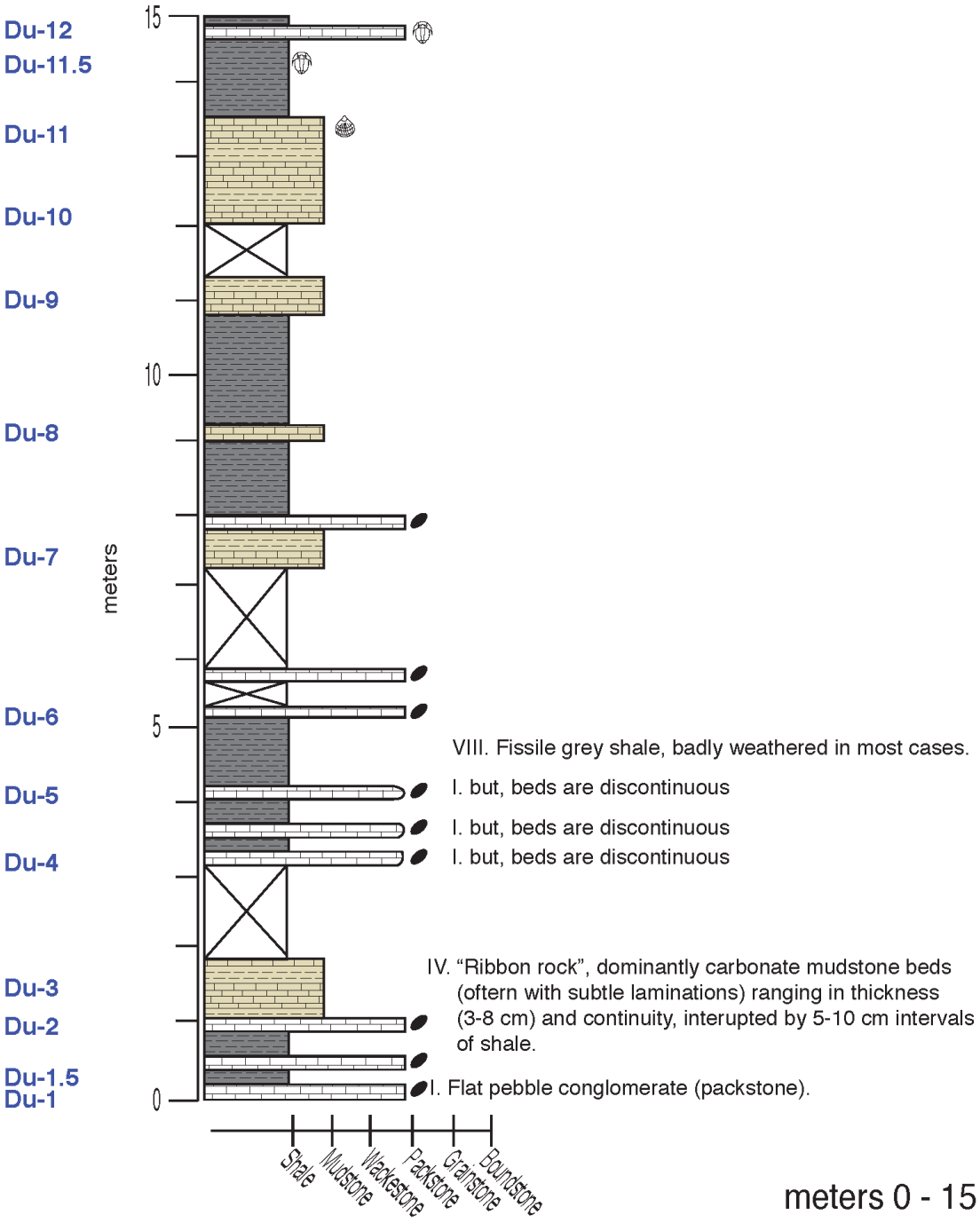

Duffield Section

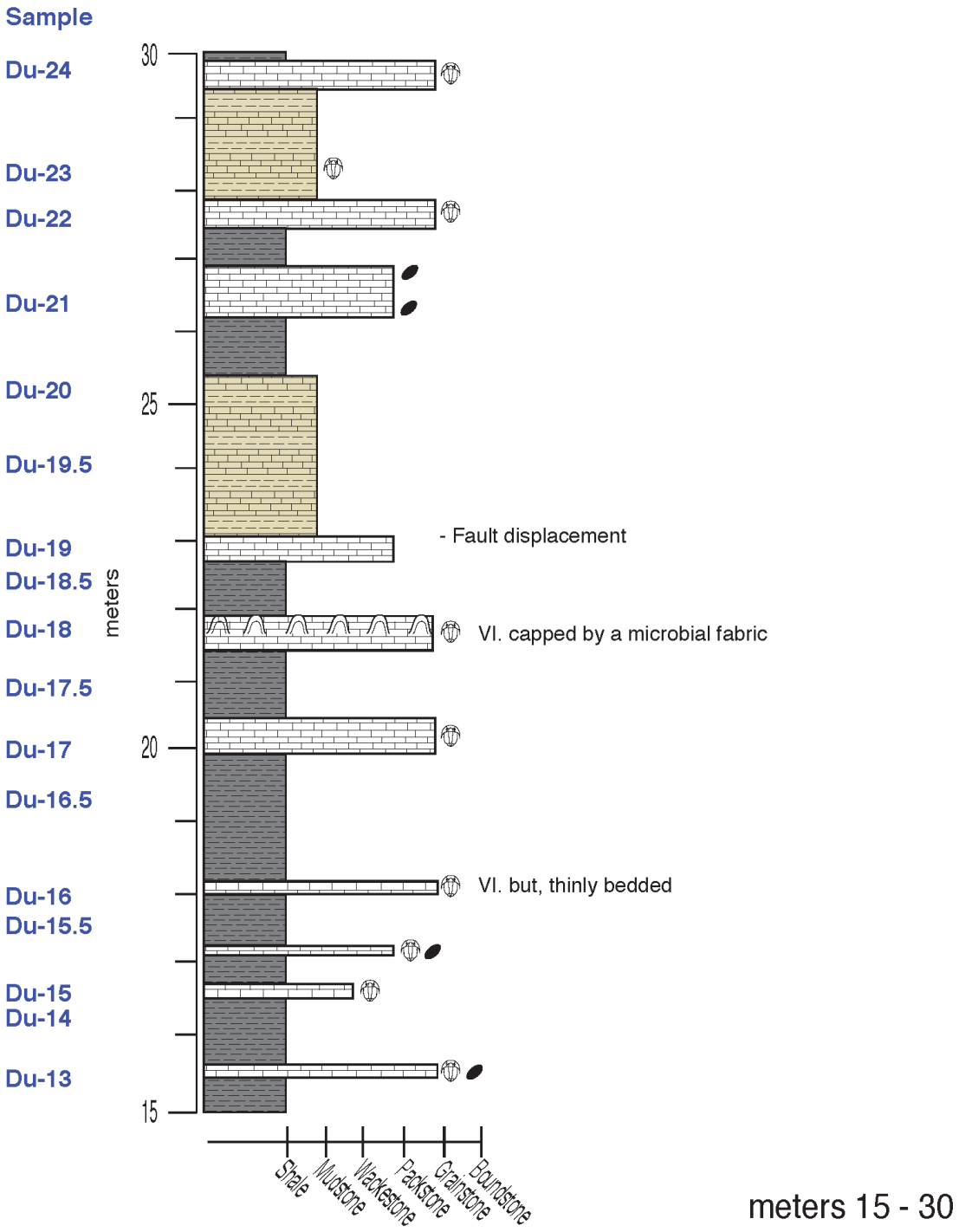

meters 15 - 30

Duffield Section

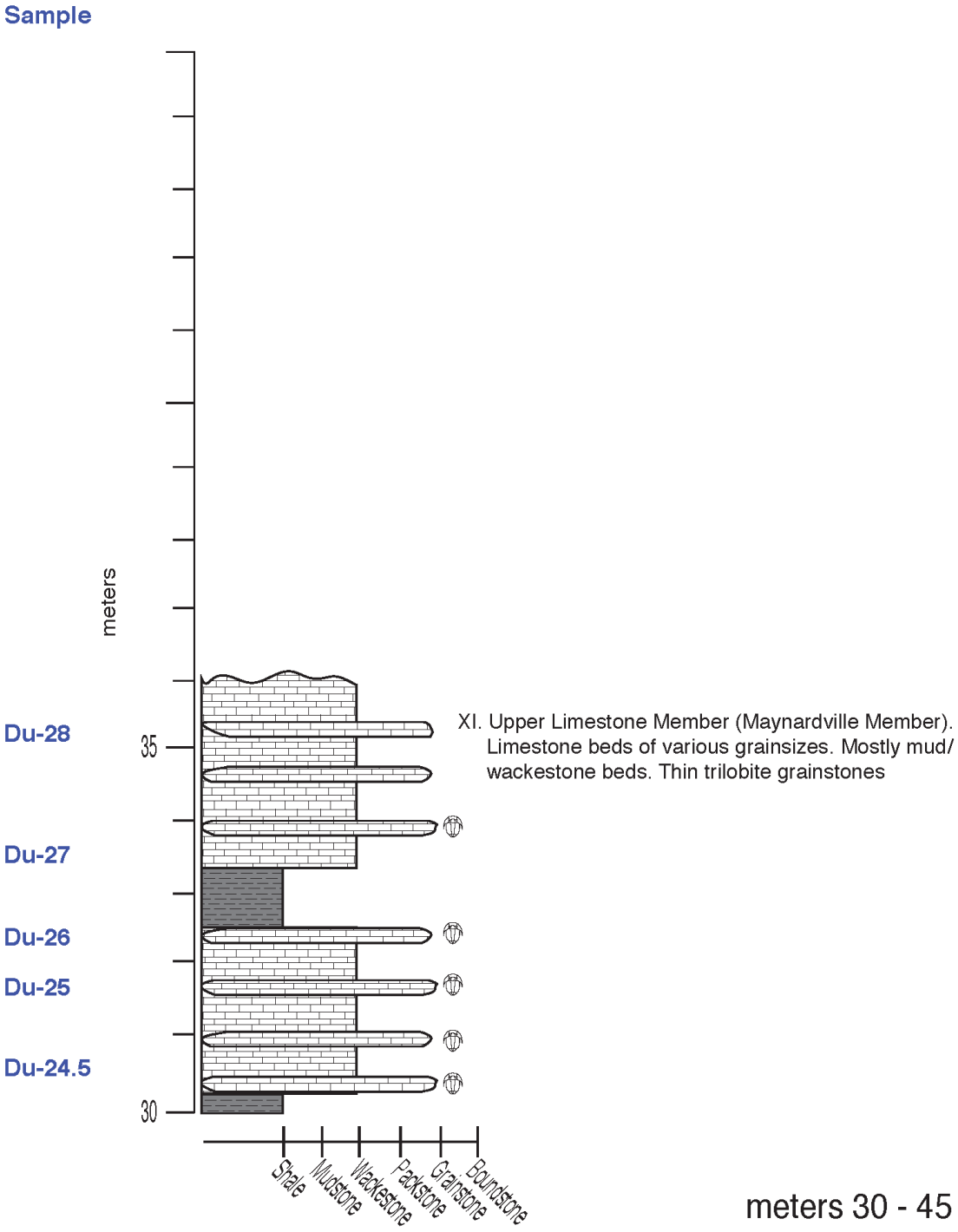

Lebanon Section

36.87977°N, 082.10737°W
Elevation: 675m , Attitude: 98°, 28°S

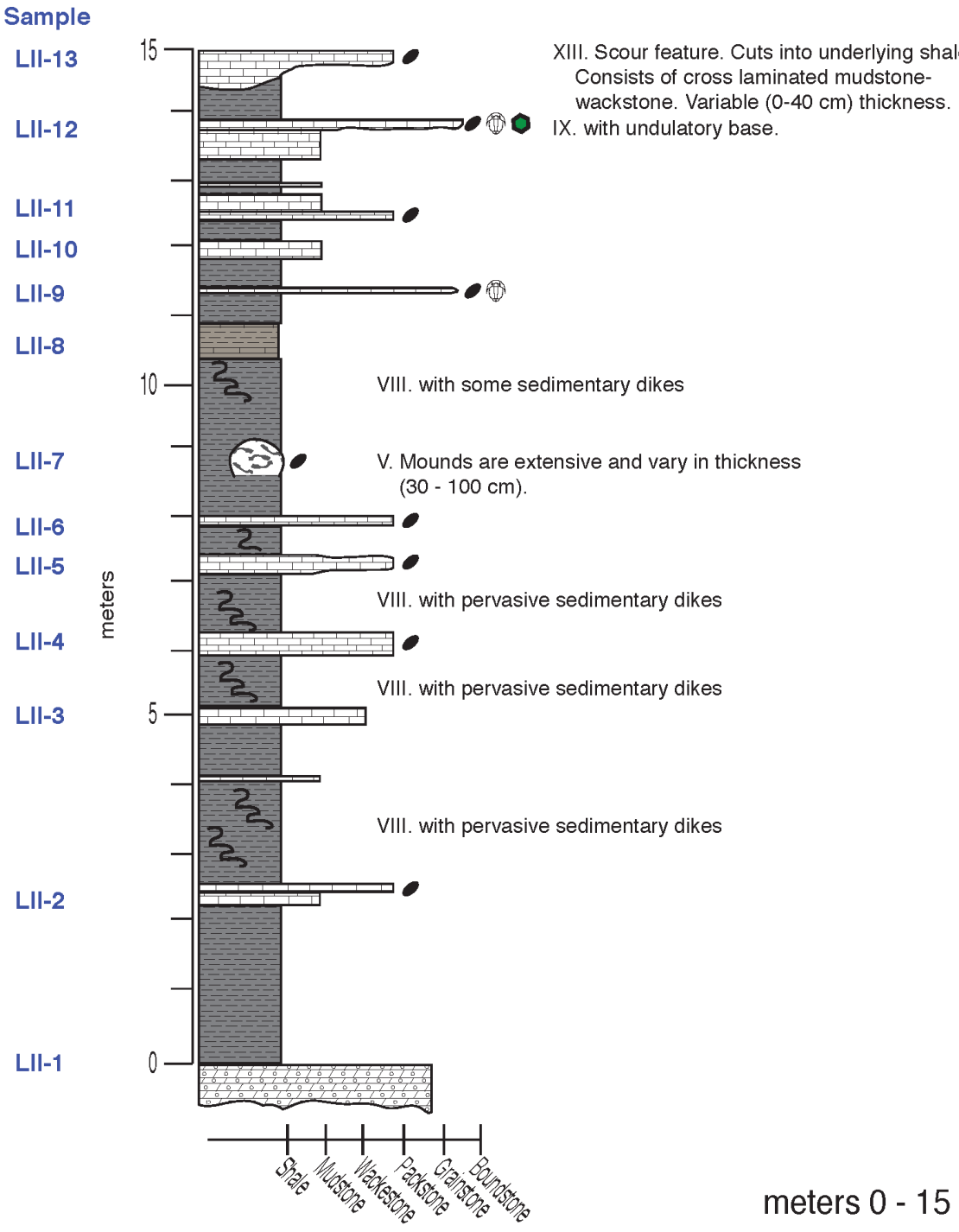

Lebanon Section

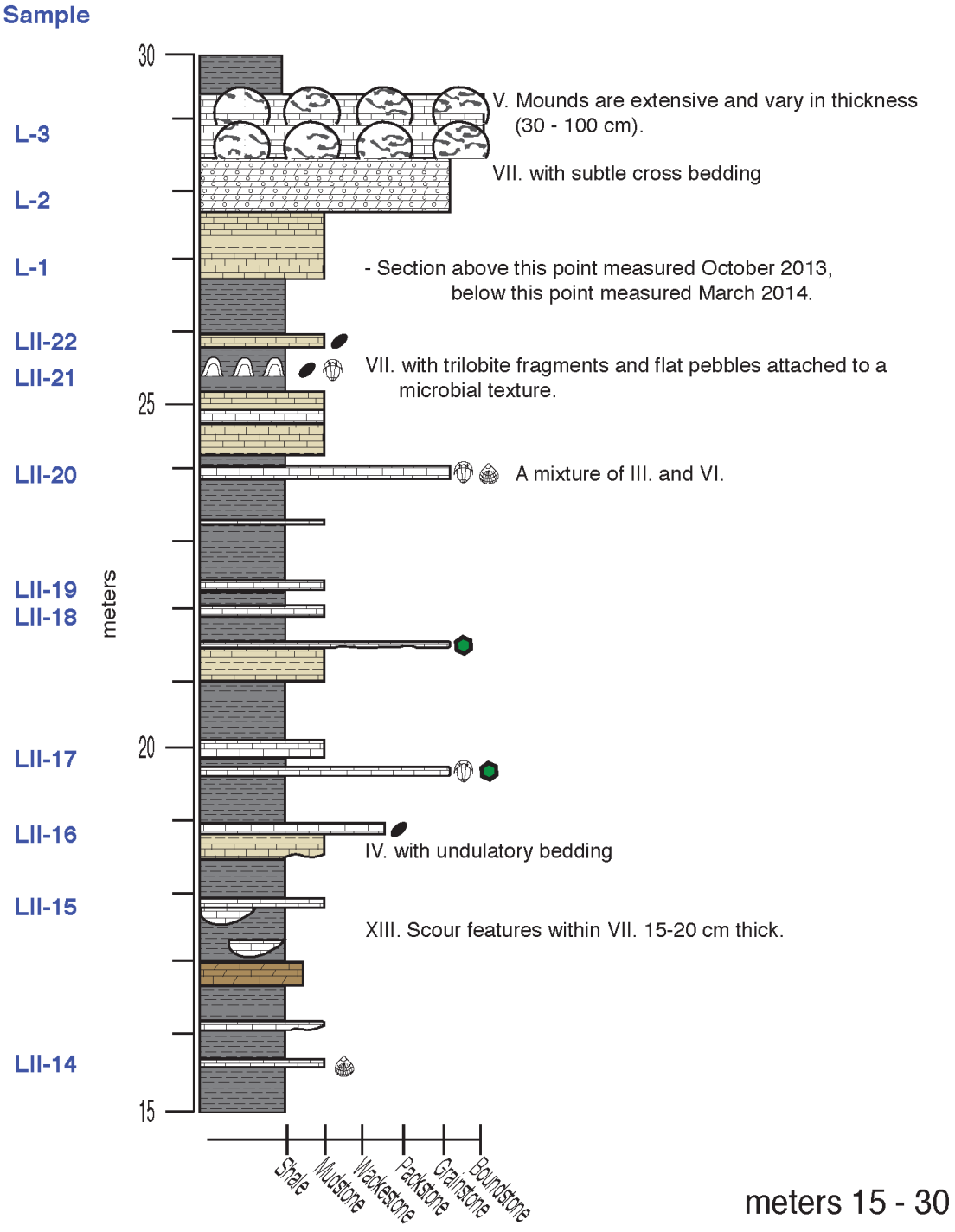

Lebanon Section

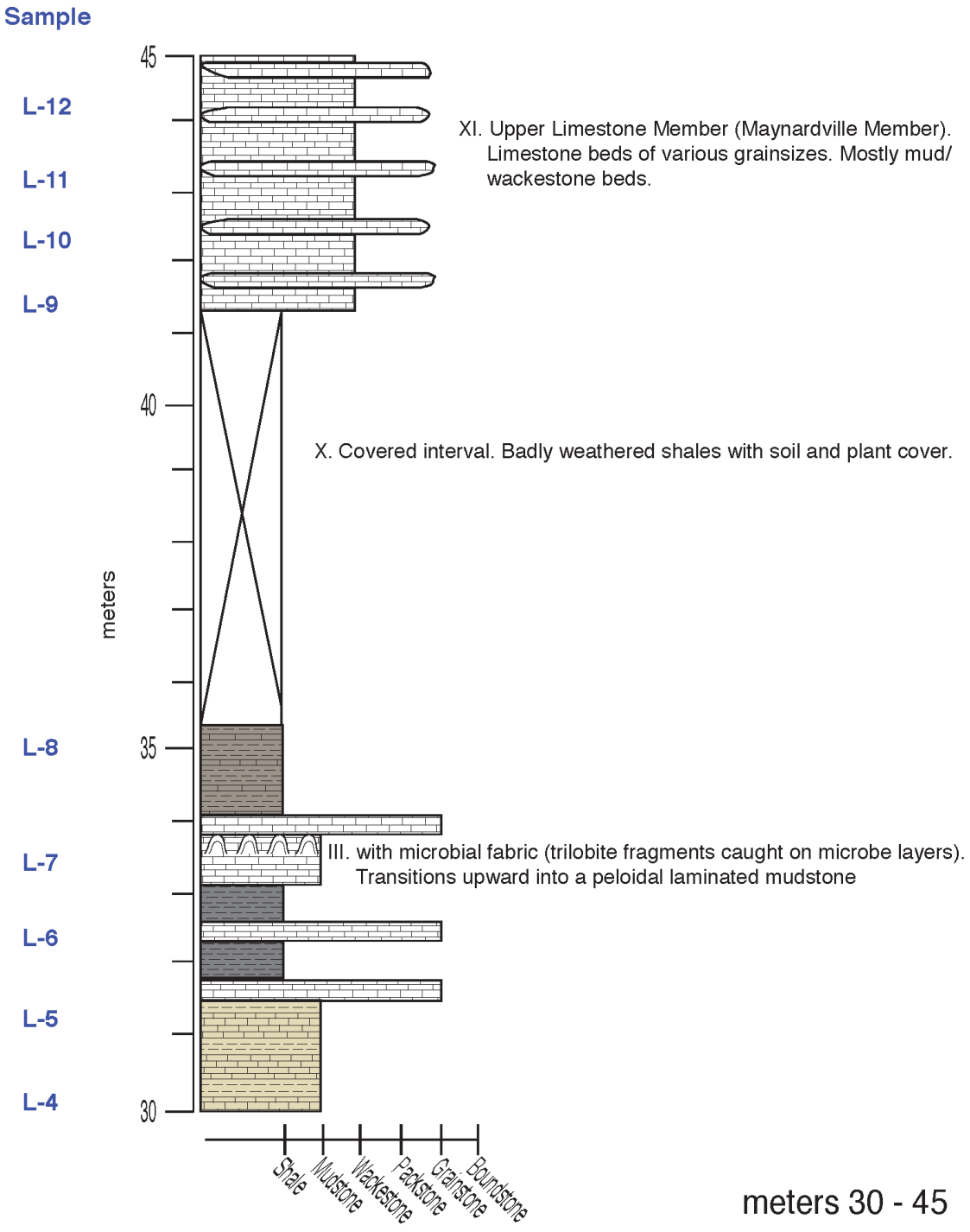

Lebanon Section

Sample

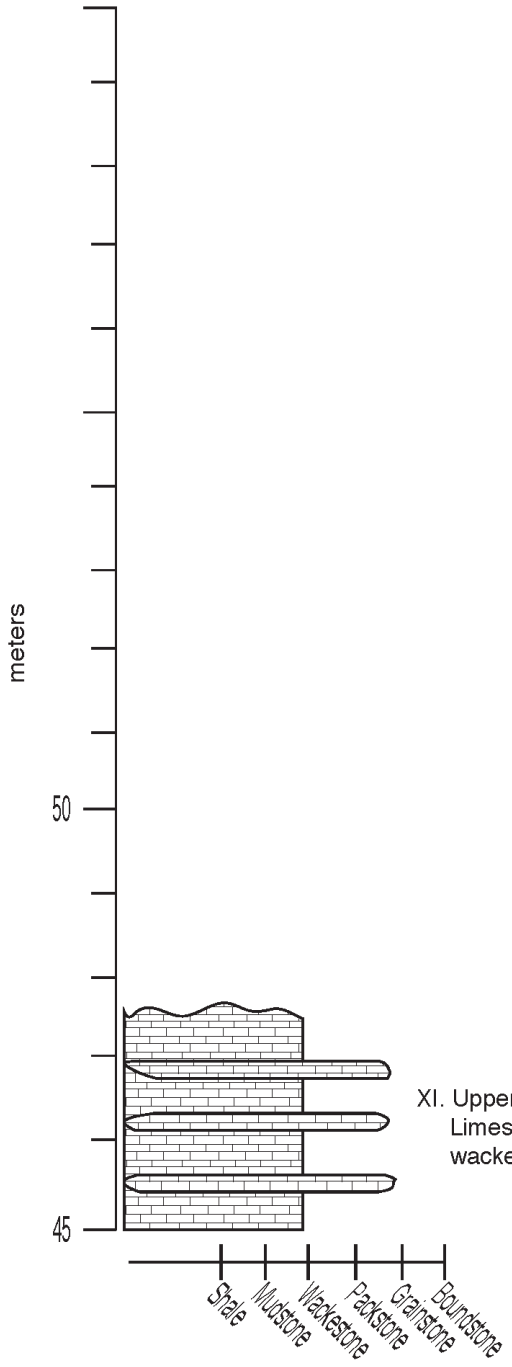

XI. Upper Limestone Member (Maynardville Member). Limestone beds of various grainsizes. Mostly mud/ wackestone beds.

L-13

meters 45 - 48

Appendix B

Geochemical data from the Nolichucky Formation:

The following is a list of abbreviations in Appendix B. FPC: flat pebble conglomerate, MSt: mudstone, WkSt: wackestone, PkSt: packstone, GSt: grainstone, Throm: thrombolite, Tr: Trilobite, Cal-Shale: Calcareous Shale, m: meters.

Nolichucky Formation – Isotope Values and Elemental Concentrations												
Sample Name	m	Description	$\delta^{13}C$	$\delta^{18}O$	[Al] ppm	[Mg] ppm	[Mn] ppm	[Sr] ppm	[Ca] ppm	[Fe] ppm	[Ca] wt%	[Mg] wt%
D-1	0.1	FPC	-0.15	-7.73	471	3848	627	335	290906	3854	29.09	0.38
D-2	1	FPC	-0.12	-7.74	147	4004	624	387	334943	3200	33.49	0.40
D-3	2	FPC	-0.04	-7.31	96	2985	551	360	291171	2913	29.12	0.30
D-4	3	FPC	-0.06	-7.49	100	3304	502	344	300687	2828	30.07	0.33
D-5	4	FPC	-0.14	-7.44	117	4168	683	401	365393	3474	36.54	0.42
D-6a	5.5	Tr PkSt/ GSt	-0.35	-8.62	1270	3077	476	246	228968	3550	22.90	0.31
D-6b	5.5	Tr PkSt/ GSt	-0.49	-7.80	243	3177	802	325	318219	4717	31.82	0.32
D-8	7.5	MSt	-0.20	-8.01	231	3106	516	319	298427	3665	29.84	0.31
D-9	8.5	Throm	-0.07	-0.07	239	3725	401	322	303004	3238	30.30	0.37
D-10	9.5	MSt	0.04	-7.51	157	3725	283	488	343318	2176	34.33	0.37
D-11a	10.5	Throm	0.06	-7.72	244	4216	228	567	348206	2131	34.82	0.42
D-11b	10.5	Throm	0.11	-7.54	193	4591	227	640	350633	2226	35.06	0.46
D-12	11.5	WkSt	-0.06	-7.65	211	3953	255	404	329241	1823	32.92	0.40
D-13	12.5	MSt	0.00	-7.83	150	3672	268	504	351113	1989	35.11	0.37
D-14a	13.75	FPC	-0.24	-7.17	127	3963	236	460	417909	2222	41.79	0.40
D-14b	13.75	FPC	-0.10	-7.52	105	4335	235	470	415191	1402	41.52	0.43
D-15	14.5	MSt	0.20	-7.50	94	3693	204	578	407775	1511	40.78	0.37
D-16	15.5	WkSt	0.18	-7.81	155	2531	253	273	266081	1922	26.61	0.25
D-17	16.5	Throm	-0.29	-7.35	248	3663	243	295	272375	1624	27.24	0.37
D-18a	17.5	Throm	0.57	-7.48	176	4360	171	689	355899	1475	35.59	0.44
D-18b	17.5	Throm			187	4552	165	703	359658	1462	35.97	0.46
D-19	18.5	Throm	0.56	-7.54	170	3532	161	508	302495	1095	30.25	0.35
D-20	19.5	Oo	0.51	-7.73	68	4135	178	382	247648	1597	24.76	0.41

D-21	20	Oo			75	7540	288	389	280557	4227	28.06	0.75
D-22	21.5	Oo	1.06	-8.41	78	4153	121	456	234921	1246	23.49	0.42
D-23	22.5	Oo	0.72	-7.66	72	3412	343	463	306816	2280	30.68	0.34
D-27	26.75	FPC	0.22	-7.82	182	3039	617	316	291784	3972	29.18	0.30
D-29a	28.5	FPC	-0.13	-7.52	256	2450	1009	262	243936	5814	24.39	0.25
D-29b	28.5	FPC	0.12	-8.04	365	3021	1076	259	262542	4984	26.25	0.30
D-30a	29.5	MSt	0.44	-8.64	431	6612	834	113	156194	7201	15.62	0.66
D-30b	29.5	FPC	0.04	-7.64	180	2292	835	216	231804	4250	23.18	0.23
D-31a	30.75	WkSt	0.19	-8.08	226	2798	957	294	294796	4533	29.48	0.28
D-31b	30.75	WkSt	-0.28	-7.64	750	1405	518	105	138382	2452	13.84	0.14
D-33a	32	FPC	0.37	-7.78	232	3396	880	341	257923	3579	25.79	0.34
D-33b	32	FPC	0.33	-7.86	269	3084	1000	326	251370	4191	25.14	0.31
D-35	34.25	FPC	0.16	-7.47	316	3584	1266	289	245550	2241	24.55	0.36
D-36a	35	MSt	-0.04	-7.68	766	1889	861	135	171590	3004	17.16	0.19
D-36b	35	MSt	0.47	-7.93	691	2382	1064	263	248842	6423	24.88	0.24
D-38	36.25	MSt	0.97	-8.35	346	3294	840	185	196160	5178	19.62	0.33
D-39	37.25	MSt	0.78	-8.87	432	5531	725	104	149325	6495	14.93	0.55
D-40a	38	FPC	0.45	-8.42	240	3136	1215	251	241253	3673	24.13	0.31
D-40b	38	FPC	0.42	-7.80	281	3074	2054	326	305035	3316	30.50	0.31
D-41	39.25	MSt	0.67	-9.54	737	7949	674	62	96691	8016	9.67	0.79
D-42	41	MSt	0.57	-9.75	400	5084	728	80	105229	5906	10.52	0.51
D-43a	42.75	MSt	0.09	-8.45	663	1266	528	83	114592	2080	11.46	0.13
D-43b	42.75	MSt	0.51	-9.71	646	5211	559	74	96806	5344	9.68	0.52
D-44	44.25	MSt	0.70	-9.15	619	7610	711	96	113208	7422	11.32	0.76
D-45	46.25	MSt	0.87	-9.13	548	12160	700	57	83307	10667	8.33	1.22
D-46	47.5	MSt	0.91	-8.73	176	2464	1210	312	263784	3481	26.38	0.25
D-47	47.6	MSt	0.16	-8.29	189	3399	2019	308	346117	1893	34.61	0.34

D-48	53	MSt	-3.82	-12.54	720	320	227	4	1372	766	0.14	0.03
D-49	59.6	MSt	3.27	-7.82	113	4328	163	749	383734	1523	38.37	0.43
D-50a	60.52	MSt	3.70	-6.44	1227	23765	164	151	78131	5874	7.81	2.38
D-50b	60.52	MSt	3.27	-7.44	171	4156	121	747	288149	1233	28.81	0.42
D-51	61.5	MSt	3.51	-7.36	190	5040	100	784	311197	943	31.12	0.50
D-52	62.52	MSt	2.78	-6.22	337	19196	172	340	195082	1470	19.51	1.92
D-53	63.52	MSt	3.39	-6.92	290	15641	129	416	204157	2530	20.42	1.56
D-54	64.6	MSt	3.57	-6.75	169	6144	82	927	383260	868	38.33	0.61
D-55	65.6	MSt	3.75	-6.45	682	17250	100	374	175474	2739	17.55	1.72
D-56	66.55	MSt	3.44	-6.88	154	4404	82	802	395703	488	39.57	0.44
D-57	67.8	MSt	3.51	-7.79	181	4154	107	362	269516	1383	26.95	0.42
L-1	0.1	MSt	0.83	-8.19	812	9099	383	34	53709	6389	5.37	0.91
L-2	1	Dolomite	-1.14	-7.03	502	2232	722	39	104498	4344	10.45	0.22
L-3	2	Throm	1.45	-8.54	105	4953	489	315	354349	2645	35.43	0.50
L-4	3.2	MSt	0.92	-8.57	836	6047	227	26	35468	4142	3.55	0.60
L-5	4.2	Tr PkSt/ GSt	0.82	-8.58	158	2201	605	197	266339	1347	26.63	0.22
L-6	5.5	MSt	0.94	-8.42	52	2169	541	208	229549	867	22.95	0.22
L-7	6.47	FPC	1.93	-6.92	550	16468	349	74	67856	6504	6.79	1.65
L-8	7.8	MSt	1.92	-6.73	555	20264	442	95	93049	7129	9.30	2.03
L-9a	8.4	MSt	3.46	-6.94	164	5841	92	940	357505	1037	35.75	0.58
L-9b	8.4	MSt	3.61	-6.06	669	27958	119	210	95745	4115	9.57	2.80
L-10a	9.4	Tr PkSt/ GSt	3.46	-6.34	363	28261	127	260	133959	3716	13.40	2.83
L-10b	9.4	Tr PkSt/ GSt	3.20	-7.36	117	10842	118	753	346106	1340	34.61	1.08
L-11a	10.3	MSt	3.61	-5.81	835	40714	142	345	133863	5049	13.39	4.07
L-11b	10.3	MSt	3.50	-6.81	209	9127	102	968	365964	1210	36.60	0.91

L-12	11.3	MSt	3.54	-6.89	160	7191	89	923	377184	872	37.72	0.72
L-13	12.3	MSt	3.53	-7.06	138	6274	97	941	380495	1027	38.05	0.63
Du-1	0.25	FPC	0.33	-7.20	174	3121	971	328	255651	1956	25.57	0.31
Du-1.5	0.5	Cal-Shale	-1.90	-10.88	873	625	52	15	8980	778	0.90	0.06
Du-2	1	FPC	0.23	-7.14	225	3080	1321	285	282785	2187	28.28	0.31
Du-3	1.25	FPC	0.97	-9.52	379	15044	1055	63	85205	11815	8.52	1.50
Du-4	3.25	FPC	0.25	-6.90	212	3768	913	231	210367	4277	21.04	0.38
Du-5	4	FPC	0.48	-7.05	291	4078	1303	374	351652	3399	35.17	0.41
Du-6	5.25	FPC	0.06	-6.79	143	3188	1361	290	232607	1948	23.26	0.32
Du-7	7.25	MSt	-0.06	-6.94	173	3733	1965	398	264400	910	26.44	0.37
Du-8	9	MSt	1.20	-9.03	779	13757	993	75	72281	11159	7.23	1.38
Du-9	11	Throm	0.72	-7.00	240	2787	1297	384	237247	1704	23.72	0.28
Du-10	12	MSt	0.92	-9.15	259	4207	1031	231	165878	4523	16.59	0.42
Du-11	13.5	MSt	1.36	-8.63	520	18752	1258	81	83388	12537	8.34	1.88
Du-12	15	Throm	1.11	-7.77	226	2919	2620	352	254275	2883	25.43	0.29
Du-13	15.5	MSt	1.59	-7.83	223	3378	1348	324	216439	3109	21.64	0.34
Du-15	16.75	MSt	1.13	-8.47	230	2229	1361	380	245330	3219	24.53	0.22
Du-16	18	MSt	1.73	-8.45	419	12113	1357	218	179272	6401	17.93	1.21
Du-17	20	MSt	0.86	-7.07	266	2790	1413	380	261660	2573	26.17	0.28
Du-18	21.75	Throm	1.00	-7.17	198	4557	1342	525	339100	2400	33.91	0.46
Du-19	22.75	MSt	0.72	-7.04	236	2958	1044	515	323625	3171	32.36	0.30
Du-20	25.25	MSt	1.99	-6.89	255	2165	1150	355	233137	2823	23.31	0.22
Du-21	26.25	FPC	1.59	-8.57	210	2572	542	260	229645	1823	22.96	0.26
Du-22		Tr GSt			88	5663	648	500	307637	2680	30.76	0.57
Du-24	27.5	MSt	2.34	-9.66	229	2812	781	355	263716	1131	26.37	0.28
Du-24.5	28.25	Throm	2.75	-8.72	580	9354	193	37	36820	4092	3.68	0.94
Du-25	31.75	MSt	2.72	-9.14	275	9084	392	167	148590	3825	14.86	0.91

Du-26	32.5	WkSt	2.52	-10.72	629	6073	154	40	37584	2930	3.76	0.61
Du-27	33.5	MSt	1.45	-6.70	297	3619	288	449	280010	996	28.00	0.36
Du-28	35.25	MSt	3.41	-6.61	391	4698	149	719	338500	1411	33.85	0.47
T-1	0.75	MSt	0.00	-10.73	599	2598	1215	231	195566	3415	19.56	0.26
T-2	2	MSt	0.43	-10.88	175	2015	1213	238	196580	3252	19.66	0.20
T-3	3.5	MSt	0.48	-10.31	114	2643	1569	335	270405	3550	27.04	0.26
T-4	4.25	FPC	0.50	-10.00	418	3788	2084	457	348087	3669	34.81	0.38
T-5	5.25	MSt	-0.34	-11.04	624	1019	729	135	117920	2680	11.79	0.10
T-6	6.25	MSt	-0.26	-10.49	590	1251	1039	177	155327	3228	15.53	0.13
T-7	8	MSt	0.30	-9.93	116	2415	1166	298	224499	2492	22.45	0.24
T-8	8.25	FPC	0.43	-10.03	276	2903	2006	348	279686	2628	27.97	0.29
T-9	10	MSt	-0.06	-10.88	602	1230	872	172	142469	2919	14.25	0.12
T-10	10.5	MSt	-0.18	-11.21	588	1076	800	159	121543	2836	12.15	0.11
T-11	11.75	FPC	0.11	-10.02	241	2587	2240	396	255045	3379	25.50	0.26
T-12	12.8	Tr WkSt			191	3372	1749	502	315472	3479	31.55	0.34
T-13	14	FPC	0.65	-10.06	358	3102	2271	465	316294	3285	31.63	0.31
T-14	15	MSt	0.31	-11.20	382	1975	983	166	146812	3516	14.68	0.20
T-15	16.75	FPC	0.17	-9.83	287	3036	2466	350	302577	2305	30.26	0.30
T-16	17.75	FPC			195	2961	1701	338	262955	1606	26.30	0.30
T-17	18.5	MSt	0.36	-11.63	365	1453	997	192	156064	3427	15.61	0.15
T-18	20.25	FPC	0.40	-9.59	220	2772	1959	299	261499	1633	26.15	0.28
T-19	21	MSt	0.41	-11.11	368	2819	813	168	132758	3588	13.28	0.28
T-20	21.5	MSt	0.75	-9.92	67	2601	872	340	238269	1376	23.83	0.26
T-20.5	22.25	FPC	0.62	-10.15	244	2838	1056	322	255375	2224	25.54	0.28
T-21	23	MSt	0.37	-11.08	467	1941	714	135	122518	3043	12.25	0.19
T-22	23.25	MSt	0.25	-10.38	253	2189	1247	285	199454	3020	19.95	0.22
T-22.3	23.5	MSt	0.25	-11.63	492	2981	827	159	125464	3855	12.55	0.30

T-22.7	24.5	MSt			118	3378	1673	419	270995	2040	27.10	0.34
T-24	25.75	MSt			86	3858	2394	505	299313	2070	29.93	0.39
T-25	26.75	MSt - ReXL	-1.20	-10.13	995	677	178	32	23617	1606	2.36	0.07
T-28	29.25	MSt	1.43	-9.38	863	5746	382	67	37520	3532	3.75	0.57
T-27	27.9	Tr GSt			43	4081	2438	613	347251	1251	34.73	0.41
T-29	30.6	Tr GSt			309	3822	1021	396	272292	3271	27.23	0.38
T-30	32	FPC	0.13	-10.64	296	3909	1611	455	296998	923	29.70	0.39
T-31	33.9	MSt			365	2858	892	334	276863	1369	27.69	0.29
T-33	36.25	MSt	1.33	-10.05	107	2180	759	354	219629	992	21.96	0.22
T-35	37.9	MSt			135	2963	378	130	102976	1957	10.30	0.30
T-36	38.75	MSt	1.59	-9.98	153	3428	573	410	277002	1228	27.70	0.34
T-37	40.75	MSt			98	4434	1827	602	332498	913	33.25	0.44
T-38	41.5	MSt	2.33	-10.54	306	1023	500	118	91958	1575	9.20	0.10
T-40	43	Tr PkSt/ GSt	0.24	-9.80	457	3988	1184	490	341290	1531	34.13	0.40
T-41	44	MSt	2.22	-8.58	305	3732	220	614	358359	1145	35.84	0.37
T-42	44.5	MSt	2.90	-7.65	482	14087	263	72	43634	4383	4.36	1.41
T-43	45.5	MSt	1.00	-8.20	120	3312	599	604	309478	980	30.95	0.33
T-44	46.75	Tr PkSt	2.82	-7.90	137	3403	319	512	275483	788	27.55	0.34
W-1	0.5	MSt	-0.17	-9.41	571	2061	769	176	184639	3249	18.46	0.21
W-2	1	FPC	0.42	-8.21	301	3664	1414	393	358904	1784	35.89	0.37
W-3	3	MSt	0.50	-7.57	113	3333	1272	404	299550	1774	29.96	0.33
W-4	3.75	MSt	0.76	-7.73	123	3464	1012	452	348331	2131	34.83	0.35
W-5	5	MSt	0.39	-7.86	179	3353	846	426	336546	2035	33.65	0.34
W-5.5	5.75	MSt	0.78	-7.73	72	3388	1043	574	355403	1996	35.54	0.34
W-6	6.33	MSt - ReXL			208	3805	1232	437	323079	2165	32.31	0.38
W-7	7		0.53	-7.77	147	3713	984	463	345100	2494	34.51	0.37

W-8a	8	MSt	0.55	-8.05	409	4279	2143	432	347325	2552	34.73	0.43
W-8b	8	MSt	0.31	-7.72	493	4160	2209	415	360660	3140	36.07	0.42
W-9	8.9				178	4395	770	332	246651	2736	24.67	0.44
W-10	9.75	MSt	0.68	-8.32	129	5126	1268	472	376268	3587	37.63	0.51
W-11	11	MSt	-0.29	-7.32	81	3267	781	522	353613	2916	35.36	0.33
W-12a	11.25	FPC	0.47	-7.92	221	3876	809	472	343892	2250	34.39	0.39
W-12b	11.25	FPC	0.45	-7.95	397	4961	982	446	344675	3187	34.47	0.50
W-13	11.75	MSt	0.78	-7.89	278	3163	1563	386	307929	1865	30.79	0.32
W-14	12.33	MSt	0.79	-7.55	106	4811	642	471	357241	2701	35.72	0.48
W-15	12.8	Tr WkSt			70	4863	619	576	387123	2058	38.71	0.49
W-19	16.5	Tr WkSt	0.02	-7.44	257	3803	2082	398	280935	1850	28.09	0.38
W-20	17.5	MSt	0.95	-7.52	433	3589	2291	416	340561	2354	34.06	0.36
W-16	14.5				87	5293	417	445	300351	1957	30.04	0.53
W-21	18.25	Conc	-0.10	-7.29	330	4255	2399	401	339438	853	33.94	0.43
W-22	19.25	Tr GSt	0.76	-7.23	140	4994	1689	556	367753	651	36.78	0.50
W-24	20	MSt	1.13	-7.41	223	3902	1554	342	303875	789	30.39	0.39
W-25	20.5	MSt	1.12	-7.49	327	3753	1456	371	344580	855	34.46	0.38
W-28	23.25	Cal-Shale	0.37	-7.70	386	2832	1152	482	304617	3210	30.46	0.28
W-29	25	MSt	0.65	-7.41	194	4547	1813	582	340851	1386	34.09	0.45
W-30	26.5	Conc	0.40	-7.46	371	3323	2873	397	364389	1008	36.44	0.33
W-31	27.9				70	3492	552	197	135947	1314	13.59	0.35
W-32	28.5	Tr WkSt	1.45	-7.54	307	3836	763	599	361721	3147	36.17	0.38
W-33	29.5	MSt	1.63	-7.45	164	4021	1116	636	367675	2062	36.77	0.40
W-34	34.75	MSt			153	4866	1813	719	384859	745	38.49	0.49
W-36	36.5	Tr PkSt	1.88	-7.22	307	5026	2012	769	358136	1230	35.81	0.50
W-37	37	MSt	1.82	-7.16	88	4318	1409	741	373698	1522	37.37	0.43
W-38a	39	Cal-Shale	2.70	-7.03	340	5268	153	622	369874	867	36.99	0.53

W-38b	39	FPC	3.14	-7.35	588	24805	352	231	126884	5830	12.69	2.48
W-39	39.5	MSt	2.07	-7.67	148	5221	363	564	361837	1514	36.18	0.52
W-40	41.5	Cal-Shale	3.57	-7.77	937	19862	204	218	112765	4783	11.28	1.99
W-41	44.5	MSt	3.29	-7.36	118	12314	104	670	297936	1652	29.79	1.23
W-42	45.5	Cal-Shale	4.06	-7.90	526	36602	157	135	118785	4934	11.88	3.66
W-44	50	Tr PkSt	1.99	-6.69	151	4064	226	675	354953	1258	35.50	0.41

Nolichucky Formation – Element/Calcium							
Sample Name	**m**	**Description**	**Al/Ca**	**Mg/Ca**	**Mn/Ca**	**Sr/Ca**	**Fe/Ca**
D-1	0.1	FPC	0.0016	0.0132	0.0022	0.0012	0.0132
D-2	1	FPC	0.0004	0.0120	0.0019	0.0012	0.0096
D-3	2	FPC	0.0003	0.0103	0.0019	0.0012	0.0100
D-4	3	FPC	0.0003	0.0110	0.0017	0.0011	0.0094
D-5	4	FPC	0.0003	0.0114	0.0019	0.0011	0.0095
D-6a	5.5	Tr PkSt/ GSt	0.0055	0.0134	0.0021	0.0011	0.0155
D-6b	5.5	Tr PkSt/ GSt	0.0008	0.0100	0.0025	0.0010	0.0148
D-8	7.5	MSt	0.0008	0.0104	0.0017	0.0011	0.0123
D-9	8.5	Throm	0.0008	0.0123	0.0013	0.0011	0.0107
D-10	9.5	MSt	0.0005	0.0108	0.0008	0.0014	0.0063
D-11a	10.5	Throm	0.0007	0.0121	0.0007	0.0016	0.0061
D-11b	10.5	Throm	0.0006	0.0131	0.0006	0.0018	0.0063
D-12	11.5	WkSt	0.0006	0.0120	0.0008	0.0012	0.0055
D-13	12.5	MSt	0.0004	0.0105	0.0008	0.0014	0.0057
D-14a	13.75	FPC	0.0003	0.0095	0.0006	0.0011	0.0053
D-14b	13.75	FPC	0.0003	0.0104	0.0006	0.0011	0.0034
D-15	14.5	MSt	0.0002	0.0091	0.0005	0.0014	0.0037
D-16	15.5	WkSt	0.0006	0.0095	0.0010	0.0010	0.0072
D-17	16.5	Throm	0.0009	0.0134	0.0009	0.0011	0.0060
D-18a	17.5	Throm	0.0005	0.0123	0.0005	0.0019	0.0041
D-18b	17.5	Throm	0.0005	0.0127	0.0005	0.0020	0.0041
D-19	18.5	Throm	0.0006	0.0117	0.0005	0.0017	0.0036
D-20	19.5	Oo	0.0003	0.0167	0.0007	0.0015	0.0064
D-21	20	Oo	0.0003	0.0269	0.0010	0.0014	0.0151

D-22	21.5	Oo	0.0003	0.0177	0.0005	0.0019	0.0053
D-23	22.5	Oo	0.0002	0.0111	0.0011	0.0015	0.0074
D-27	26.75	FPC	0.0006	0.0104	0.0021	0.0011	0.0136
D-29a	28.5	FPC	0.0010	0.0100	0.0041	0.0011	0.0238
D-29b	28.5	FPC	0.0014	0.0115	0.0041	0.0010	0.0190
D-30a	29.5	MSt	0.0028	0.0423	0.0053	0.0007	0.0461
D-30b	29.5	FPC	0.0008	0.0099	0.0036	0.0009	0.0183
D-31a	30.75	WkSt	0.0008	0.0095	0.0032	0.0010	0.0154
D-31b	30.75	WkSt	0.0054	0.0101	0.0037	0.0008	0.0177
D-33a	32	FPC	0.0009	0.0132	0.0034	0.0013	0.0139
D-33b	32	FPC	0.0011	0.0123	0.0040	0.0013	0.0167
D-35	34.25	FPC	0.0013	0.0146	0.0052	0.0012	0.0091
D-36a	35	MSt	0.0045	0.0110	0.0050	0.0008	0.0175
D-36b	35	MSt	0.0028	0.0096	0.0043	0.0011	0.0258
D-38	36.25	MSt	0.0018	0.0168	0.0043	0.0009	0.0264
D-39	37.25	MSt	0.0029	0.0370	0.0049	0.0007	0.0435
D-40a	38	FPC	0.0010	0.0130	0.0050	0.0010	0.0152
D-40b	38	FPC	0.0009	0.0101	0.0067	0.0011	0.0109
D-41	39.25	MSt	0.0076	0.0822	0.0070	0.0006	0.0829
D-42	41	MSt	0.0038	0.0483	0.0069	0.0008	0.0561
D-43a	42.75	MSt	0.0058	0.0111	0.0046	0.0007	0.0182
D-43b	42.75	MSt	0.0067	0.0538	0.0058	0.0008	0.0552
D-44	44.25	MSt	0.0055	0.0672	0.0063	0.0009	0.0656
D-45	46.25	MSt	0.0066	0.1460	0.0084	0.0007	0.1280
D-46	47.5	MSt	0.0007	0.0093	0.0046	0.0012	0.0132
D-47	47.6	MSt	0.0005	0.0098	0.0058	0.0009	0.0055
D-48	53	MSt	0.5250	0.2330	0.1652	0.0030	0.5580

D-49	59.6	MSt	0.0003	0.0113	0.0004	0.0020	0.0040
D-50a	60.52	MSt	0.0157	0.3042	0.0021	0.0019	0.0752
D-50b	60.52	MSt	0.0006	0.0144	0.0004	0.0026	0.0043
D-51	61.5	MSt	0.0006	0.0162	0.0003	0.0025	0.0030
D-52	62.52	MSt	0.0017	0.0984	0.0009	0.0017	0.0075
D-53	63.52	MSt	0.0014	0.0766	0.0006	0.0020	0.0124
D-54	64.6	MSt	0.0004	0.0160	0.0002	0.0024	0.0023
D-55	65.6	MSt	0.0039	0.0983	0.0006	0.0021	0.0156
D-56	66.55	MSt	0.0004	0.0111	0.0002	0.0020	0.0012
D-57	67.8	MSt	0.0007	0.0154	0.0004	0.0013	0.0051
L-1	0.1	MSt	0.0151	0.1694	0.0071	0.0006	0.1190
L-2	1	Dolomite	0.0048	0.0214	0.0069	0.0004	0.0416
L-3	2	Throm	0.0003	0.0140	0.0014	0.0009	0.0075
L-4	3.2	MSt	0.0236	0.1705	0.0064	0.0007	0.1168
L-5	4.2	Tr PkSt/ GSt	0.0006	0.0083	0.0023	0.0007	0.0051
L-6	5.5	MSt	0.0002	0.0094	0.0024	0.0009	0.0038
L-7	6.47	FPC	0.0081	0.2427	0.0051	0.0011	0.0958
L-8	7.8	MSt	0.0060	0.2178	0.0047	0.0010	0.0766
L-9a	8.4	MSt	0.0005	0.0163	0.0003	0.0026	0.0029
L-9b	8.4	MSt	0.0070	0.2920	0.0012	0.0022	0.0430
L-10a	9.4	Tr PkSt/ GSt	0.0027	0.2110	0.0010	0.0019	0.0277
L-10b	9.4	Tr PkSt/ GSt	0.0003	0.0313	0.0003	0.0022	0.0039
L-11a	10.3	MSt	0.0062	0.3041	0.0011	0.0026	0.0377
L-11b	10.3	MSt	0.0006	0.0249	0.0003	0.0026	0.0033
L-12	11.3	MSt	0.0004	0.0191	0.0002	0.0024	0.0023
L-13	12.3	MSt	0.0004	0.0165	0.0003	0.0025	0.0027
Du-1	0.25	FPC	0.0007	0.0122	0.0038	0.0013	0.0077

Du-1.5	0.5	Cal-Shale	0.0972	0.0696	0.0058	0.0017	0.0866
Du-2	1	FPC	0.0008	0.0109	0.0047	0.0010	0.0077
Du-3	1.25	FPC	0.0045	0.1766	0.0124	0.0007	0.1387
Du-4	3.25	FPC	0.0010	0.0179	0.0043	0.0011	0.0203
Du-5	4	FPC	0.0008	0.0116	0.0037	0.0011	0.0097
Du-6	5.25	FPC	0.0006	0.0137	0.0059	0.0012	0.0084
Du-7	7.25	MSt	0.0007	0.0141	0.0074	0.0015	0.0034
Du-8	9	MSt	0.0108	0.1903	0.0137	0.0010	0.1544
Du-9	11	Throm	0.0010	0.0117	0.0055	0.0016	0.0072
Du-10	12	MSt	0.0016	0.0254	0.0062	0.0014	0.0273
Du-11	13.5	MSt	0.0062	0.2249	0.0151	0.0010	0.1503
Du-12	15	Throm	0.0009	0.0115	0.0103	0.0014	0.0113
Du-13	15.5	MSt	0.0010	0.0156	0.0062	0.0015	0.0144
Du-15	16.75	MSt	0.0009	0.0091	0.0055	0.0015	0.0131
Du-16	18	MSt	0.0023	0.0676	0.0076	0.0012	0.0357
Du-17	20	MSt	0.0010	0.0107	0.0054	0.0015	0.0098
Du-18	21.75	Throm	0.0006	0.0134	0.0040	0.0015	0.0071
Du-19	22.75	MSt	0.0007	0.0091	0.0032	0.0016	0.0098
Du-20	25.25	MSt	0.0011	0.0093	0.0049	0.0015	0.0121
Du-21	26.25	FPC	0.0009	0.0112	0.0024	0.0011	0.0079
Du-22		Tr GSt	0.0003	0.0184	0.0021	0.0016	0.0087
Du-24	27.5	MSt	0.0009	0.0107	0.0030	0.0013	0.0043
Du-24.5	28.25	Throm	0.0157	0.2541	0.0052	0.0010	0.1111
Du-25	31.75	MSt	0.0018	0.0611	0.0026	0.0011	0.0257
Du-26	32.5	WkSt	0.0167	0.1616	0.0041	0.0011	0.0780
Du-27	33.5	MSt	0.0011	0.0129	0.0010	0.0016	0.0036
Du-28	35.25	MSt	0.0012	0.0139	0.0004	0.0021	0.0042

T-1	0.75	MSt	0.0031	0.0133	0.0062	0.0012	0.0175
T-2	2	MSt	0.0009	0.0102	0.0062	0.0012	0.0165
T-3	3.5	MSt	0.0004	0.0098	0.0058	0.0012	0.0131
T-4	4.25	FPC	0.0012	0.0109	0.0060	0.0013	0.0105
T-5	5.25	MSt	0.0053	0.0086	0.0062	0.0011	0.0227
T-6	6.25	MSt	0.0038	0.0081	0.0067	0.0011	0.0208
T-7	8	MSt	0.0005	0.0108	0.0052	0.0013	0.0111
T-8	8.25	FPC	0.0010	0.0104	0.0072	0.0012	0.0094
T-9	10	MSt	0.0042	0.0086	0.0061	0.0012	0.0205
T-10	10.5	MSt	0.0048	0.0089	0.0066	0.0013	0.0233
T-11	11.75	FPC	0.0009	0.0101	0.0088	0.0016	0.0132
T-12	12.8	Tr WkSt	0.0006	0.0107	0.0055	0.0016	0.0110
T-13	14	FPC	0.0011	0.0098	0.0072	0.0015	0.0104
T-14	15	MSt	0.0026	0.0134	0.0067	0.0011	0.0239
T-15	16.75	FPC	0.0009	0.0100	0.0081	0.0012	0.0076
T-16	17.75	FPC	0.0007	0.0113	0.0065	0.0013	0.0061
T-17	18.5	MSt	0.0023	0.0093	0.0064	0.0012	0.0220
T-18	20.25	FPC	0.0008	0.0106	0.0075	0.0011	0.0062
T-19	21	MSt	0.0028	0.0212	0.0061	0.0013	0.0270
T-20	21.5	MSt	0.0003	0.0109	0.0037	0.0014	0.0058
T-20.5	22.25	FPC	0.0010	0.0111	0.0041	0.0013	0.0087
T-21	23	MSt	0.0038	0.0158	0.0058	0.0011	0.0248
T-22	23.25	MSt	0.0013	0.0110	0.0063	0.0014	0.0151
T-22.3	23.5	MSt	0.0039	0.0238	0.0066	0.0013	0.0307
T-22.7	24.5	MSt	0.0004	0.0125	0.0062	0.0015	0.0075
T-24	25.75	MSt	0.0003	0.0129	0.0080	0.0017	0.0069
T-25	26.75	MSt - ReXL	0.0421	0.0287	0.0075	0.0014	0.0680

T-28	29.25	MSt	0.0230	0.1532	0.0102	0.0018	0.0941
T-27	27.9	Tr GSt	0.0001	0.0118	0.0070	0.0018	0.0036
T-29	30.6	Tr GSt	0.0011	0.0140	0.0038	0.0015	0.0120
T-30	32	FPC	0.0010	0.0132	0.0054	0.0015	0.0031
T-31	33.9	MSt	0.0013	0.0103	0.0032	0.0012	0.0049
T-33	36.25	MSt	0.0005	0.0099	0.0035	0.0016	0.0045
T-35	37.9	MSt	0.0013	0.0288	0.0037	0.0013	0.0190
T-36	38.75	MSt	0.0006	0.0124	0.0021	0.0015	0.0044
T-37	40.75	MSt	0.0003	0.0133	0.0055	0.0018	0.0027
T-38	41.5	MSt	0.0033	0.0111	0.0054	0.0013	0.0171
T-40	43	Tr PkSt/ GSt	0.0013	0.0117	0.0035	0.0014	0.0045
T-41	44	MSt	0.0009	0.0104	0.0006	0.0017	0.0032
T-42	44.5	MSt	0.0111	0.3228	0.0060	0.0016	0.1004
T-43	45.5	MSt	0.0004	0.0107	0.0019	0.0020	0.0032
T-44	46.75	Tr PkSt	0.0005	0.0124	0.0012	0.0019	0.0029
W-1	0.5	MSt	0.0031	0.0112	0.0042	0.0010	0.0176
W-2	1	FPC	0.0008	0.0102	0.0039	0.0011	0.0050
W-3	3	MSt	0.0004	0.0111	0.0042	0.0014	0.0059
W-4	3.75	MSt	0.0004	0.0099	0.0029	0.0013	0.0061
W-5	5	MSt	0.0005	0.0100	0.0025	0.0013	0.0060
W-5.5	5.75	MSt	0.0002	0.0095	0.0029	0.0016	0.0056
W-6	6.33	MSt - ReXL	0.0006	0.0118	0.0038	0.0014	0.0067
W-7	7		0.0004	0.0108	0.0029	0.0013	0.0072
W-8a	8	MSt	0.0012	0.0123	0.0062	0.0012	0.0073
W-8b	8	MSt	0.0014	0.0115	0.0061	0.0012	0.0087
W-9	8.9		0.0007	0.0178	0.0031	0.0013	0.0111
W-10	9.75	MSt	0.0003	0.0136	0.0034	0.0013	0.0095

W-11	11	MSt	0.0002	0.0092	0.0022	0.0015	0.0082
W-12a	11.25	FPC	0.0006	0.0113	0.0024	0.0014	0.0065
W-12b	11.25	FPC	0.0012	0.0144	0.0028	0.0013	0.0092
W-13	11.75	MSt	0.0009	0.0103	0.0051	0.0013	0.0061
W-14	12.33	MSt	0.0003	0.0135	0.0018	0.0013	0.0076
W-15	12.8	Tr WkSt	0.0002	0.0126	0.0016	0.0015	0.0053
W-19	16.5	Tr WkSt	0.0009	0.0135	0.0074	0.0014	0.0066
W-20	17.5	MSt	0.0013	0.0105	0.0067	0.0012	0.0069
W-16	14.5		0.0003	0.0176	0.0014	0.0015	0.0065
W-21	18.25	Conc	0.0010	0.0125	0.0071	0.0012	0.0025
W-22	19.25	Tr GSt	0.0004	0.0136	0.0046	0.0015	0.0018
W-24	20	MSt	0.0007	0.0128	0.0051	0.0011	0.0026
W-25	20.5	MSt	0.0009	0.0109	0.0042	0.0011	0.0025
W-28	23.25	Cal-Shale	0.0013	0.0093	0.0038	0.0016	0.0105
W-29	25	MSt	0.0006	0.0133	0.0053	0.0017	0.0041
W-30	26.5	Conc	0.0010	0.0091	0.0079	0.0011	0.0028
W-31	27.9		0.0005	0.0257	0.0041	0.0015	0.0097
W-32	28.5	Tr WkSt	0.0008	0.0106	0.0021	0.0017	0.0087
W-33	29.5	MSt	0.0004	0.0109	0.0030	0.0017	0.0056
W-34	34.75	MSt	0.0004	0.0126	0.0047	0.0019	0.0019
W-36	36.5	Tr PkSt	0.0009	0.0140	0.0056	0.0021	0.0034
W-37	37	MSt	0.0002	0.0116	0.0038	0.0020	0.0041
W-38a	39	Cal-Shale	0.0009	0.0142	0.0004	0.0017	0.0023
W-38b	39	FPC	0.0046	0.1955	0.0028	0.0018	0.0459
W-39	39.5	MSt	0.0004	0.0144	0.0010	0.0016	0.0042
W-40	41.5	Cal-Shale	0.0083	0.1761	0.0018	0.0019	0.0424
W-41	44.5	MSt	0.0004	0.0413	0.0003	0.0022	0.0055

W-42	45.5	Cal-Shale	0.0044	0.3081	0.0013	0.0011	0.0415
W-44	50	Tr PkSt	0.0004	0.0115	0.0006	0.0019	0.0035